INFORMATION TO USERS

This manuscript has been reproduced from the microfilm master. UMI films the text directly from the original or copy submitted. Thus, some thesis and dissertation copies are in typewriter face, while others may be from any type of computer printer.

The quality of this reproduction is dependent upon the quality of the copy submitted. Broken or indistinct print, colored or poor quality illustrations and photographs, print bleedthrough, substandard margins, and improper alignment can adversely affect reproduction.

In the unlikely event that the author did not send UMI a complete manuscript and there are missing pages, these will be noted. Also, if unauthorized copyright material had to be removed, a note will indicate the deletion.

Oversize materials (e.g., maps, drawings, charts) are reproduced by sectioning the original, beginning at the upper left-hand corner and continuing from left to right in equal sections with small overlaps. Each original is also photographed in one exposure and is included in reduced form at the back of the book.

Photographs included in the original manuscript have been reproduced xerographically in this copy. Higher quality 6" x 9" black and white photographic prints are available for any photographs or illustrations appearing in this copy for an additional charge. Contact UMI directly to order.

UMI

A Bell & Howell Information Company
300 North Zeeb Road, Ann Arbor MI 48106-1346 USA
313/761-4700 800/521-0600

Mixed-State Hall Effect of High-T_c Superconductors

by

Byeongwon Kang

Submitted to the Department of Physics and Astronomy and the Faculty of the Graduate School of the University of Kansas in partial fulfillment of the requirements for the degree of Doctor of Philosophy

Dissertation Committee

Chair

Dissertation defended on Nov. 5th, 1998

Abstract

In this dissertation, we presented the study on the mixed-state Hall effect of high-T_c superconductors (HTSs). In order to understand the mechanisms of the puzzling phenomena in the mixed-state Hall effect of HTSs, the Hall sign anomaly and scaling behavior, Hall measurements are conducted in several HTS thin films.

We investigate the mechanism of the sign reversal of the Hall resistivity in Tl-2201 films when the electronic band structure is varied through the underdoped, optimally doped, and overdoped regions. It is found that the Hall sign reversals are an intrinsic property of HTSs and determined by electronic band structure. Although pinning is not found to be the mechanism behind sign reversals, pinning can suppress the appearance of the Hall sign reversal. Therefore, it is concluded that two (or more) sign reversals are a generic behavior of HTSs.

From a systematic study of the vortex phase diagram, we discover several new features of the vortex liquid. In the presence of pinning, the vortex-liquid phase can be divided into two regions, a glassy liquid (GL) where vortices remain correlated as manifested in non-Ohmic resistivity, and a regular liquid (RL) where resistivity becomes Ohmic as vortices become uncorrelated. The field dependence of the Hall angle is found to be linear in the RL and nonlinear in the GL. Generally the decoupling line (H_k-T), which is defined as a boundary between the GL and the RL, is lower than the depinning line (H_d-T). As pinning increases the H_k-T may approach the H_d-T, thus vortices are decoupled and depinned nearly simultaneously. For a weak pinning system, on the other hand, the H_k-T and the H_d-T are well separated so that single vortices remain pinned in the region $H_k \leq H \leq H_d$. The behavior of σ_{xy} is

also investigated in the GL and the RL. In the GL σ_{xy} is observed to strongly depend on pinning due to the inter-vortex correlation whereas in the RL σ_{xy} is independent of pinning since the pinning effect is scaled out.

Byeongwon Kang, Ph. D.
Department of Physics and Astronomy, 1998
University of Kansas

This dissertation is dedicated

to

my late father

Acknowledgment

When I look back the last 5 years, I have been very lucky to meet unforgettable people who have helped me to go through this definitely not-easy process. It is my great pleasure to have the opportunity to acknowledge them.

My first and foremost and also the deepest gratitude will go to my research advisor, Prof. Judy Z. Wu. She has provided me such a wonderful graduate training and environment together with enduring guidance, encouragement and caring during the whole my graduate studies. Without her help, I could not have taken the first step for a researcher. I have admired and will admire her passion and devotion for the research, which has never failed to motivate me to grow as an independent and competitive scientist. For all the appreciation I am feeling for her, however, I would like to say just one word to her now. That is " THANKS". The rest of the words of gratitude I will tell her bit by bit during all of my life as a serious scientist.

I am also very grateful to Dr. Kai-Wai Wong, Dr. Douglas W. McKay, Dr. Brian B. Laird and Dr. David K. Christen for serving on my dissertation committee and for their valuable suggestions and comments on my dissertation. I owe a great deal of gratitude to Dr. David K. Christen for his insightful comments regarding the interpretation of experimental data, which has broadened my perspective in physics. I deeply appreciate his sacrifice to make long trips to University of Kansas to serve as a committee.

My special thanks go to TcSUH and Midwest Superconductivity Inc. for providing access to various experimental facilities. I cannot forget Dr. Wei-Kan Chu and Dr. Quark Y. Chen in TcSUH for their endless encouragement and invaluable

help. They also helped me feel really comfortable and enjoyable during the time I was doing experiment in TcSUH. Without Dr. Q. Y. Chen's tremendous help and warmth during my experiment, this work couldn't be finished.

Dr. Won-Nam Kang and Dr. Sang-Ho Yun also deserve my special thanks for their valuable help in my growth as an experimentalist. I vividly remember 5 years ago when I entered KU as a real beginner in experiment. They are the ones who taught me all experimental techniques I need to know with kindness and patience. I am sincerely thankful for their insightful comments on the interpretation of the data and for providing high quality Hg-1212 films I used in the experiment as well.

It was my privilege to be able to get the high-quality samples from our colleagues. I wish to express my sincere appreciation to Dr. Z.F. Ren and Dr. J.H. Wang at SUNY Buffalo for high quality Tl-2201 films and Dr. Shaolin Yan and Mr. Yi-yuan Xie at KU for high-quality Hg-1212 and Tl-2212 films.

For over five years, the Condensed Matter Physics Group of KU has provided a great environment in which I could work with confidence and comfort. I am very thankful to Dr. Shaolin Yan, Dr. Lan Fang, Mr. Albert A. Gapud, Mr. Tolga Aytug, Mr. Yi-yuan Xie and Mr. Robert Aga for their kindness, concern and help which made my graduate studies memorable. Their warm celebration for my wedding and sincere consolation for the loss of my father are still vivid in my memory. My special thanks go to Mr. A. A. Gapud not only for his help in measurements at MSI and at TcSUH, and assistance in editing a large portion of this dissertation but also for his faithful friendship and encouragement.

My interest and affection in physics developed through my undergraduate training at Ewha Womans University in Korea, which also provided a solid foundation for my present study. I am greatly benefited by the lectures and training from Prof. Hae-jeong Moh, Prof. Sung-Ku Kim, Prof. Jongman Yang among others. My heartfelt thanks go to my M.A. thesis advisor, Prof. Hae-jeong Moh who guided and encouraged me to open my eyes to the bigger and more competitive world of science. I also wish to say thank to Dr. So-yeon Jeong for her moral support and warm

encouragement since I entered the university. I owe a great thank to Dr. Hye-kyung Lee for her caring and help during my stay in Houston.

Now I extend my special gratitude to my family. I couldn't find any appropriate phrases to express my thanks to my parents not only for their love and encouragement but also for their patience and sacrifice during their whole life. Especially, I wish to appreciate my late father who had long waited to see the completion of this work but could not. His love, support and confidence in me had always been a firm ground on which I could grow up to be what I am. I am also deeply grateful to my parents-in-law for their deep understanding, attention and love. My special thanks go to my three sisters and brothers-in-law for their endless encouragement, concern and confidence in my study.

I owe my deepest thanks to my husband, Hangyoo Khym, who has never failed to provide me a shelter during my entire graduate career. He has been my eternal supporter and at the same time, my well-meant rival as a companion and a better-half. I can not thank him enough for his deep love, understanding, and caring as well as his incredible patience for editing this dissertation.

Finally, I would like to thank God who allows me everything that I have done and will do.

Contents

List of Figures

Chapter 1

Introduction

The Hall effect in the mixed state of high-T_c superconductors (HTSs) has been a topic of great interest in the fundamental research because it provides important information on vortex dynamics. There are two puzzling behaviors recognized; (1) the Hall resistivity (ρ_{xy}) changes its sign once or twice upon cooling down from the normal state to the superconducting state, and (2) ρ_{xy} and the longitudinal resistivity (ρ_{xx}) show an unusual scaling behavior of $\rho_{xy} \sim \rho_{xx}^{\beta}$ at the onset of resistivity. Since none of these features is expected within the standard models of the flux motion such as the Bardeen-Stephen (BS) model [1] or the Nozieres-Vinen (NV) model [2], understanding of these phenomena is of primary importance in the study of vortex dynamics in the mixed state of HTSs. Despite great efforts attempted in both theoretical and experimental investigations, no consensus has been achieved.

1.1 Hall effect in the mixed-state of high-T_c superconductors

The Hall sign anomaly (as shown in Fig. 1.1) has been observed in most HTSs[3-13] and even in low T_c superconductors (LTSs), such as Nb [14], MoGe/Ge

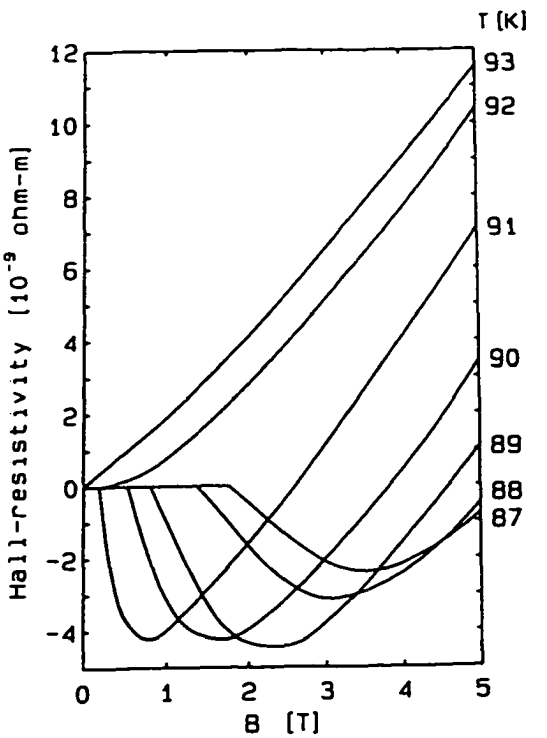

Fig. 1.1: Hall resistivity vs. magnetic field at constant temperature between 84 and 93 K for polycrystalline YBCO sample (Ref. [3]). Note the sign change of Hall resistivity below T_c from positive to negative with decreasing field.

multilayers [15] and α-$MoSi_3$ [16], while the number of the sign anomaly differs from system to system. Since all these superconductors have a large Ginzberg-Landau parameter ($\kappa \equiv \lambda/\xi >> 1$), so-called type-II superconductors, the Hall sign anomaly is regarded as a unique feature of the type-II superconductors. The first sign reversal always occurs near the transition temperature (T_c) while the second one usually appears at much lower temperatures for the relatively weak pinning systems such as Bi-, Tl- [5,6,10,11] and recently discovered Hg-based cuprates [13]. It is generally believed that the sign reversal is due to vortex motion because charge carriers (electrons or holes) are not expected to change the sign at the normal to

superconducting transition.

The puzzling scaling behavior between ρ_{xy} and ρ_{xx} (Fig. 1.2) has been also observed as the relation of $\rho_{xy} \sim \rho_{xx}^{\beta}$ in most HTS, but with the different scaling exponent $1.5 < \beta < 2$ for various systems [10-12]. Originally the scaling behavior of ρ_{xy} against ρ_{xx} has been explained in terms of the general picture of the glassy scaling near the vortex-glass transition by Dorsey and Fisher [17]. They showed that ρ_{xy} and ρ_{xx} should scale with a universal power, which was observed by Luo *et al.* [9] in YBCO films, further predicted that the nonlinear Hall electric field should scale with a universal power of current at the vortex-glass transition, later confirmed by Wöltgens *et al.* [18].

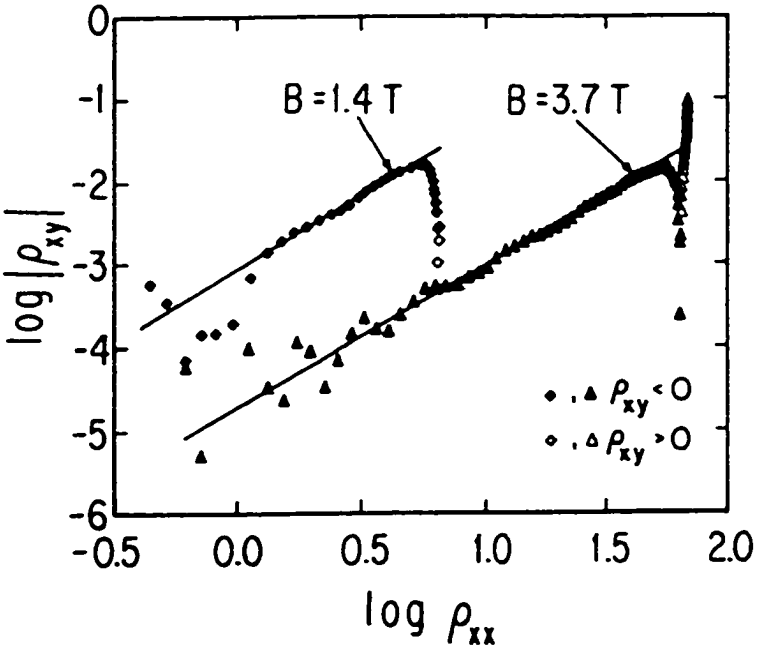

Fig. 1.2: Log-log plot of $|\rho_{xy}|$ vs. ρ_{xx} obtained for temperature sweep at two magnetic field values. Note apparent $|\rho_{xy}| \sim \rho_{xx}^{\beta}$ behavior with $\beta = 1.7 \pm 0.2$. Solid symbols for $\rho_{xy} < 0$, open for $\rho_{xy} > 0$ (Ref. [9]).

1.2 Theoretical models

Numerous mechanisms based on both intrinsic or extrinsic superconducting properties have been proposed to understand the mechanism of the Hall effect. Among them the models proposed by Vinokur, Geshkenbein, Feigel'man and Blatter (VGFB) [19] and Wang, Dong and Ting (WDT) [20] have received much attention since these models seem to agree with most of the experimental results. Besides these phenomenological models, important progress has been made recently on microscopic theories [21,22] which attracted attention since these theories provide much more quantitative descriptions of the Hall effect.

1.2.1 VGFB model

Based on a phenomenological model of force balance, Vinokur, Geshkenbein, Feigel'man and Blatter (VGFB) [19] calculated the effect of pinning on ρ_{xx} and ρ_{xy} from the force balance equation for an individual vortex line, which is obtained by balancing the Lorentz force $(c/e)n_s\Phi_0(\mathbf{v}_s - \mathbf{v}) \times \mathbf{n}$ with a drag force $\eta\mathbf{v} + \eta'\mathbf{v} \times \mathbf{n}$. In this expression $\mathbf{v}_s$ and n_s are superfluid velocity and the density of superconducting electrons, respectively, $\mathbf{v}$ is the average velocity of vortices, $\mathbf{n}$ is the unit vector along the vortex line, and $\Phi_0 = hc/2e$ (hereafter $c = 1$) is the flux quantum. The friction term η comes from the dissipation in the normal core with the Bardeen-Stephen form $\eta = \Phi_0 H_{c2}/\rho_n$, where ρ_n is the normal state resistivity. With consideration of interactions between vortices $\mathbf{F}_{int,i}$, pinning $\mathbf{F}_{pin,i}$, and thermal noise $\mathbf{F}_{T,i}$, the force balance equation for a given ith vortex acquires the form

$$\eta\mathbf{v}_i + \alpha\mathbf{v}_i \times \mathbf{n} = \Phi_0 \mathbf{j} \times \mathbf{n} + \mathbf{F}_{int,i} + \mathbf{F}_{pin,i} + \mathbf{F}_{T,i} \qquad (1.1)$$

Here $\boldsymbol{j} = en_s\mathbf{v}_s$ is the transport current density and $\mathbf{v}_i$ is the velocity of the vortex with respect to the crystal lattice. The coefficient α determines the sign and the magnitude of the Hall angle θ_H via the relation $\tan\theta_H = \alpha/\eta$. It is the particular behavior of α

that determines such an effect as the sign change of the Hall resistivity, however, the specific form of α is irrelevant. It will be shown that pinning renormalizes the friction η leaving the Hall coefficient α unchanged.

On averaging Eq. (1.1) over disorder, thermal fluctuation and vortex positions one arrives at

$$\eta \mathbf{v} + \alpha \mathbf{v} \times \mathbf{n} = \Phi_0 \mathbf{j} \times \mathbf{n} + \langle \mathbf{F}_{pin,i} \rangle \tag{1.2}$$

where $\mathbf{v}$ denotes the average velocity of vortices. The averaged interaction force is zero due to Newton's third law. In the discussion of the resistivity scaling, a question is the *direction* of the averaged pinning force. The pinning force is the gradient of the random potential and this potential is determined by the relative positions of the vortices with respect to the pins and is invariant under time reversal. Hence, the averaged pinning force is invariant under the reversal of the magnetic field. Then, after averaging the only vectorial quantity that characterizes the vortex motion is independent of the sign of the magnetic field and is the vortex velocity $\mathbf{v}$. Therefore pinning force can be written in the form

$$\langle \mathbf{F}_{pin,i} \rangle = -\gamma(v)\mathbf{v} \tag{1.3}$$

where the coefficient $\gamma(v) > 0$ can be in principle calculated by the summation of the perturbation series. The above statement can be illustrated by the lowest order calculation in the perturbation expansion over the disorder potential:

$$\left\langle \mathbf{F}^{(1)}_{pin,i} \right\rangle = -\left\langle \sum_i V(\mathbf{r}) \left[\mathbf{u}_{pin}(\mathbf{r},t) \cdot \nabla \right] \nabla_p \left(\mathbf{r}_\perp - \mathbf{r}_{\perp i} - \mathbf{v}t \right) \right\rangle \tag{1.4}$$

where $V(\mathbf{r})$ is the short range disorder potential, $p(\mathbf{r})$ is the vortex core form factor, $\mathbf{u}_{pin}(\mathbf{r},t)$ is the disorder induced displacement field of the vortex configuration and the summation is performed over the positions of the vortex lines $\mathbf{r}_{\perp i}$. Straightforward calculation shows that the perpendicular to $\mathbf{v}$ terms cancel in Eq. (1.4). Hence the equation of vortex motion is:

$$[\eta + \gamma(v)]\, \mathbf{v} + \alpha \mathbf{v} \times \mathbf{n} = \mathbf{f}_L \tag{1.5}$$

with $\mathbf{f}_L = \Phi_0\, \mathbf{j} \times \mathbf{n}$. It can be seen that pinning normalizes the friction coefficient γ only, whereas the Hall conductivity α remains unchanged. A solution to Eq. (1.5) is easily found as

$$\mathbf{v} = \frac{1}{\bar{\gamma}(v)}\left[1+\frac{\alpha^2}{\bar{\gamma}^2}\right]^{-1}\left[\mathbf{f}_L - \frac{\alpha}{\bar{\gamma}(v)}\mathbf{f}_L \times \mathbf{n}\right] \tag{1.6}$$

where $\bar{\gamma}(v) = \gamma(v) + \eta$. The Hall angle and the ratio $\alpha / \bar{\gamma}(v)$ are assumed to be very small and hence, the term $\alpha^2 / \bar{\gamma}^2(v)$ will be neglected with respect to 1. The electric field induced by the vortex motion is $\mathbf{E} = \mathbf{B} \times \mathbf{v}$ and from Eq. (1.6), $E_x = [B\Phi_0 / \bar{\gamma}(v)]\, j$, $E_y = [\alpha B\Phi_0 / \bar{\gamma}^2(v)]\, j$. For resistivity defined as $\rho = E/j$ one immediately gets

$$\rho_{xy} = \rho_{xx}^2\, \alpha / B\Phi_0 \tag{1.7}$$

The main result of this analysis is that since the coefficient α is nearly temperature and pinning independent, the Hall conductivity σ_{xy} ($\cong \rho_{xy}/\rho_{xx}^2$) does not depend on disorder. This result is general to the regimes of flux flow, thermally assisted flux flow (TAFF) and vortex glass behavior (creep), regardless of the type of defects. The temperature dependence of ρ_{xy} is determined by that of ρ_{xx} and α. In particular the sign of ρ_{xy} follows the sign of α. Regarding the origin of the sign change in ρ_{xy}, one can conclude that the sign change is not related to the pinning and may even take place above T_c provided the magnetic field is low enough. In the vicinity of the resistive onset where pinning is effective, ρ_{xx} dominates the temperature dependence of ρ_{xy} since α has a much weaker temperature dependence in this region. Consequently, the existence of a second sign change depends on whether the pinning is strong enough as to suppress ρ_{xy} before the second sign change occurs or afterwards. This explains in a natural way the occurrence of the double sign change in the strongly layered Bi- and Tl-compounds, where pinning is reduced due to the large anisotropy, whereas the second sign change in YBCO is suppressed by the stronger pinning.

1.2.2 WDT model

The different number of the sign reversal observed for different systems leads one to believe that the sign reversal might be caused by the extrinsic property of HTSs such as pinning. Based on this idea, Wang, Dong and Ting (WDT) [20] developed a theory of the flux motion including both pinning-induced backflow and thermal fluctuations in the standard BS model. Let us consider a moving flux carrying a quantum of flux $\Phi_0 = hc/2e$ (hereafter $c = 1$) in the z direction (unit vector $\mathbf{n}$). Then an equation of motion for the charge fluid inside the core of the ith flux in the presence of thermal fluctuation (per unit length in the z direction) is well established as

$$\mathbf{F}_{nc(i)} + \mathbf{F}^{in}_{T(i)} + \mathbf{F}^{in}_{p(i)} = (Nm/\tau)\, \pi a^2\, \mathbf{v}_{nc(i)} \tag{1.8}$$

where N is the normal charge carrier density and τ is the momentum relaxation time of charge carriers. The term $(Nm/\tau)\ \pi a^2\ \mathbf{v}_{nc(i)}$ denotes the momentum dissipated inside the normal core with $\mathbf{v}_{nc(i)}$ the drift velocity of carriers. $\mathbf{F}^{in}_{T(i)}$ is the force due to thermal fluctuations resulting from the random thermal motions of the normal charge carrier inside the core. At finite temperature, thermal fluctuations definitely exist. Especially for high T_c superconductors and when the temperature is not too far below T_c, the pinning energy could be comparatively low so that the thermal fluctuation plays a crucial role in assisting the motion of a flux within the TAFF and creep region. $\mathbf{F}^{in}_{p(i)}$ and $\mathbf{F}_{nc(i)}$ are the effective pinning and the external driving forces acting on the charge fluid inside the normal core.

$$\mathbf{F}_{nc(i)} = \int_{\Omega^-} N\left[e\mathbf{E} + e\mathbf{v}_{nc} \times \mathbf{H} - \nabla\mu_0\right] d\Omega$$

where $\mathbf{E}$ and $\mathbf{H}$ are, respectively, local electric and magnetic fields, μ_0 is the chemical potential in the absence of currents and fields, and Ω^- represents the volume of the unit-length cylinder. Using the approach similar to that adopted in Ref. [23], in the presence of thermal fluctuations the force balance equation on a flux can be written as

$$\mathbf{F}_{(i)} + \mathbf{f}_{drag(i)} + \mathbf{F}_{T(i)} + \mathbf{F}_{pin(i)} = 0 \qquad (1.9)$$

where $\mathbf{F}_{T(i)}$ and $\mathbf{F}_{pin(i)}$ are, respectively, thermal noise and pinning force acting on the flux, $\mathbf{F}_{(i)} = Ne(\mathbf{v}_T - \mathbf{v}_{\varphi(i)}) \times \Phi_0$ is the magnus force with $Ne\mathbf{v}_T = \mathbf{J}$ as the applied current along the x direction, and $\mathbf{f}_{drag(i)}$ is the drag force which has the following form:

$$\mathbf{f}_{drag(i)} = Ne\mathbf{v}_{\varphi(i)} \times \Phi_0 - \eta\mathbf{v}_{\varphi(i)} + \Phi_0\beta_0(1 - \bar{\gamma})\,\mathbf{J} - \beta_0(1 + \bar{\gamma})\,\mathbf{F}_{pin(i)} \times \mathbf{n} \qquad (1.10)$$

where $\mathbf{v}_{\varphi(i)}$ is the velocity of the flux line, $\beta_0 = \mu_m H_{c2}$ with μ_m being the mobility of the charge carrier and H_{c2} being the upper critical field, η is the usual viscous coefficient, $\bar{\gamma} = \gamma(1 - \bar{H}/H_{c2})$ with $\bar{H}$ the average magnetic field over the core and γ as the parameter describing the contact force on the surface of core, which depends on temperature in the following way [23]: $\gamma \sim 0$ (NV limit) for $\xi/l \ll 1$ and $\gamma \sim 1$ (BS limit) for $\xi/l \geq 1$ with ξ and l as the superconducting coherence length and the mean free path of the carrier, respectively. In detail, Eq. (1.9) is rewritten as

$$\eta\mathbf{v}_{\varphi(i)} = \mathbf{F}_L + \mathbf{F}_{pin(i)} + \mathbf{F}_{T(i)} - \beta_0(1 - \bar{\gamma})\mathbf{F}_L \times \mathbf{n} - \beta_0(1 + \bar{\gamma})\mathbf{F}_{pin(i)} \times \mathbf{n} \qquad (1.11)$$

where $\mathbf{F}_L = \boldsymbol{J} \times \Phi_0$ is the Lorentz force. Note that Eq. (1.11) is rigorously derived in terms of the well known normal core model, and the transverse term $\mathbf{F}_{pin(i)} \times \mathbf{n}$ is induced due to the backflow current inside the normal core, which constitutes the essential physics of Wang and Ting (WT) theory [23]. Eq. (1.11) is the basic equation to describe the flux motion in the presence of thermal fluctuation and the pinning. In principle, the equation can be solved, i.e., $\mathbf{v}_{\varphi(i)}(t) = \Psi(\mathbf{F}_L, \mathbf{F}_{p(i)}(t), \mathbf{F}_{p(i)}(t))$, at least by numerical calculations, but it is unnecessary to solve Eq. (1.11) in detail. Taking the time average on $\mathbf{v}_{\varphi(i)}$, i.e., $\langle \mathbf{v}_{\varphi(i)} \rangle_t (t) = \langle\, \Psi(\mathbf{F}_L, \mathbf{F}_{p(i)}(t), \mathbf{F}_{p(i)}(t))\, \rangle_t$, Eq. (1.11) becomes

$$\eta\mathbf{v}_L = \mathbf{F}_L + \langle \mathbf{F}_p \rangle_t - \beta_0(1 - \bar{\gamma})\mathbf{F}_L \times \mathbf{n} - \beta_0(1 + \bar{\gamma})\langle \mathbf{F}_{pin} \rangle_t \times \mathbf{n} \qquad (1.12)$$

where $\mathbf{v}_L = \langle \mathbf{v}_{\varphi(i)} \rangle_t$ and $\langle \mathbf{F}_p \rangle_t$ are, respectively, time averaged flux-motion velocity and

pinning force. Although Eq. (1.12) seems to be similar to the case of neglecting the thermal fluctuations, the regime of the validity and the meaning for $\langle \mathbf{F}_p \rangle_t$ are quite different from this without the thermal noise. In the absence of thermal noise, $\mathbf{F}_p$ is merely a space-average quantity, and so the flux can move if and only if $F_L \geq F_p$ (flux flow region), while in the present case, with the assistance of the force due to thermal fluctuations, flux moves as long as $F_L > 0$ (whole flux motion region). Here $\mathbf{F}_p$ is significantly different from $\langle \mathbf{F}_p \rangle_t$ in the TAFF and creep region. By considering the fact that $\langle \mathbf{F}_p \rangle_t$ should be antiparallel to $\mathbf{v}_L$, i.e., $\langle \mathbf{F}_p \rangle_t = -\Gamma(\upsilon_L)\mathbf{v}_L$ with $-\Gamma(\upsilon_L)$ a positive scale function being generally dependent on υ_L (including temperature and pinning energy dependence) and F_L, it is straight forward to obtain

$$\upsilon_{Lx} = \beta_0 \frac{F_L\{(1-\bar{\gamma})\bar{\Gamma} - (1+\bar{\gamma})\Gamma(\upsilon_L)\}}{\bar{\Gamma}^2 + \beta_0^2(1+\bar{\gamma})\Gamma^2(\upsilon_L)} \tag{1.13}$$

$$\upsilon_{Ly} = -\frac{F_L\{\bar{\Gamma} + \beta_0^2(1-\bar{\gamma}^2)\Gamma(\upsilon_L)\}}{\bar{\Gamma}^2 + \beta_0^2(1+\bar{\gamma})^2\Gamma^2(\upsilon_L)} \tag{1.14}$$

where $\bar{\Gamma} = \Gamma(\upsilon_L) + \eta$. Considering the experimental fact that the Hall angle $|\theta_H| = |tg^{-1}(\upsilon_{Lx}/\upsilon_{Ly})| \sim \beta_0 << 1$, then $\upsilon_{Ly} \approx -F_L / \bar{\Gamma}$, and $\upsilon_{Lx} \approx (\beta_0 F_L / \bar{\Gamma}^2)\{\eta(1-\bar{\gamma}) - 2\bar{\gamma}\Gamma(\upsilon_L)\}$. In terms of the relationships $\rho_{xx} = -\upsilon_{Ly}B / J$ and $\rho_{xy} = \upsilon_{Lx}B / J$ with B as the magnetic induction, it is easy to obtain

$$\rho_{xy} = (\beta_0 \rho_{xx}^2 / H\Phi_0)\{\eta(1-\bar{\gamma}) - 2\bar{\gamma}\Gamma(\upsilon_L)\} \tag{1.15}$$

Eq. (1.15) is the main result of the WDT model. From the above equation, it can be noticed that when $\gamma = 0$ (NV limit, usually in the low-temperature region for some superconductor), the scaling law $\rho_{xy} \sim \rho_{xx}^2$ holds strictly for J dependence and works well for T dependence because η is independent of J, and is only weakly dependent on T in the TAFF region as compared with the exponent dependence of $\rho_{xx} \sim e^{-Uo/kT}$. Although this result may seem to be similar to that in the VGFB model, it should be

noted that the origin is totally different. If Eq. (1.11) is written in the form $\eta \mathbf{v}_\varphi + \alpha \mathbf{v}_\varphi \times \mathbf{n} = \mathbf{F}_L + \mathbf{F}_{pin} + \mathbf{F}_T$ [19], α should be dependent on the pinning and υ_φ explicitly. Only after renormalizing α due to the pinning with the thermal fluctuation effect could it become J independent and T weakly dependent in the NV limit. This is contrary to the starting point of the VGFB model in which α is assumed to be "constant" and then is claimed not to be renormalized by the pinning. Second, when $\gamma \sim 1$ (BS limit: usually in a relatively higher temperature region), the negative Hall effect could automatically appear as long as the magnetic field is low enough and the pinning is not negligible. This model could also explain the double sign reversals observed in Bi-, Tl- and Hg-based cuprates. For a fixed magnetic field, by increasing temperature, there is an apparent reduction of ρ_{xy} during its increase. If the field is low enough and the pinning is relatively strong, ρ_{xy} will change its sign from positive to negative (the second sign reversal). As temperature further increases, the pinning will become less important, i.e., the second term is less than the first term in the bracket and the sign of ρ_{xy} undergoes another change.

For the systems with weak pinning (such as BSCCO) there are two distinct regimes for the Hall scaling behavior in the region of $\gamma \sim 1$. As $\Gamma(\upsilon_L) << \eta\ \bar{H}/H_{c2}$ in the intermediate field, the scaling relation $\rho_{xy} \sim A\rho_{xx}^2$ with A being positive and approximately independent of field is still valid. With higher $\bar{H}$, the observable scaling region may become widened. If the field is very low, however, there could exist a negative ρ_{xy} region because of $\Gamma(\upsilon_L) > \eta\ \bar{H}/H_{c2}$ in which the scaling law with $\beta \approx 2$ does not hold well. On the other hand, for systems with strong pinning (such as YBCO), a vortex glass state may form near the low-temperature end T_2 of the negative Hall region and pinning is dominant [i.e., $\Gamma(\upsilon_L) >> \eta\ \bar{H}/H_{c2}$ for $\gamma \sim 1$]. Thus when T is near but a little bit above T_2 and also close to the vortex-glass transition temperature T_g, rough estimation yields $\Gamma(\upsilon_L) \sim \upsilon_L^{-1/2}$ [19], which leads to $\beta \sim 1.5$. Therefore, depending on the pinning strength, various β ranges from 1.5 to 2 is expected.

1.2.3 Microscopic theory: TDGL model

Recently significant progress has been made on microscopic theories. Based on the time-dependent Ginzburg-Landau (TDGL) equation, Dorsey [21] and Kopnin, Ivlev and Kalasky (KIK) [22] have independently calculated the Hall angle (θ_H) and Hall conductivity (σ_{xy}). Since the results of the calculation are very similar to each other, only the KIK model is described in the following.

In the KIK model, the TDGL theory is modified to account for two mechanisms responsible for the transverse voltage. The first is the usual effect of the magnetic field on the normal current and the second mechanism is the vortex traction by the superflow: the vortex has a velocity component parallel to the transport supercurrent. It gives rise to a Hall voltage since the average electric field is perpendicular to the vortex velocity $\mathbf{v}_L$:

$$\mathbf{E}_{av} = 1/c\,[\mathbf{B} \times \mathbf{v}_L] \tag{1.16}$$

The TDGL equation can be written in the form

$$-\gamma\left(\frac{\partial\Psi}{\partial t} + 2ie\phi\Psi\right) = \frac{\delta F_{sn}}{\delta\Psi^*} \tag{1.17}$$

$$-\frac{\mathbf{j}_s}{c} = \frac{\delta F_{sn}}{\delta\mathbf{A}} \tag{1.18}$$

Here F_{sn} is the condensation free energy of a superconductor,

$$F_{sn} = \int\left[C_1|\Psi|^2 + \frac{1}{2}C_2|\Psi|^4 + \frac{1}{2m}\left|\left(-i\nabla - \frac{2e}{c}\mathbf{A}\right)\Psi\right|^2\right]dV \tag{1.19}$$

$\mathbf{j}_s$ is the supercurrent,

$$\mathbf{j}_s = \mathbf{j} - \mathbf{j}_n \tag{1.20}$$

where $\mathbf{j}$ is the total current, and

$$\mathbf{j}_n = \sigma_n E = \sigma_n\left(-\frac{1}{c}\frac{\partial \mathbf{A}}{\partial t} - \nabla\phi\right) \tag{1.21}$$

is the normal current. The constant γ is real; it controls the relaxation of the order parameter Ψ to its equilibrium value.

It is known that the TDGL model in the form of Eqs. (1.17), (1.18), (1.20) and (1.21) does not describe the Hall effect: it only gives the longitudinal flux-flow conductivity σ_f. To account for the Hall effect within the TDGL formalism, the most obvious modification would be to incorporate the Hall component into the normal current

$$\mathbf{j}_n = \sigma_n \mathbf{E} + \frac{\sigma_n^H}{H}[\mathbf{E} \times \mathbf{H}] \tag{1.22}$$

where σ_n^H is the normal-state Hall conductivity.

This contribution, however, is not the only one. In the dissipative flux-flow regime, vortices move perpendicular to the transport current, so that the averaged electric field, Eq. (1.16), induced in the superconductor is parallel to the transport current. On the other hand, in the ideal fluid, a vortex moves together with the flow; this vortex traction by the flow is the consequence of the Galilean invariance. For the TDGL model, there is no Galilean invariance since the condensate interacts strongly with the excitations which are at rest with the crystal lattice. However, some traces of the Galilean invariance can still exist: they can appear as a small imaginary part of the relaxation constant γ in Eq. (1.17). Indeed, if γ were purely imaginary Eq. (1.17) would be a (nonlinear) Schrödinger equation which is Galilean invariant.

In the following the modified TDGL equations in the form of Eqs. (1.17), (1.18), (1.20), (1.22) with a complex $\gamma = \gamma' + i\gamma''$ is used. It will be shown that in the basis of a simple model of gapless superconductivity with the BCS pairing potential that the ratio $\zeta = -\gamma''/\gamma'$ is proportional to the energy derivative of the density of states at the Fermi level. It is of the relative order of T_c/E_F; nevertheless, it plays a very important role for the Hall effect in the mixed-state of superconductors.

To calculate the force on a vortex produced by its interaction with the thermostat, the free energy variation caused by the displacement of the vortex by an arbitrary vector **d**. The total free energy consists of the condensation energy of Eq. (1.19) and the magnetic energy

$$F_{em} = \int \frac{H^2}{8\pi} dV \tag{1.23}$$

The variation of the total free energy $F = F_{sn} + F_{em}$ is

$$\delta F = \int \left((\mathbf{d}\cdot\nabla)\Psi \frac{\delta F_{sn}}{\delta \Psi} + c.c. + (\mathbf{d}\cdot\nabla)\mathbf{A} \frac{\delta F_{sn}}{\delta \mathbf{A}} + \frac{1}{4\pi}\mathbf{H}\cdot(\nabla\times[(\mathbf{d}\cdot\nabla)\mathbf{A}]) \right) dV \tag{1.24}$$

omitting the surface term. One obtains from Eqs. (1.17), (1.18), (1.19), and (1.20)

$$\delta F = \int \left(-\gamma(\mathbf{d}\cdot\nabla)\Psi^* \left(\frac{\partial \Psi}{\partial t} + 2ie\phi\Psi \right) - c.c. + \frac{\sigma_n}{c}[(\mathbf{d}\cdot\nabla)\mathbf{A}]\mathbf{j}_n \right) dV \tag{1.25}$$

The free energy variation in Eq. (1.25) is the work done by the force produced by excitations

$$\delta F = -\mathbf{d}\cdot\mathbf{f}_{exc} L$$

where L is the length of vortices, f_{exc} being the force per unit length. If the integration in Eq. (1.25) is extended over the area S_0 of one unit cell in the vortex lattice, the force acting on one vortex can be obtained. This force should be balanced by the external Lorentz force from the transport supercurrent:

$$\mathbf{f}_{exc} + \phi_0/c\,[\mathbf{j}_{tr}\times\mathbf{n}] = 0$$

Here **n** is the unit vector of the vortex calculation, and $\phi_0 = hc/2e$ is the flux quantum. Therefore,

$$\frac{\phi_0}{c}(\mathbf{d}[\mathbf{j}_{tr}\times\mathbf{n}]) = \int_{S_0} \left(-\gamma(\mathbf{d}\nabla)\Psi^* \left(\frac{\partial \Psi}{\partial t} + 2ie\phi\Psi \right) - c.c. + \frac{\sigma_n}{c}[(\mathbf{d}\nabla)\mathbf{A}]\mathbf{j}_n \right) dS \tag{1.26}$$

The scalar potential ϕ in Eq. (1.26) appears as a result of the vortex motion; it is proportional to v_L. It can be found from the equation which follows from the facts that $\nabla \cdot \mathbf{j} = 0$, and

$$\frac{\delta F}{\delta \chi} \equiv i\left(\Psi \frac{\delta F}{\delta \Psi} - \Psi^* \frac{\delta F}{\delta \Psi^*}\right) = -\frac{1}{2e}\nabla \cdot \mathbf{j}_s \qquad (1.27)$$

where χ is the phase of the order parameter. From Eq. (2) together with its complex conjugated equation one obtains

$$\nabla^2 \Phi - \frac{8e^2\gamma'|\Psi|^2}{\sigma_n}\Phi = -\frac{1}{c}\nabla \cdot \frac{\partial \mathbf{Q}}{\partial t} + \frac{2e\gamma''}{\sigma_n}\frac{\partial|\Psi|^2}{\partial t} - \frac{4\pi\sigma_n^H}{\sigma_n^2 Hc}\left(\mathbf{E}\cdot\mathbf{j} + \frac{\partial}{\partial t}\left(\frac{H^2}{8\pi}\right)\right) \qquad (1.28)$$

Here $\Phi = \phi + (1/2e)(\partial\chi/\partial t)$, and $\mathbf{Q} = \mathbf{A} - (c/2e)\nabla\chi$. The last two terms in the right-hand side of Eq. (1.28) are associated with the Hall effect. The term with σ_n^H is obtained under the assumption that $\sigma_n^H \propto H$. For a slow vortex motion with a velocity v_L, the time derivative $\partial/\partial t$ in Eqs. (1.26) and (1.28) can be replaced with $-\mathbf{v}_L \cdot \nabla$ acting on variables describing a static vortex. Therefore, Eq. (1.26) contains either the known functions or the function Φ which can be found from Eq. (1.28). The boundary conditions for Φ require that: (1) $\Phi = 0$ for large distances from the vortex, and (2) the scalar potential ϕ is finite at the center of the vortex.

Let us consider superconductors with a large Ginzberg-Landau parameter κ. In this case the term with the vector potential in Eq. (1.26) can be neglected. As a result we get

$$\frac{\phi_0}{c}(\mathbf{d}\cdot[\mathbf{j}_{tr}\times\mathbf{n}]) = \int_{S_0}\Big[2\gamma'\Big(((\mathbf{d}\cdot\nabla)|\Psi|)((\mathbf{v}_L\cdot\nabla)|\Psi|) - ((\mathbf{d}\cdot\nabla)\chi)2e\Phi|\Psi|^2\Big)$$

$$+ 2\gamma''\Big(((\mathbf{d}\cdot\nabla)|\Psi|)2e\Phi|\Psi| + ((\mathbf{d}\cdot\nabla\chi)|\Psi|)((\mathbf{v}_L\cdot\nabla)|\Psi|)\Big)\Big]dS \qquad (1.29)$$

For $H << H_{c2}$ one can consider a single vortex. Let us introduce the cylindrical coordinate frame (ρ, φ, z) with the z-axis along the vortex. The magnitude of the order parameter $|\Psi|$ is a function of the distance from the vortex axis ρ, and its phase is just the azimuthal angle $\chi = \varphi$. For a large κ, the gauge invariant vector potential is $Q = (0, -c/2e\rho, 0)$. Moreover, the estimates show that the normal-state contribution to the Hall current originating from Eq. (1.22) contains additional powers of both $1/\kappa$ and $(1 - T/T_c)$ as compared to the traction term. Therefore one can neglect the term with σ_n^H in Eq. (1.28). If

$$|\Psi| = |\Psi_0| f(\rho) \tag{1.30}$$

where $|\Psi_0|$ is the equilibrium magnitude of the Ginzberg-Landau order parameter, and the normalized function f satisfies the equation

$$\xi^2\left(\frac{d^2 f}{d\rho^2} + \frac{1}{\rho}\frac{df}{d\rho} - \frac{f}{\rho^2}\right) + f - f^3 = 0 \tag{1.31}$$

with $f = 0$ at $\rho = 0$ and $f \to 1$ for $\rho = \infty$. Here ξ is the temperature-dependent coherence length. The gauge invariant scalar potential can be written as a sum of two terms, $\Phi = \Phi_0 + \Phi_1$, where

$$\Phi_0 = -(v_{L\varphi}/2e\xi)\,\mu_0(\rho), \qquad \Phi_1 = -\zeta(v_{L\rho}/2e\xi)\,\mu_1(\rho) \tag{1.32}$$

The function μ_0 satisfies the equation

$$\xi^2\left(\frac{d^2 f}{d\rho^2} + \frac{1}{\rho}\frac{df}{d\rho} - \frac{f}{\rho^2}\right)\mu_0 - u f \mu_0^2 = 0 \tag{1.33}$$

with the boundary conditions $\mu_0 = 0$ for $\rho \to \infty$ and $\mu_0 = \xi/\rho$ for $\rho \to 0$. Here $u = 8e^2\gamma'\xi^2|\Psi_0|^2/\sigma_n$ is the numerical factor equal to the ratio squared of ξ and the electron-field penetration length. For a weak pair breaking, $\tau_0 T_c >> 1$, the factor $u = 5.79$. For $\tau_0 T_c << 1$ (high concentration of magnetic impurities) $u = 12$. The term with Φ_0 is the

one which has been obtained earlier for purely dissipative flux flow. The new term μ_1 satisfies the equation

$$\xi^2\left(\frac{d^2f}{d\rho^2}+\frac{1}{\rho}\frac{df}{d\rho}-\frac{f}{\rho^2}\right)\mu_1-uf^2\mu_1=-u\xi f\frac{df}{d\rho} \tag{1.34}$$

with the boundary conditions $\mu_1 = 0$ for $\rho = 0$ and $\rho \to \infty$. Collecting all the terms in Eq. (1.29) it can be obtained

$$\mathbf{j}_{tr}=\frac{2\pi c}{|\phi_0|}\gamma'|\Psi_0|^2\left(\alpha[\mathbf{n}_H\times\mathbf{v}_L]+sign(e)\zeta\beta\mathbf{v}_L\right) \tag{1.35}$$

The sign of the charge carriers appears since the unit vector of the vortex circulation and the unit vector of the magnetic field $\mathbf{n}_H$ are coupled through $\mathbf{n}$ = sign(e)$\mathbf{n}_H$, the circulation of the phase being chosen in Eq. (14) for the positive charge. The constant α and β are

$$\alpha=\int_0^\infty\left(\rho\left(\frac{df}{d\rho}\right)^2+\frac{f^2\mu_0}{\xi}\right)d\rho \tag{1.36}$$

$$\beta=\int_0^\infty\left(\frac{1}{2}\left(1+\frac{\rho\mu_0}{\xi}\right)\frac{df^2}{d\rho}-\frac{f^2\mu_1}{\xi}\right)d\rho \tag{1.37}$$

From Eq. (1.16)

$$\mathbf{j}_{tr}=\sigma_f\mathbf{E}+\sigma_f^H\mathbf{E}\times\mathbf{n}_H \tag{1.38}$$

where

$$\sigma_f=\frac{\alpha u\sigma_n}{2}\left(\frac{H_{c2}}{B}\right) \tag{1.39}$$

is the well-known flux-flow conductivity and

$$\sigma_f^H=sign(e)\frac{\zeta\beta u\sigma_n}{2}\left(\frac{H_{c2}}{B}\right) \tag{1.40}$$

is the Hall conductivity in the flux-flow regime.

In the limit of high magnetic fields, $H_{c2} - H << H_{c2}$, one needs to solve the linearlized TDGL equation with $\phi = -E_x x - E_y y$. Assuming $A_y = Bx$, $A_x = 0$, one finds the solution within the first term in **E**:

$$\Psi = \sum_n C_n \exp\left[i(qn + 2eE_y t)(y + cE_x t/B)\right]$$
$$\times \exp\left[-\frac{1}{2\xi^2}\left(x - \frac{cE_y t}{B} - \frac{cqn}{2eB}\right)^2 + 2me\xi^2\gamma(iE_x - sign(e)E_y)\left(x - \frac{cqn}{2eB}\right)\right] \quad (1.41)$$

This solution describes a slightly modified vortex lattice moving with the velocity $\mathbf{v}_L = (eE_y/B; -cE_x/B)$. The order-parameter magnitude can be found from the nonlinear GL equation. The coefficient C_n correspond to the Abrikosov vortex lattice with the parameter $\beta_A \approx 1.16$. After calculating the averaged total current using Eqs. (1.22) and (1.38) with

$$\sigma_f = \sigma_n + 4e^2\xi^2\gamma'\left\langle|\Psi|^2\right\rangle = \sigma_n\left[1 + \frac{u}{2}\frac{H_{c2} - B}{\beta_A H_{c2}}\right] \quad (1.42)$$

$$\sigma_f^H = \sigma_n^H + sign(e)\sigma_n\left[\frac{\zeta u}{2}\frac{H_{c2} - B}{\beta_A H_{c2}}\right] \quad (1.43)$$

Let us calculate the imaginary part of the constant $\gamma = \gamma' + i\gamma''$ in the TDGL theory. It is well known that the TDGL equations can be derived microscopically only for gapless superconductors. For simplicity, let us consider the case of weak pair-braking, $\tau_0 T_c >> 1$, where τ_0 is a characteristic time for pair-braking time. It can be the spin-flip time, or the inelastic electron-phonon collision time. To be more specific, the pair-breaking by magnetic impurities is considered. It will be shown that the small correction γ'' is proportional to the energy derivative of the density of states at the Fermi level.

Within the BCS model of superconductivity, the equation for the order parameter has the form

$$\frac{\Delta_\omega(\mathbf{k})}{|g|} = \int F_{\varepsilon_+,\varepsilon_-}(\mathbf{p}_+,\mathbf{p}_-)\frac{d^3\mathbf{p}}{(2\pi)^3}\frac{d\varepsilon}{4\pi i} \tag{1.44}$$

where g is the BCS pairing interaction and $\varepsilon_\pm = \varepsilon \pm \omega/2$; $\mathbf{p}_\pm = \mathbf{p} \pm \mathbf{k}/2$. The total Green's function is

$$F_{\varepsilon_+,\varepsilon_-}(\mathbf{p}_+,\mathbf{p}_-) = \left[F^R_{\varepsilon_+,\varepsilon_-}(\mathbf{p}_+,\mathbf{p}_-) - F^A_{\varepsilon_+,\varepsilon_-}(\mathbf{p}_+,\mathbf{p}_-)\right]\tanh\left(\frac{\varepsilon}{2T}\right)$$
$$-\frac{\omega}{4T}\cosh^{-2}\left(\frac{\varepsilon}{2T}\right)\left[F^R_{\varepsilon_+,\varepsilon_-} + F^A_{\varepsilon_+,\varepsilon_-}\right] + F^{(a)}_{\varepsilon_+,\varepsilon_-}(\mathbf{p}_+,\mathbf{p}_-) \tag{1.45}$$

The so-called anomalous function $F^{(a)}$ is found from the Dyson equation. Expansion in Δ is made assuming $\Delta\tau_0 << 1$ and $\Delta/T_c << 1$. The regular functions are

$$F^{R(A)}_{\varepsilon_+,\varepsilon_-} = G_0^{R(A)}\tilde{\Delta}^{R(A)}_\omega \bar{G}_0^{R(A)} - \frac{1}{2}(\omega - 2e\phi)\tilde{\Delta}^{R(A)}_\omega \frac{\partial}{\partial\xi_p}\left[G_0^{R(A)}\bar{G}_0^{R(A)}\right] \tag{1.46}$$

plus third-order terms in Δ, where

$$\tilde{\Delta}^{R(A)} = \Delta\frac{\varepsilon \pm (i/2\tau)}{\varepsilon \pm (i/\tau_0)}$$

The function $G_0^{R(A)}$ are the Green's functions in the normal state:

$$G_0^{R(A)} = \frac{1}{\xi_p - \varepsilon \mu(i/2\tau)}, \qquad \bar{G}_0^{R(A)} = \frac{1}{\xi_p + \varepsilon \mu(i/2\tau)}$$

Here $\xi_p = \varepsilon_p - \varepsilon_F$, and ε_p is the quasiparticle spectrum while ε_F is the Fermi energy. Strictly speaking, the expression for $\tilde{\Delta}^{R(A)}$ has to be calculated including the corrections to the scattering process proportional to the derivative $\partial v/\partial\xi_p$, as well. However, in the limit of a weak pair-breaking, $\tau_0 T_c >> 1$, the scattering times drop out of the relaxation constant γ and one can neglect these corrections.

The impurity self-energies are

$$\sum_1 = \frac{1}{2\pi\nu(0)\tau_1}\int G^{(a)}(\mathbf{p}_+,\mathbf{p}_-)\frac{d^3\mathbf{p}}{(2\pi)^3}$$
$$\sum_2 = \frac{1}{2\pi\nu(0)\tau_2}\int F^{(a)}(\mathbf{p}_+,\mathbf{p}_-)\frac{d^3\mathbf{p}}{(2\pi)^3} \qquad (1.47)$$

The self-energies $\bar{\Sigma}_1$ and Σ_2^+ are obtained from Eq. (1.47) by replacing G and F with $\bar{G}$ and F^+, respectively. The scattering mean-free times define the spin-flip time $\tau_0^{-1} = (2\tau_1)^{-1} - (2\tau_2)^{-1}$.

After inserting the total Green's function in the form of Eq. (1.45) into Eq. (1.44), the ω-independent terms in the right-hand side of Eq. (1.45) give the variational derivative of the free energy respect to the order parameter, i.e., the usual Ginzberg-Landau part of Eq. (1.17). Within the first-order terms in Δ, the contribution to the total Green's function proportional to ω and ϕ is

$$F' = -\frac{\omega}{4\pi}\left(F^R + F^A\right)\cosh^{-2}\frac{\varepsilon}{2T} - \frac{\omega - 2e\phi}{2}\frac{\partial}{\partial\xi_p}\left(F^R - F^A\right)\tanh\frac{\varepsilon}{2T}$$
$$+\frac{\omega}{2T}G_0^R\Delta\bar{G}_0^A\cosh^{-2}\frac{\varepsilon}{2T} + G_0^R\Sigma_2\bar{G}_0^A + G_0^R\Sigma_1F^A + F^R\bar{\Sigma}_1\bar{G}_0^A \qquad (1.48)$$

Here one has to take only the first term in Eq. (1.46) for the function $F^{R(A)}$.

The self-energies Σ_1 and $\bar{\Sigma}$ are proportional to ϕ. Let us consider only the first term with $\partial\Delta/\partial t$ since ϕ appears in a gauge-invariant way. One has to calculate the integral

$$\int F'\frac{d^3\mathbf{p}}{(2\pi)^3} = \int F'\nu(\xi_p)d\xi_p\frac{d\Omega_\mathbf{p}}{4\pi}$$

The integral of the first term in Eq. (1.48) is always real. To find the imaginary

contribution to the relaxation constant, it is necessary to take into account the energy independence of the density of states $\nu(\xi_p)$. Since

$$\int G_0^R \overline{G}_0^A \nu(\xi_p) \frac{d\xi_p}{\pi i} = \frac{\partial \nu}{\partial \xi_p}$$

one has

$$\int F' \frac{d^3 p}{(2\pi)^3} \frac{d\varepsilon}{4\pi i} = -\nu(0) \frac{\partial \Delta}{\partial t} \left(\frac{\pi}{8T_c} - \frac{i}{2\nu(0)} \frac{\partial \nu(0)}{\partial \xi_p} \left(\frac{1+\lambda}{\lambda} \right) \right) \tag{1.49}$$

where $\lambda = |g| \nu(0)$ is the pairing constant. It appears due to the logarithmic divergence of the second term in Eq. (1.48). Comparing the two terms in the right-hand side of Eq. (1.49) one obtains the ratio of the imaginary and the real parts of γ:

$$\zeta \equiv -\frac{\gamma''}{\gamma'} = \frac{4T}{\pi \nu(0)} \left[\frac{\partial \nu(0)}{\partial \xi_p} \right] \left(\frac{1+\lambda}{\lambda} \right) \tag{1.50}$$

This model can be summarized as the following. The Hall conductivity (σ_{xy}) is decomposed into two terms:

$$\sigma_{xy} = \sigma_{xy}^n + \sigma_{xy}^f \tag{1.51}$$

where σ_{xy}^n is the contribution of the quasiparticles inside the vortex core and σ_{xy}^f is arising from the Magnus term due to vortex flow. Since the quasiparticle term σ_{xy}^n always has the same sign as in the normal state, sign reversal could occur when σ_{xy}^f has an opposite sign to σ_{xy}^n. The sign of σ_{xy}^f depends on the sign of ζ. Within the BCS pairing model, ζ is proportional to the energy derivative of the density of states averaged over the Fermi surface. Therefore, the Hall conductivity could be negative if quasiparticles have a positive derivative ($\partial \nu(0)/\partial \xi_p$) and vice versa.

1.3 Controversy in experimental investigation

1.3.1 Hall sign reversal

The Hall sign reversal has been observed in most HTSs but the details are system dependent. For example, $RBa_2Cu_3O_{7-\delta}$ (RBCO, R represents rare-earth) [3-9,12] and $La_{2-x}Sr_xCuO_4$ (La-214, $x \leq 0.2$) [24], which are relatively strong pinning systems, show only one sign reversal while in the weak pinning systems such as Bi-, Tl-based cuprates, two sign reversals have been observed [5,6,10,11]. This led one to suspect that the sign reversal is caused by extrinsic effects such as disorders of pinning [20]. According to the WDT model, ρ_{xy}, $\tan\theta_H$ ($= \rho_{xy}/\rho_{xx}$) or $\sigma_{xy}(\cong \rho_{xy}/\rho_{xx}^2)$ are expected to be more negative as the pinning strength is increased, which therefore makes the sign reversal more pronounced.

Experimental investigations of this model have been conducted by either increasing pinning in weak-pinning HTSs to suppress the second sign reversal, or by decreasing pinning in strong pinning HTSs to reveal the second sign reversal. The results, however, were inconsistent and thus inconclusive. Budhani *et al.* [10] observed on $Tl_2Ba_2Ca_2Cu_3O_{10-\delta}$ (Tl-2223) films that both sign reversals were diminished with increasing concentration of columnar defects produced by 276 *MeV* silver ions. Their results contradict the WDT model, but indicate that pinning is relevant to the Hall sign reversal. It should be noticed, however, that even though the disappearance of the second sign reversal is expected from theory [19], the first sign reversal occurring near T_c in the flux flow region should not be affected by pinning. Considering a significantly low $T_c \sim 105$ K (compared to the bulk value of 125 K) for their Tl-2223 film, the high-T behavior of resistivity could possibly be dominated by degradation of the weak links across grain boundaries during the ion-beam irradiation. Samoilov *et al.* [26] studied the Hall effect on $Tl_2Ba_2CaCu_2O_{8-\delta}$ (Tl-2212) thin films and YBCO single crystals. By comparing ρ_{xy} before and after a 2 Tesla dose (i.e., 10^{11} ions/cm^2) of columnar defects were introduced into the sample they

reported that the first sign reversal was unaffected by the increased pinning while the second (in Tl-2212) was shifted towards higher T, instead of being diminished. Ideally, the second Hall sign reversal may be observable in single-crystal YBCO where pinning is negligible. The small crystal dimensions, however, prohibits accurate measurements of Hall effect when the signal becomes small near the resistive onset [26]. On the other hand, Kunchur *et al.* [25] used high pulsed current to suppress the pinning in YBCO thin films and found that the first sign reversal is even enhanced but the second sign reversal is still invisible. This finding suggests that pinning is not the mechanism for the first sign reversal that occurs immediately below T_c in YBCO. However, the results of these experiments do not necessarily exclude pinning as a possible mechanism for the second sign reversal in Bi-, Tl- and Hg-based HTSs since in none of them the pinning effective region can be clearly identified in the H-T phase diagram. Furthermore, the question of whether or not the observed number of the sign reversal in different systems is an intrinsic property of the material remains unanswered.

1.3.2 Scaling behavior and Hall conductivity

The puzzling scaling behavior as a form of $\rho_{xy} \sim \rho_{xx}^{\beta}$ has also been observed in most HTSs, but with different exponent β for different systems. There exist two controversial theories which seem to be successful in explaining the observed experimental results. Since the scaling behavior is usually observed near the onset of resistivity where pinning is quite effective, the WDT model [20] predicts the different scaling exponent ranging from 1.5 to 2, depending on the pinning strength. On the other hand, the VGFB model [19] concludes that β should be ~ 2 in the regimes of flux flow, thermally assisted flux flow (TAFF) and vortex glass behavior (creep), regardless of the type of defects. For the weak pinning systems, both models agree that β should be ~ 2, and the experimental results observed in the $Bi_2Sr_2CaCu_2O_8$ (Bi-2212) and $Tl_2Ba_2CaCu_2O_8$ (Tl-2212) [10,11,26] are consistent with this prediction.

On the other hand, the results in relatively strong pinning systems contradict each other, so which model gives the correct mechanism of the scaling behavior remains controversial. In the YBCO system, β has been observed in the range of 1.5 to 1.7 [9,12] which seems to be consistent with the WDT model. In addition, for YBCO/PBCO superlattices [27] and Hg-1212 films [13], magnetic field dependent β has been observed. It has been found that in the stronger field, the larger β due to weaker pinning, which also supports this model. On the other hand, in the strongly pinned system of heavy ion irradiated TBCCO films, β has been found as ~ 1.85 [10], which is rather closer to the VFGB model than the WDT model.

Since σ_{xy} can be expressed as $\sigma_{xy} \equiv \rho_{xy}/(\rho_{xx}^2 + \rho_{xy}^2) \cong \rho_{xy}/\rho_{xx}^2$, another interesting question as to whether or not σ_{xy} depends on pinning of the system is automatically raised. Samoilov *et al.* [26] showed that σ_{xy} is nearly unchanged before and after columnar tracks were added by 5.6 GeV and 1 GeV *Pb* ion irradiation into YBCO crystal and Tl-2212 films, respectively, supporting the VGFB model. Almost the same experiment has been conducted on YBCO crystals with 740 MeV *Xe* and *Sn* ion irradiation by Kang *et al.* [12]. Interestingly, they have found that before and after irradiation σ_{xy} curves coincide at a high temperature region as in Ref. [26] and then diverge at a low temperature region near the onset of resistivity if σ_{xy} is plotted as a function of reduced temperature (T/T_c). This result is consistent with the WDT model.

Besides this controversy, Smith *et al.* [28] have reported that σ_{xy} is independent of pinning on the YBCO and α-Mo_3Si films where pinning is varied by different current densities. In contrary, a clearly pinning dependent σ_{xy} has been found from a study of angular dependence of σ_{xy} in ion-irradiated YBCO films [29].

1.3.3 Scaling laws of ρ_{xx}

Besides the two puzzling phenomena, special attention has been focused on the scaling law of ρ_{xx} since the dissipative flux motion is closely related to the flux pinning mechanism. Due to the considerably high thermal energy kT near the

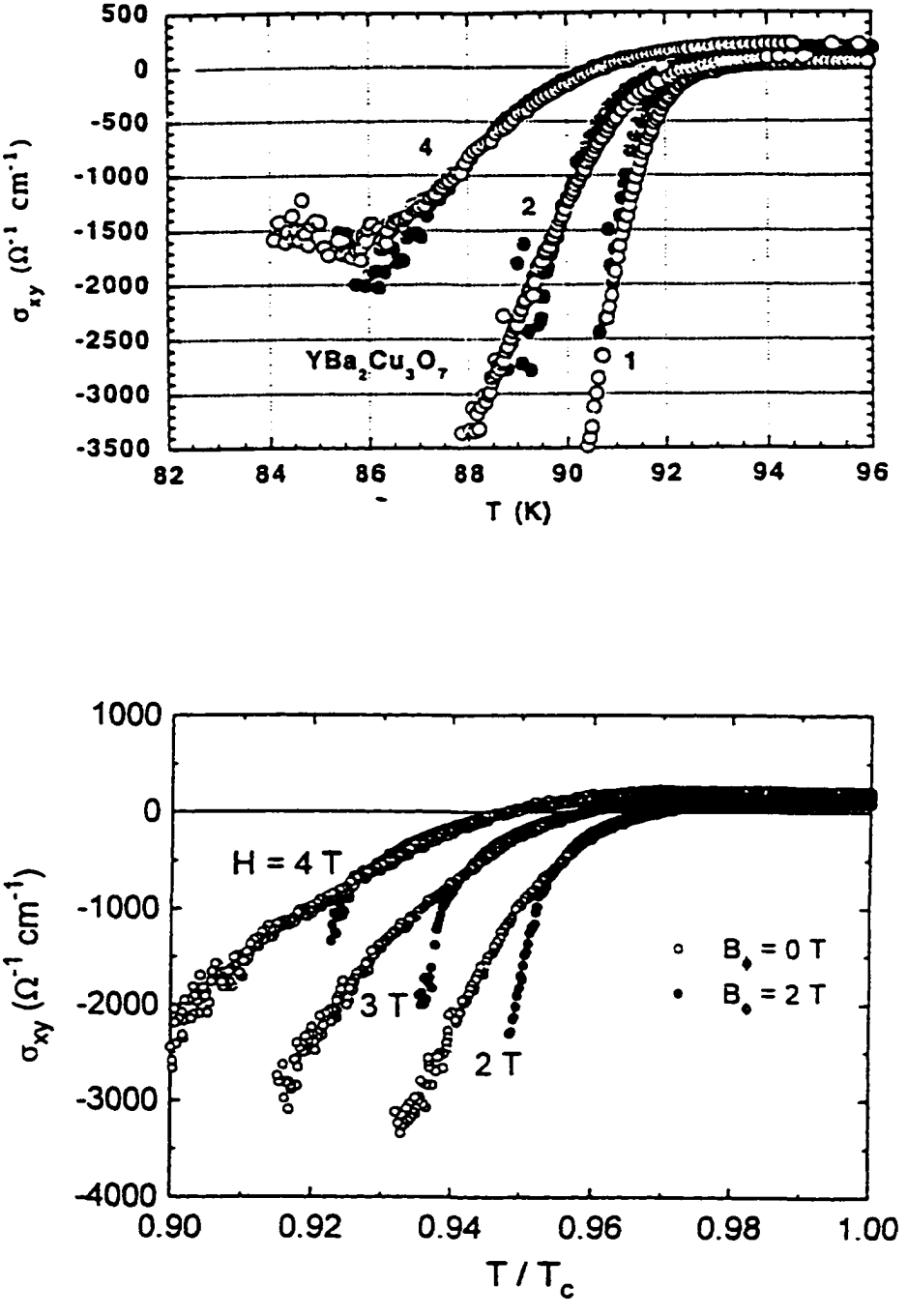

Fig. 1.3: (Top) Hall conductivity of $YBa_2Cu_3O_7$ crystals before and after irradiation dose of $B_\phi = 2$ T by Samoilov *et al.* [26]; (bottom) Almost the same measurement by Kang *et al.* [12].

superconducting transition of HTSs', thermally activated flux motion plays an important role during the onset of finite resistance in the superconducting mixed state. This thermally activated flux motion is generally expressed as $\rho_{xx} \sim \exp(-U_e / kT)$, therefore, the effective activation energy U_e, which measures the depth of the activation energy well, is a critical parameter for the interpretation of the thermally activated flux motion in the mixed state.

It is generally accepted that U_e scales as U_e (T, H) $\sim (1 - T/T_c)^m g(H)$ for HTSs, where $g(H)$ describes the field dependence. Different scaling laws, however, have been discovered for different HTS systems [5,7,30-33]. The YBCO system has been found to have m = 1.5 –1.8 and $g(H) = 1/H$ [7,30,31]. The same measurements on the Bi/Tl-2212 systems, however, revealed a different scaling behavior such as $m \sim 1.0$ and $g(H) = 1/\sqrt{H}$ [5,32,33]. One of the major discrepancies between YBCO and Bi/Tl-2212 is the dimensionality of the system which is inferred from the anisotropy of the electronic band structure. Since the dimensionality constrains the flux motion, it has been used as a key parameter to understand the observed different scaling behaviors in different HTSs. YBCO has been regarded as a three-dimensional-like (3D-like) system due to its small effective mass anisotropy $\{\gamma = \sqrt{m_c / m_{ab}} = 5.5$ [34]$\}$. On the other hand, Bi-2212 and Tl-2212 have been considered to be two-dimensional-like (2D-like) systems due to their much larger mass anisotropies such as $\gamma \sim 55 - 200$ [35] and $\gamma \sim 100 - 300$ [36], respectively.

Yeshurun and Malozmoff [37] and Tinkham [38] proposed a model for the less anisotropic YBCO system. They argued that for fields greater that $0.2H_{c2}$, the relevant correlation length which is perpendicular to the field becomes the flux line spacing a_0 due to collective pinning effect. U_e is, thus, scaled as $U_e \propto H_c^2 a_0^2 \xi_c \sim (1 - T/T_c)^{3/2} / H$, which is consistent with the experimental results of YBCO [30,31]. Nikolo *et al.* [33] use the same approach to explain the $(1 - T/T_c) / \sqrt{H}$ dependence of the 2D-like Tl-2212 system. According to their argument, the vortex length along the c-axis scales as a_0, the flux line spacing, at the low field and high temperature limit, and therefore vortex occupies a characteristic volume of $\xi^2 a_0$, where ξ is the

coherence length in the *ab*-plane. On the other hand, the model proposed by Geshkenbein *et al.* [39] and later extended by Vinokur *et al.* [40] associated the scaling behavior of the 2D-like Bi/Tl-2212 systems with the plastic deformation of the flux-line lattice at flux-line-lattice dislocations. They regarded U_e as the energy required to create a double-link configuration, which scales as $U_e \sim \phi_0^2 a_0 / \lambda^2 \propto (1 - T/T_c) / \sqrt{H}$ near T_c.

Previous observations imply that the scaling laws are related with the dimensionality of the system. Recall that the dimensionality here is defined based on the anisotropy of the material. However, recent studies on ultra thin YBCO films with a thickness of 24 – 200 Å, which is a 2D-like system, reveal a different scaling behavior from the above [41,42]. The exponent for the temperature scaling is $m = 1.0 - 1.2$ which is consistent with the Bi/Tl-2212 systems whereas $g(H) = -\ln H$ is different from the expected $1/\sqrt{H}$ law. These different results for different systems leave us a question as to what kind of scaling behavior a system with dimensionality between YBCO and Bi/Tl-2212 system would have.

1.4 Motivation

The discovery of HTSs has stimulated great interest in the vortex dynamics of these fascinating materials. Since the most important properties of HTSs, such as the critical current, are determined by vortex dynamics in the superconducting mixed state, the study of vortex dynamics has tremendous implications not only for fundamental research but also for potential applications of HTSs. Among many properties of HTSs, the mixed-state Hall effect provides very important information on vortex dynamics. Therefore, understanding the mixed-state Hall effect is of primary importance in understanding vortex dynamics of HTSs. Despite tremendous efforts both in experiment and theory devoted to this subject, the controversies of earlier studies motivate us to do a comprehensive study of the mixed-state Hall effect

of HTSs.

Several issues remain controversial in the study of the mixed-state Hall effect. Among them, three important issues will be addressed in this thesis: (1) mechanism of the Hall sign reversals, whether it is an intrinsic or an extrinsic property of HTSs; (2) how vortex dissipative state is modified by the presence of pinning; and (3) how the vortex dissipation is reflected in the scaling law of ρ_{xx} and ρ_{xy}.

The TDGL theory [21] suggests that the Hall sign is determined by the detailed electronic structure. Since electronic band structure can be perturbed by charge carrier doping, we measure the Hall effect in the samples with various charge doping levels in order to identify the mechanism of the Hall sign reversals. Anion (oxygen) doping is adopted because it may provide a change only in electronic band structure that is unlike cation doping used in earlier studies, and can be performed in the same sample, eliminating uncertainty from sample to sample. The Tl-2201 system is selected for this study since its charge carrier density can be continuously controlled from underdoped to overdoped regions by oxygen annealing. In addition, unlike the systems with one sign reversal that have been examined earlier, Tl-2201 has two sign reversals in the mixed-state, so that the mechanism of the two sign reversals can be probed.

In order to investigate the effect of pinning on the vortex dissipative mechanism, fine control of pinning is required. Two ways are adopted in our study: (1) selecting two systems which have intrinsically different pinning; and (2) increasing pinning of a system using ion beam irradiation. For the first case, Tl-2212 and Hg-1212 are selected as a weak pinning system and a moderate pinning system, respectively. For the second case, the pinning of Hg-1212 and Tl-2212 is tuned in a wide range by varying the concentration of the columnar defects generated by high-energy ion beam irradiation. We study the Hall effect on Hg-1212 as a function of columnar defects. This experiment is designed to examine if enhanced pinning can cover the appearance of the second sign reversal as in YBCO. In addition, the effect of pinning on the H-, T-dependence of $\tan\theta_H$ and σ_{xy} is examined quantitatively.

Fitting the experimental data with the microscopic TDGL model without considering the effect of pinning, will enable us to define the boundary between pinning effective and pinning ineffective regions. After identification of the two regions, the effect of pinning on the scaling behavior between ρ_{xy} and ρ_{xx} (or σ_{xy}) can be clarified by comparing σ_{xy} of samples with different pinning in the two regions.

The scaling law of ρ_{xx} is examined by measuring ρ_{xx} with sweeping magnetic field. This method is adopted because ρ_{xx} vs. H plot reflects the change in vortex dissipation mechanism as the inter-vortex spacing varies systematically by sweeping magnetic field, while ρ_{xx} vs. T plot, which has been conventionally used in earlier studies, does not. Comparative study of ρ_{xx} - H measurements on various HTSs ranging from weak pinning (Tl-2212), moderate pinning (Hg-1212) and strong pinning (Hg-1212 with columnar defects) system could provide a quantitative pinning dependence of the scaling law of ρ_{xx}.

In chapter 2, a general introduction for the Hall effect measurement in a normal metal and in a high-T_c superconductor is described. The two different fabrication processes of Hg-1212 thin films are also described. In addition, a description is given of an experimental set up used for the Hall measurement. In chapter 3, we investigated the doping dependence of the Hall sign reversal on $Tl_2Ba_2CuO_{6+\delta}$ thin films with anion doping. In chapter 4, the effect of pinning the Hall sign reversals is studied in Hg-1212 thin films with various pinning tuned by heavy ion irradiation. In chapter 5, we examine the scaling law of ρ_{xx} in systems with various pinning. Based on the different behavior in ρ_{xx}, the vortex-liquid phase is distinguished into two phases and the characteristics of these phases are studied. The T- and H-dependence of tan θ_H and σ_{xy} in the two phases are compared in chapter 6. In chapter 7, the pinning dependence of σ_{xy} in the two regions is examined in Tl-2212 and Hg-1212 with columnar defects. Chapter 8 contains summary of conclusions and future experiment proposal is presented in chapter 9.

Chapter 2

Measurement of Hall Effect

2.1 Hall effect in normal metal

The Hall effect employs crossed electric and magnetic fields to obtain information on the sign and mobility of the charge carriers. The experimental

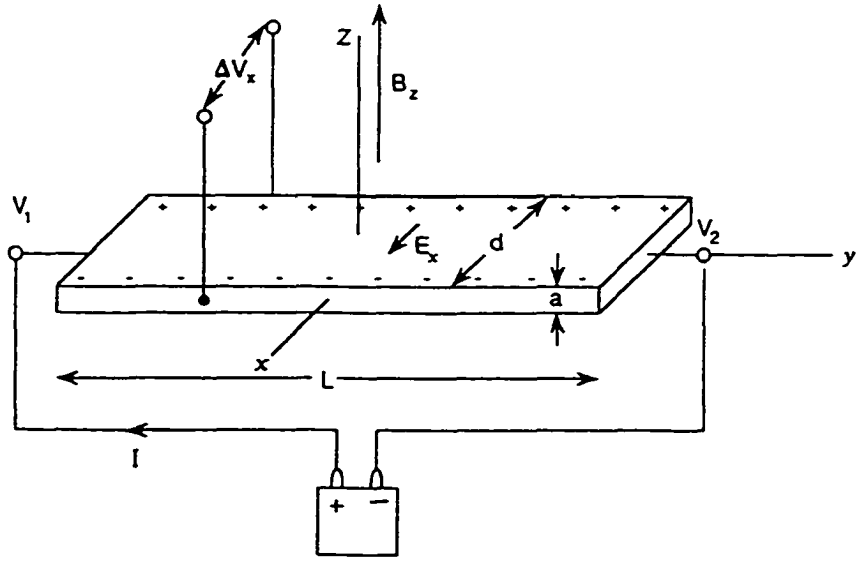

Fig. 2.1: Experimental arrangement for Hall effect measurements. The figure is drawn for negative charge carriers (electrons).

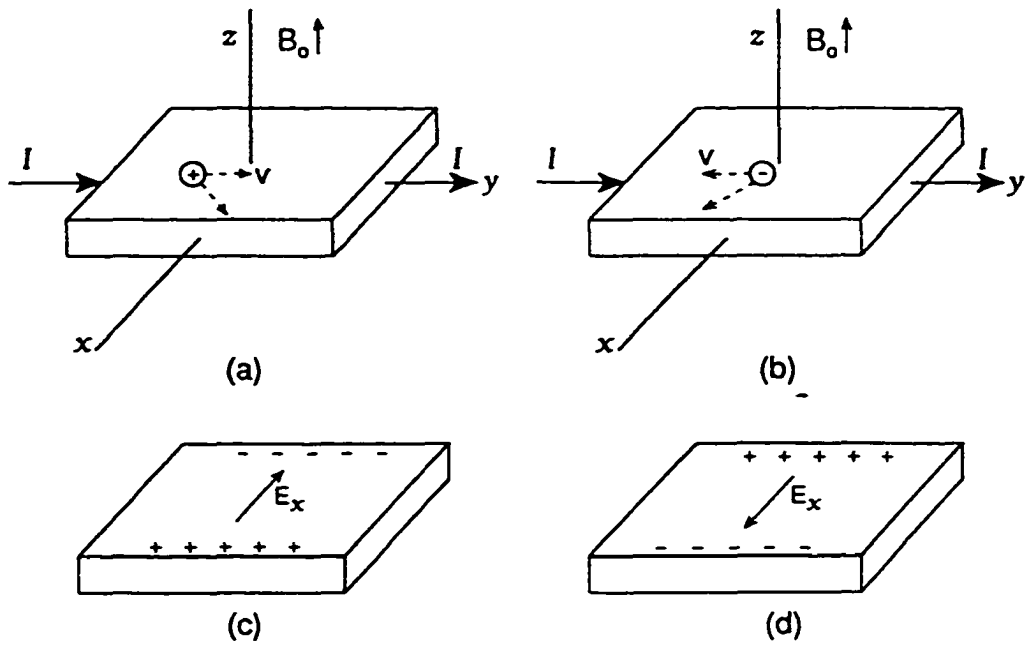

Fig. 2.2: Charge carrier motion and transverse electric field direction for the Hall effect experimental arrangement of Fig. 2.1. Positive charge carriers deflect as indicated in (a) and produce the transverse electric field E_x shown in (c). The corresponding deflection and resulting electric field for negative charge carries are sketched in (b) and (d), respectively.

arrangement illustrated in Fig. 2.1 shows a magnetic field B_0 applies in the z-direction perpendicular to a slab and a battery that establishes an electric field E_y in the y-direction that causes a current $I = JA$ to flow, where $J = nev$ is the current density. The Lorentz force

$$\mathbf{F} = q\mathbf{v} \times \mathbf{B}_0 \tag{2.1}$$

of the magnetic field on each moving charge q is in the positive x-direction for both positive and negative charge carriers, as shown in Fig. 2.2(a) and 2.2(b), respectively. This causes a charge separation to build up on the sides of the plate, which produces an electric field E_x perpendicular to the directions of the current (y) and magnetic fields (z). The induced electric field is in the negative x-direction for positive q, and in

the positive x-direction for negative q, as shown in Figs. 2.2(c) and 2.2(d), respectively. After the charge separation has built up, the electric force $q\mathbf{E}_x$ balances the magnetic force $q\mathbf{v} \times \mathbf{B}_0$,

$$q\mathbf{E}_x = q\mathbf{v} \times \mathbf{B}_0 \tag{2.2}$$

and the charge carrier q proceed along the wire.

The Hall coefficient R_H is defined as a ratio,

$$R_H \equiv \frac{E_x}{J_y B_z} \tag{2.3}$$

Substituting the expressions for $\mathbf{J}$ and $\mathbf{E}_x$ from Eq. (2.2) in Eq. (2.3) we obtain for holes ($q = e$) and electrons ($q = -e$), respectively,

$$R_H = \frac{1}{ne} \qquad \text{(holes)}$$

$$R_H = -\frac{1}{ne} \qquad \text{(electrons)} \tag{2.4}$$

where the sign of R_H is determined by the sign of the charges. The Hall angle θ_H is defined by

$$\tan\theta_H = \frac{E_x}{E_y} \tag{2.5}$$

Sometimes the dimensionless Hall number is reported,

$$\text{Hall \#} = \frac{V_0}{R_H e} \tag{2.6}$$

where V_0 is the volume per chemical formula unit. Thus the Hall effect distinguishes electrons from holes, and when all of the charge carriers are the same this experiment provides the charge carrier density n. When both positive and negative charge carriers are present, partial (or total) cancellation of their Hall effect occurs.

The mobility μ is the charge carrier drift velocity per unit electric field,

$$\mu = \frac{|v_{av}|}{E} \tag{2.7}$$

and with the aid of Eqs. (2.1), (2.4) we can write

$$\mu_H = \frac{R_H}{\rho} = \frac{1}{ne\rho} \tag{2.8}$$

where the Hall mobility μ_H is the mobility determined by a Hall effect measurement. It is a valid measure of the mobility (2.7) if only one type of charge carrier is present.

By Ohm's law, the resistivity is the ratio of the applied electric field in the direction of current flow to the current density,

$$\rho = \frac{E_y}{J} \tag{2.9}$$

In the presence of a magnetic field, this expression is written as

$$\rho_m = \frac{E_y}{J} \tag{2.10}$$

where ρ_m is called the *transverse* magnetoresistivity. There is also a *longitudinal* magnetoresistivity defined when E and B_0 are parallel. For the present case the resistivity does not depend of the applied field, so $\rho_m = \rho$. For very high magnetic fields ρ_m and ρ can be different, In the superconducting state ρ_m arises from the movement of quantized magnetic flux lines, so that it can be called the flux flow resistivity ρ_{ff}. Finally, the Hall effect resistivity ρ_{xy} is defined by [43]

$$\rho_{xy} \equiv \frac{E_x}{J_y} \tag{2.11}$$

2.2 Hall effect in high-T_c superconductor

The Hall effect provides information on the sign, concentration, and mobility of charge carriers in the normal state, with a positive sign for the Hall coefficient $R_H = E_x/JB_0 = \pm 1/ne$ of Eqs. (2.3) and (2.4) indicating that the majority carriers are

holes. In the superconducting state, the Hall voltage arises from the electric field induced by flux motion.

2.2.1 Normal-state Hall effect

The most important result that has been obtained from the Hall effect measurement above T_c is that the charge carriers in the copper-oxide planes of most of the high-temperature superconductors are holes. Included in this group are the La-, Y-, Bi-, Tl-, and Hg-based compounds. The major exception is compounds with the Nd_2CuO_4 structures and their charge carriers are electron-like.

It is easy to explain on the basis of chemical considerations as to why the La-, and Y-compounds are hole-like [44]. Replacing a La^{3+} by a Sr^{2+} without changing oxygen content can convert a Cu^{2+} to Cu^{3+} on one of the CuO_2 planes, which is the same thing as introducing a hole in a plane. The stoichiometric $YBa_2Cu_3O_7$ compound has an average *Cu* charge of 2.33, corresponding to one Cu^{3+} and two Cu^{2+} ions, so there is already one trivalent copper ion to contribute a hole. It has also been suggested that the hole might exist on oxygen, corresponding to the ion O^-. From a band structure viewpoint it can be said that the hole is in an oxygen $2p$ band.

In contrast, an electron superconductor can be created by doping with a cation having a higher carrier, such as substituting Ce^{4+} for Nd^{3+} in $(Nd_{1-x}Ce_x)_2CuO_4$, or substituting a trivalent rare earth such as $R = Gd^{3+}$ for Ca^{2+} in the compound $TlCa_{1-x}R_xSr_2Cu_2O_7$ perhaps to convert Cu^{2+} to Cu^{+} or add an electron to the conduction band.

2.2.2 Mixed-state Hall effect

In type-II superconductors, in which most high-T_c superconductors belong to, an applied magnetic field B_{app} penetrates a superconductor in the mixed-state, $B_{c1} < B_{app} < B_{c2}$. Penetration occurs in the form of tubes, called vortices, which serve to

confine the flux. The highest field is in the core, which has a radius of superconducting coherence length ξ. The core is surrounded by a region of larger radius λ within which magnetic flux and screening currents flowing around the core are present together. The current density J_s of these shielding current decays with distance from the core in an approximately exponential manner.

When transport current flows in the presence of an applied magnetic field, the vortices arising from the field interact with the current. This interaction can lead to vortex motion and heat dissipation, and the result is a resistive term called flux-flow resistance. It is a type of magnetoresistance, and limits the achievable critical current in many samples.

When the Lorentz force $\mathbf{J} \times \Phi_0$ exceeds the pinning force F_p,

$$|\mathbf{J} \times \Phi_0| > F_p \tag{2.12}$$

where Φ_0 is the quantum of flux, the vortices move with the velocity $\mathbf{v}_\phi$ in accordance with the equation of motion

$$\mathbf{J} \times \Phi_0 - \alpha n_s e (\mathbf{v}_\phi \times \Phi_0) - \beta \mathbf{v}_\phi = m_\phi (d\mathbf{v}/dt) \tag{2.13}$$

where m_ϕ is the effective mass per unit length of the vortex. The vortex velocity is limited by the frictional drag force $\beta \mathbf{v}_\phi$, while the Magnus force $\alpha n_s e (\mathbf{v}_\phi \times \Phi_0)$ shifts the direction of this motion through an angle θ_ϕ away from the direction perpendicular to **J**, as shown in Fig. 2.3.

By Faraday's law, the motion of the vortices transverse to the current density induces a time-averaged macroscopic electric field **E**, which is given by

$$\mathbf{E} = -\mathbf{v}_\phi \times \mathbf{B}_{in} \tag{2.14}$$

as indicated in Fig. 2.3, where $\mathbf{B}_{in}$ is the average internal field due to the presence of the vortices. The component of this electric field E_y along the current flow direction $E_y = E \cos \theta_\phi$ shown in Fig. 2.4, produces a voltage drop along this direction. The other component of the induced electric field perpendicular to the direction of the

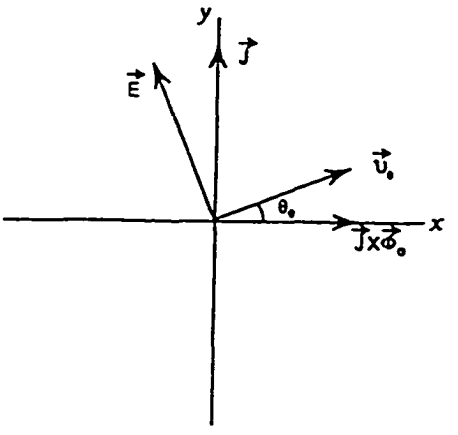

Fig. 2.3: Electric field E induced by the motion of a vortex Φ_0 moving a velocity υ_ϕ through an applied magnetic field B_{app} directed upward from the page. The vectors **E**, $\mathbf{v}_\phi$ and $\mathbf{B}_{app}$ are mutually perpendicular.

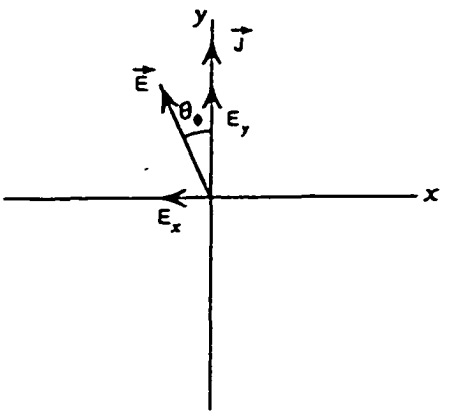

Fig. 2.4: Resolution of the induced electric field of Fig.2.3 into components transverse (E_x) and longitudinal (E_y) to the current density direction (**J**).

current, $E_x = E \sin\theta_\phi$, produces a Hall-effect voltage. The Hall resistivity ρ_{xy} defined by (2.11)

$$\rho_{xy} = E_x / J_y$$

is close to zero for very low applied fields in the mixed state below T_c and negative for intermediate fields. Thereafter, it becomes positive and increases linearly with further increases in field.

2.3 Experimental preparation

2.3.1 Film fabrication

In this thesis, various HTS thin films, such as $HgBa_2CaCu_2O_6$ (Hg-1212), $Tl_2Ba_2CaCu_2O_7$ (Tl-2212), and $Tl_2Ba_2CuO_6$ (Tl-2201), have been used for the Hall measurement. The fabrication process for Tl-2212 and Tl-2201 films are described in Ref. [45] and Ref. [46] in detail, respectively. In the following, the synthesis of Hg-1212 films is described. For the last few years, we have developed two different processes to obtain high quality Hg-1212 thin films: thermal-reaction process with fast temperature ramping annealing (FTRA) and newly developed cation-exchange process.

Thermal-reaction process with FTRA

It is well known that the Hg-based superconducting phases, like Tl-based superconducting phases, is formed through a solid/vapor reaction during annealing [47,48]. This reaction could happen in a carefully controlled Hg atmosphere at a precise temperature and O_2 partial pressure when a precursor sample is sealed in a quartz tube together with an unreacted stoichiometric pellet of Hg-based cuprates. The much more volatile nature of Hg-compounds than Tl-compound, however, has caused tremendous difficulty in fabrication of Hg-based cuprates thin films. For example, HgO decomposes at around 500 °C and Hg ion then reacts with Ca in the precursor to form an impurity phase $HgCaO_2$ which degrades the superconducting properties of the thin film significantly. As a result, poor reproducibility has been found in the existing two-step process used for fabrication of Hg-based cuprates thin films. Moreover, only $SrTiO_3$ substrates have been used previously for the growth of the Hg-based thin films because $SrTiO_3$ substrates are chemically stable in the presence of Hg-vapor while they have severe disadvantages of high cost, less availability with large size, and poor microwave properties. Even though high-quality films of other high-T_c superconductors have been obtained on $LaAlO_3$ substrates, which has much lower-cost, large size availability and excellent microwave properties, poor quality Hg-based thin films are obtained by using the same procedure as that for $SrTiO_3$ substrates [49]. A major reason is that the chemical stability of

$LaAlO_3$ is not as good as $SrTiO_3$ at high temperatures in the presence of Hg-vapor, so chemical reactions and interdiffusion near the film/substrate interface may seriously degrade the superconducting properties of the film.

A solution to the above problems is to reduce the period of high temperature Hg-vapor processing. In the conventional annealing process previously used for Hg-based cuprates, the sample temperature is increased slowly (4-6 hours) to the annealing temperature (780 - 860 °C) in order to maintain a phase equilibrium and the annealing temperature to form the superconducting phase. The slow heating thus makes the high temperature annealing above 500 °C unnecessarily long, worsening the problems of $CaHgO_2$ impurity formation, and film/substrate interface chemical reaction and interdiffusion. By adopting a FTRA process, considerable progress has been made. Instead of using a slow heating rate during the Hg-vapor annealing, the precursor films are brought to annealing temperature in a short period ranging from 1 minute to a few tens of minutes. The two problems mentioned above have been effectively reduced and high-quality Hg-1212 films can be fabricated reproducibly via the FTRA process.

The film fabrication process is composed of three steps: deposition of non-Hg-containing rare-earth copper precursor films, high temperature Hg-vapor annealing, and low temperature oxygen annealing. The precursor films were deposited at room temperature in a *rf* magnetron sputtering system. In our experiment, a stoichiometric target of composition $Ba_2CaCu_2O_x$ was used. Substrates were mounted in the on-axis configuration to the magnetron sputtering gun. The sputtering pressure of the *Ar* gas was 50 –70 *mTorr*.

The precursor films are amorphous and insulating and thus need to be annealed at high temperatures and controlled Hg-vapor pressure to form a superconducting phase. We encapsulated the precursor films together with bulk pellets into a quartz tube to achieve the Hg-vapor pressure, which is necessary for the superconducting Hg-1212 phase. Two bulk pellets were used: a non-Hg-containing rare-earth copper precursor ($Ba_2CaCu_2O_x$) pellet and a Hg-containing stoichiometric

pellet ($HgBa_2CaCu_2O_x$). The mass ratio of non-Hg-containing pellet to stoichiometric pellet is approximately 1 to 3. To increase local Hg-vapor pressure effectively, a precursor film is placed in close proximity to the Hg-containing stoichiometric pellet used as a Hg source. The sealed sample is then quickly heated with a rate of ~50 °C/*min* to 780 – 810 °C and kept at this temperature for period ranging from 30 minutes to 1 hour before being quenched with a cooling rate of 2.5 °C/*min*.

After high temperature Hg-vapor annealing, the samples are annealed between 300 – 400 °C with a slow heating rate (2.5 °C/*min*) in O_2 atmosphere in order to compensate possible O_2 deficiency of the samples when fast temperature ramping rate and short period of annealing is adopted.

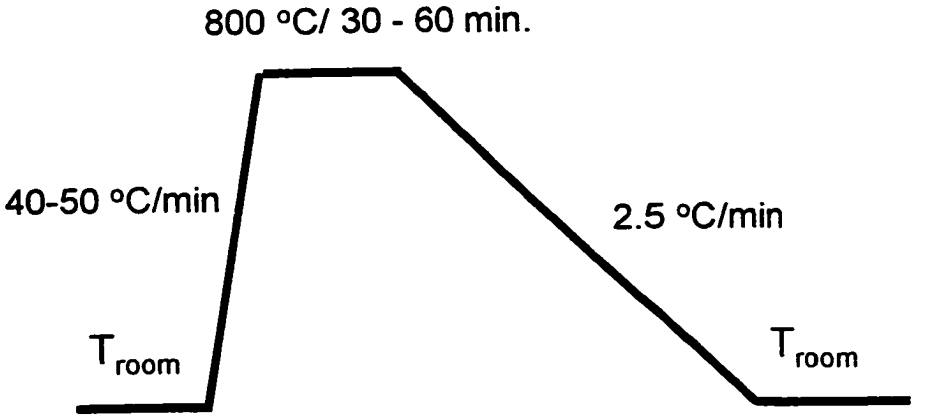

Fig. 2.5: Diagram of FRTA process

Cation-exchange process [49]

In conventional thermal-reaction process [50-54], a mixture of simple oxides of Hg, Ba, Ca, and Cu (precursor) is reacted at high temperatures of 750 – 860 °C, in controlled high Hg-vapor pressure of 5 – 10 atmospheres to form Hg-based HTSs. Even though high T_cs and high critical current densities (J_cs) on Hg-HTSs have been reported, there are technical difficulties in obtaining epitaxial growth of Hg-HTS thin films. First of all, it is nearly impossible to accurately control the processing parameters, such as Hg-vapor pressure due to the high volatile nature of the Hg-based compounds. This results in typically multiple superconducting phases plus significant amount of non-superconducting impurities in Hg-HTS samples, which substantially degrades the sample quality. Second, Hg vapor reacts with most metals as well as oxides, which prohibits epitaxial growth of Hg-HTS thin films on most technologically compatible substrates. Even on few chemically stable substrates such as $SrTiO_3$, serious film/substrates interface chemical diffusion was observed [54]. Consequently, most Hg-HTS films have to be made with fairly large thickness in the order of 1 μm and most of them are *c*-oriented uniaxial films with rough surface. Finally, the precursors are extremely sensitive to air. As short as a few second air exposure of the precursor may result in severely degraded samples. Even with special sample handling, such as the use of dry-box, sample reproducibility is poor which prevents any practical application of Hg-HTSs.

In order to circumvent these difficulties, we recently developed a novel cation-exchange technique, which is composed of two steps: selection of a precursor matrix with pre-designed structure and composition followed by cation-exchange processing. In the cation-exchange process, the precursor matrices are chosen to have a similar structure and composition to that of the target material and should have at least one weakly bonded cation to be replaced later by another cation to form the target material. When the weakly bonded cation is perturbed via different methods such as thermal heating of light/particle-beam irradiation, it will vibrate around the equilibrium site where the Gibbs free energy is minimized. The spatial deflection of

this cation is proportional to the energy of perturbation. When the threshold perturbation energy (U_{th}) is reached, at which the deflection of the original cation is comparable to the lattice constant, the precursor matrix may collapse due to escape of the cation. In the cation-exchange process, however, the perturbation energy is maintained to be close to but below U_{th} so that the precursor matrix is well kept while the original cation is slowly escaping. If the vapor of another cation is provided for replacement, the overwhelming population of this cation induces the replacement of the original cation with a new cation, and the target material is formed.

Based on this concept of the cation exchange, $TlBa_2CaCu_2O_7$ (Tl-1212) was selected as a matrix for $HgBa_2CaCu_2O_6$ (Hg-1212). Tl-1212 and Hg-1212 have nearly the same structure while Tl-1212 is much less volatile, insensitive to air, and thus easy to be grown epitaxially on many single-crystal substrates [39]. Tl-1212 is also a superconductor with its T_c ranging 90 – 94 K which is ~ 30 K lower than that of Hg-1212. Since the U_{th} for Tl-1212 is estimated to be 800 - 820 °C in air, the processing temperature for Tl/Hg exchange (T_{Hg}) was chosen slightly below 800 °C. The thickness of the precursor is in the range of 150 – 200 *nm*. Two bulk pellets, $HgBa_2CaCu_2O_x$ and $Ba_2CaCu_2O_x$ with the mass ratio 3:1 and total weight of 1.7 ~ 2.0 *g*, were sealed together with the precursor Tl-1212 film to control Hg-vapor pressure (P_{Hg}). Different P_{Hg}s were obtained by using different weights of HgO in the $HgBa_2CaCu_2O_x$ pellet while leaving the other ingredients unchanged. For all Hg-1212 samples, superconducting transition occurs at ~ 115 K, an increase of near 30 K over that of the precursor Tl-1212 film, indicating that Hg-1212 phase was formed through the Tl/Hg exchange. No second superconducting transition was observed on the Hg-1212 films, which implies that the remains of Tl-1212 phase are negligible under the processing condition used.

The precursor matrix may have a different structure from that of the target compound and may have more than one weakly-bonded cations to be replaced. One such example is the use of superconducting $Tl_2Ba_2CaCu_2O_8$ (Tl-2212) films as the matrices for Hg-1212 films. Tl-2212 has two identical Tl-O layers so that U_{th} ~ 785 –

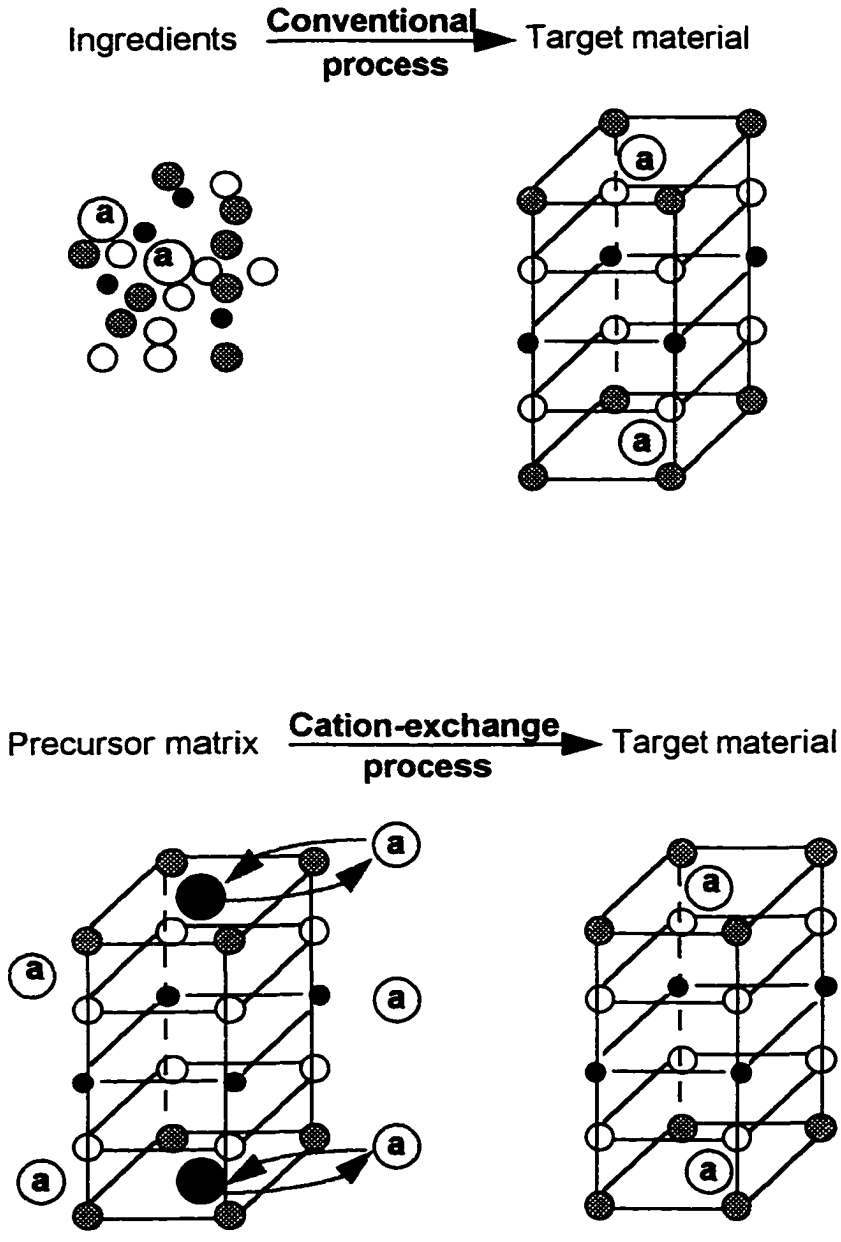

Fig. 2.6: Schematic diagram of (a) conventional thermal-reaction process; and (2) cation-exchange process

800 °C is assumed to be the same for the two *Tl* cations. Two films processed in different conditions, one at T_{Hg} = 700 °C for 12 hours and the other at T_{Hg} = 780 °C for 3 hours, show similar crystalline structures and superconducting properties indicating that the precursor Tl-2212 films were fully converted to Hg-1212 films in both cases. The XRD spectrum of the two precursor Tl-2212 films confirms that the Tl-2212 precursor film is *c*-axis oriented with a lattice constant of $c \sim 2.93$ *nm* while the resulting Hg-1212 films remain *c*-axis oriented but with a different lattice constant of $c \sim 1.27$ *nm*. This suggests that one unit cell of Tl-2212 splits into two unit cells of Hg-1212 during Tl/Hg exchange, accompanied by lattice shrink in c-axis by ~ 13 %. The measurement of film thickness with Rutherford back scattering (RBS) confirmed the reduction of film thickness from ~ 300 *nm* for the Tl-2212 precursor film to ~ 260 *nm* for the two Hg-1212 films. This yields 13.3 % thickness reduction, agreeing well with the XRD data.

The quality of the sample made in cation-exchange process is superior to that made in the conventional process. Hg-1212 thin films synthesized at optimized conditions are all nearly pure phase and show high T_cs of 120 - 124 *K* which are the same as the best reported for Hg-1212. Much higher J_cs, however, have been obtained on the films made by using cation exchange. These Hg-1212 films (with a thickness around 200 –300 *nm*) have their J_cs typically in the range of 1-2 MA/cm^2 at 100 K and self field. $J_c \sim 0.8$ MA/cm^2 at 110 *K* observed on the two films is nearly an order of magnitude higher than the best value previously reported on Hg-1212 thin films [56]. Such improvement on sample quality can be attributed to the high-quality epitaxy achieved on the films made in the cation-doping exchange process.

2.3.2 Experimental setup

. Fig. 2.7 shows the experimental set up used for measuring the Hall effect. A Keithly 220 current source produces an oscillating *dc* current to eliminate offset signals. Applied current is 1 – 4 *mA*, which can give a current density ranging 200 –

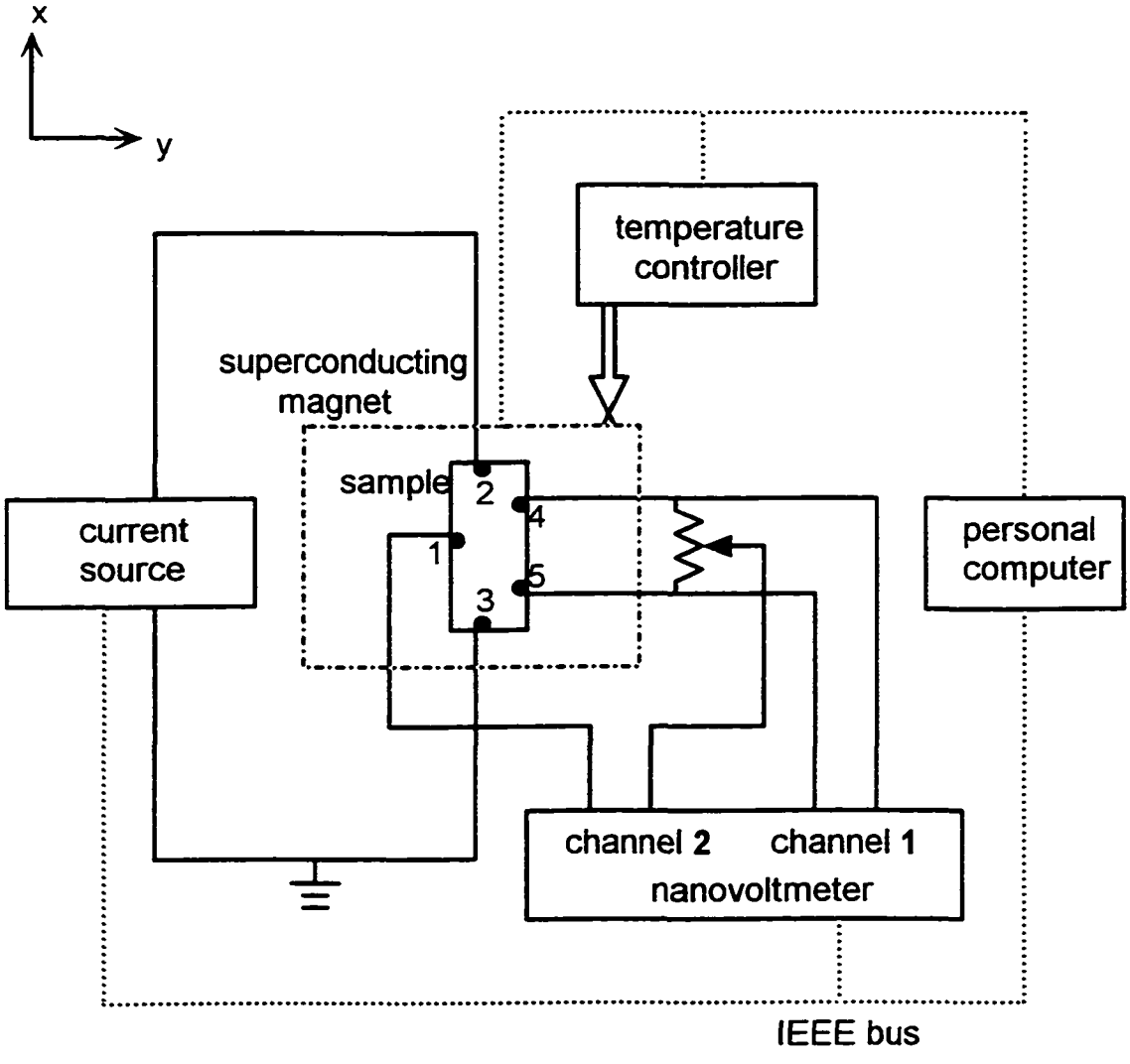

Fig. 2.7: Schematic diagram of the experimental setup used for the Hall effect measurements.

250 A/cm^2. Temperature is measured by a Lakeshore Cernox sensor placed at the top of the sample stage and in close proximity to the sample to probe the temperature of the sample as accurately as possible. The uncertainty of the Cernox sensor at temperature range from 20 to 300 K and in field up to 0 – 19 Tesla is less than 0.05 % and temperature is controlled by a Lakeshore DRC91CA temperature controller.

The longitudinal voltage (V_{xx}) is measured from the voltage drop of terminals 4 and 5, and Hall voltage (V_{xy}) is from the terminal 1 and the point between 4 and 5. A potentiometer finds an equipotential point of the terminal 1 in-between terminal 4 and 5 before a magnetic field is applied. In order to eliminate a temperature mismatch between the V_{xx} and V_{xy}, they are measured simultaneously by a Hewlett Packard HP34420A two-channel nanovoltmeter. The ρ_{xy} is calculated from the antisymmetric part of the V_{xy} under the magnetic field reversal. This measurement is conducted in a Janis 8 T superconducting magnet, in which a pair of split Helmholtz coils produces a magnetic field uniform to 0.1 % within a 1" spherical volume. A FW Bell BHT-921 cryogenic Hall sensor is installed in the sample stage with the surface of the sensor being parallel to an applied magnetic field to determine the magnetic field inside the magnet precisely.

The temperature controller, the current source, the nanovoltmeter, and the superconducting magnet power supply are controlled by a personal computer via IEEE-488 bus. The data acquisition is completely automated, enabling us to measure the V_{xx} and V_{xy} for many fields and temperatures at a fixed current density.

Chapter 3

Mechanism of Hall Sign Reversals

Since the first observation of the Hall sign reversal in YBCO [3], numerous models based on both intrinsic and extrinsic mechanisms have been proposed to explain this puzzling phenomenon. The experimental results [25,26], however, exclude pinning from a possible mechanism of the Hall sign reversals. This leads us to believe that the Hall sign reversal is an intrinsic property of HTSs in the mixed state. In order to prove this hypothesis, the relation between the Hall sign reversal and electronic band structure, which can be perturbed by charge carrier doping, is examined. In this chapter, we present the results of the Hall effect measurements on Tl-2201 films with different oxygen doping level.

3.1 Correlation between Hall sign reversal and electronic band structure

Recently, a phenomenological theory based on the time-dependent Ginzburg-Landau (TDGL) equation [21,22,57] and a microscopic theory [58] attracted much attention since they relate the Hall sign reversal directly to the electronic band structure. In the frame of these two theories, the Hall conductivity (σ_{xy}) is

decomposed into two terms such as $\sigma_{xy} = \sigma_{xy}^{n} + \sigma_{xy}^{f}$, where σ_{xy}^{n} is the contribution of the quasiparticles inside the vortex core. σ_{xy}^{f}, arising from the Magnus term due to vortex flow, is determined by the electronic band structure according to both TDGL [22,57] and microscopic theories [58]. Since σ_{xy}^{n} always has the same sign as in the normal state and is positive (hole-like) for HTSs, sign reversal could occur only when σ_{xy}^{f} is negative. Calculations from the TDGL equation [22,57] suggest that $\sigma_{xy}^{f} \sim \partial N(0)/\partial\mu$, where $N(0)$ is the density of states (DOS) at the Fermi surface and μ is the Fermi energy. Based on BCS theory, $\partial N(0)/\partial\mu$ is positive in the underdoped region, where the hole concentration (n_h) is below its optimal value (n_h^{opt}), and negative in the overdoped region where $n_h > n_h^{opt}$. Accordingly the Hall sign anomaly is expected only in the overdoped region. It should be noticed that the same conclusion was reached also by microscopic calculation. Aronov, Hikami and Larkin (AHL) [58] have shown that $\sigma_{xy}^{f} \sim \mathrm{sgn}(e)\partial\, lnT_c/\partial\, ln\mu$, where sgn($e$) is the sign of the carrier, namely "positive" for holes and "negative" for electrons. In the case of holes (electrons) as charge carriers, μ increases (decreases) monotonically with n_h in both the underdoped and overdoped region [59,60]. On the other hand, T_c shows a bell-shape dependence on n_h with its maximum (T_c^{opt}) staying at n_h^{opt}. Consequently, σ_{xy}^{f} is positive in the underdoped region and negative in the overdoped region. This implies that the Hall sign anomaly should occur only in the overdoped region, as concluded from the TDGL calculation, and it will be switched "off" as the charge carrier doping enters the underdoped region from the optimal doping level. In addition, both TDGL and microscopic calculations suggest a possible, complicated temperature dependence of σ_{xy}^{f}, which may result in more than one sign change in the Hall effect. In fact, *two* sign reversals have been observed in Bi-, Tl-, and Hg-based HTSs [5,6,10,12,26].

Examination of the theory requires measurements of the Hall effect when the electronic band structure of the superconductor is perturbed via charge carrier doping. The key point is to show that the Hall sign anomaly can be switched "on" and "off"

when the system is switched between underdoped and overdoped sides and the triggering point is near the n_h^{opt}. Two ways may be pursued to drive the system from the underdoped to the overdoped region: cation doping (ion substitution) or anion (oxygen) doping. Few experimental results were reported on the Hall effect of the overdoped samples due to low availability of overdoped HTS samples. Recently, Matsuda *et al.* [24] and Nagaoka *et al.* [61] studied the Hall effect in cation-doped $La_{2-x}Sr_xCuO_4$ (x = 0.1, 0.15, 0.2, 0.24 and 0.28) and $Y_{1-x}Ca_xBa_2Cu_3O_y$ (x = 0, 0.1, 0.2 and 0.4). Inconsistent with theory, the Hall sign anomaly was observed in underdoped, optimally-doped and partially in overdoped region. In other words, switching "on" or "off" of the Hall sign anomaly does not occur near n_h^{opt}. In fact, the Hall sign anomaly disappears only for the heavily overdoped samples ($T_c/T_c^{opt} < 0.7$). For sligthly overdoped samples with $T_c \sim 0.9\ T_c^{opt}$, the Hall anomaly has been found to be sample dependent. It should be mentioned that, unlike anion doping, cation doping has been found to cause additional effects on the electronic band structure besides the change in charge carrier density [62]. If these additional effects are responsible for the shift of the switching point from T_c^{opt} to $\sim 0.7\ T_c^{opt}$ on the overdoped side, anion doping will be more favorable since only the change in charge carrier density will be produced upon doping. In addition, anion doping can be performed on the same sample by annealing oxygen in or out, eliminating uncertainty from sample to sample typically seen in the cation doping case. In fact, anion doping has been attempted by Nagaoka *et al.* [61] on the $Bi_2Sr_2CuO_{6+\delta}$ (Bi-2201) system. They examined three samples, one with $T_c/T_c^{opt} = 0.6$ in the underdoped region and two overdoped samples with $T_c/T_c^{opt} = 0.57$ and 0.17, respectively. All of these doping levels are far from the n_h^{opt} value. Though it is similar to that for cation doping case, this result is inconclusive in terms of confirmation of the theory. In addition, since all the systems examined show only one sign reversal, the experimental test on the system with two sign reversals is necessary to explore the mechanism for both Hall sign reversals.

3.2 Experimental details

$Tl_2Ba_2CuO_{6+\delta}$ (Tl-2201) thin film is an ideal system for such a study. The T_c^{opt} is 83 K and T_c can be reduced continuously and reversibly close to 0 K in both underdoped and overdoped regions by changing the excess oxygen content δ in the range of 0 to 0.1 as shown in Fig. 3.1[63]. δ can be estimated from T_c values using a nearly linear relationship reported by Shimakawa *et al.* [62] and the optimum doping is realized at $\delta \approx 0.01$. The Hall measurements clearly demonstrate that the hole carriers are doped by the excess oxygen [64]. Unlike the systems previously studied in the cation doping cases, Tl-2201 shows *two* sign reversals. The study of the Hall effect on Tl-2201 thin films with different oxygen contents will allow investigation of (1) correlation between the Hall sign anomaly and the electronic band structure modified only via charge carrier concentration; and (2) the mechanism of the two Hall sign reversals. In this paper, we present the experimental study of the Hall effect on Tl-2201 thin films with different oxygen contents.

C-axis oriented Tl-2201 films with different oxygen contents (underdoped, optimally doped and overdoped) were prepared on $SrTiO_3$ (100) substrates by *rf* magnetron sputtering technique. The detailed fabrication process and the physical properties of the films are described elsewhere [48,65]. Briefly, four heavily overdoped films were fabricated in the same batch and then annealed in *Ar* for different periods to reach different δ's with two optimally doped, one underdoped and one overdoped. Mid-transition T_cs of the underdoped, optimally doped and overdoped samples were 81.4 K, 82 K and 71.5 K, and the estimated δ's are ≤ 0.01, 0.01 and ~ 0.025, respectively. For the underdoped and optimally doped samples, their T_cs are very close each other, though significantly different annealing conditions such as $485\ ^oC \times 8\ hrs.$ and $435\ ^oC \times 7\ hrs.$, were used, respectively. Since T_c is very sensitive to the oxygen level, it may be possible that these two samples are in nearly optimally doped region, one in slightly underdoped region and the other in slightly

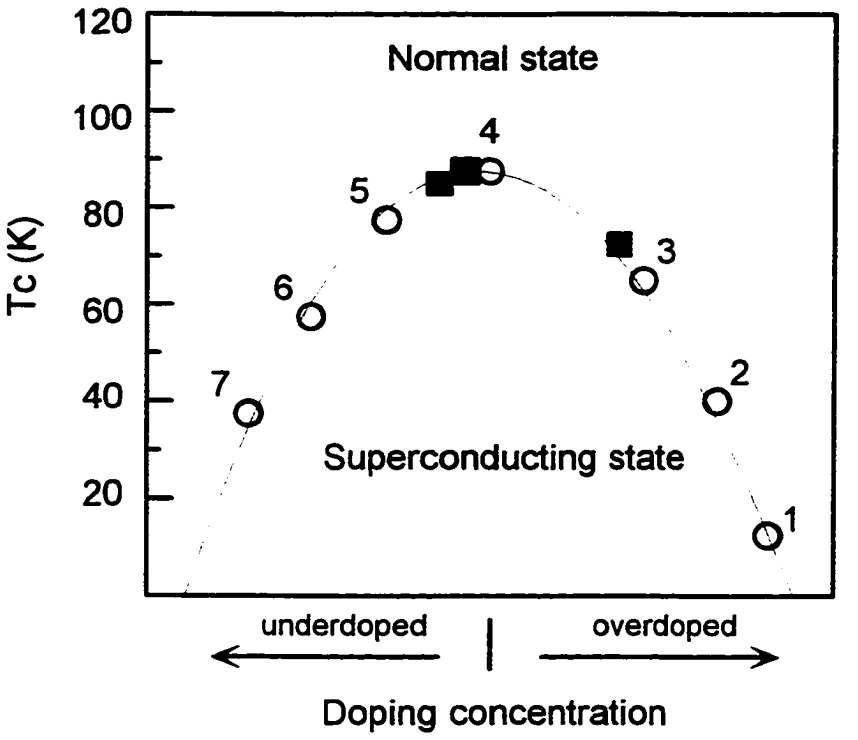

Fig. 3.1: Schematic phase diagram of Tl-2201 films as a function of doping concentration (Ref. [92]). The annealing temperature and time for each point are: 1 - as grown; 2 - 360 °C for 20 min; 3 - 360 °C for 40 min; 4 - 360 °C for 1 hour; 5 - 380 °C for 7 hr; 6 - 410 °C for 7 hr and 7 - 440 °C for 7 hr. The solid symbols indicate the samples used in this experiment.

overdoped region. We labeled the former "underdoped" and the latter "optimally doped" to distinguish these two results despite their close T_cs. These films of ~ 350 *nm* thickness have typical dimension of 5 x 10 mm^2. ρ_{xy} and the longitudinal resistivity (ρ_{xx}) were measured simultaneously by a two-channel nanovoltmeter (HP34420A) in an 8 *T* superconducting magnet system using the standard five-probe *dc* method. The magnetic field was applied parallel to the *c*-axis of the films, and ρ_{xy} was calculated from the antisymmetric part of the Hall voltage under the magnetic field reversal. The current density used for these measurements was ~ 240 A/cm^2.

3.3 Doping dependence of Hall sign reversals

Fig. 3.2 shows the temperature dependence of ρ_{xy} for the optimally doped sample. Two sign reversals can be clearly seen at the field of H = 1 T. At higher fields, a dip near T_c and a peak at lower temperature are observed as the trace of two sign reversals. The general pattern of ρ_{xy} observed in the optimally doped Tl-2201, including the two sign reversals and the temperature-dependence/field-dependence of ρ_{xy}, qualitatively resembles that for Bi-, Tl- and Hg-based cuprates previously reported [5,6,10,12,26]. The second sign reversal, however, can be

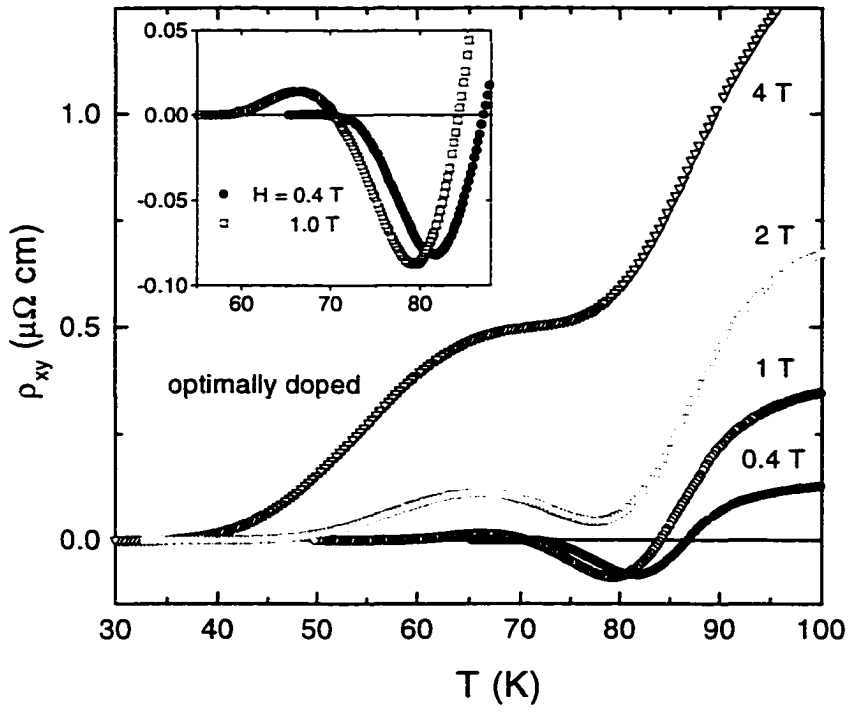

Fig. 3.2: The temperature dependence of ρ_{xy} for the optimally doped Tl-2201 sample at different magnetic fields. Two sign reversals are observed at H = 1 T. Inset: the magnified plot of ρ_{xy} vs. temperature at H = 0.4 T and 1.0 T, respectively. The second sign reversal is suppressed by relatively strong pinning at H = 0.4 T.

suppressed at very low field, as shown in the inset of Fig. 3.2 for $H = 0.4$ T. This can be explained by the fact that the pinning of the system at $H = 0.4$ T is much stronger than that at $H = 1$ T. Consequently, the second sign reversal is suppressed by pinning, as proposed by Vinokur *et al.* [19]. The first Hall sign reversal near T_c, however, remains at all the fields used up to 8 T.

In Fig. 3.3, the normalized ρ_{xy} is plotted as a function of the reduced temperature (T/T_c) for the underdoped, optimally doped and overdoped samples at $H = 1$ T. In order to compare ρ_{xy} for samples with difference in T_c, the figure is

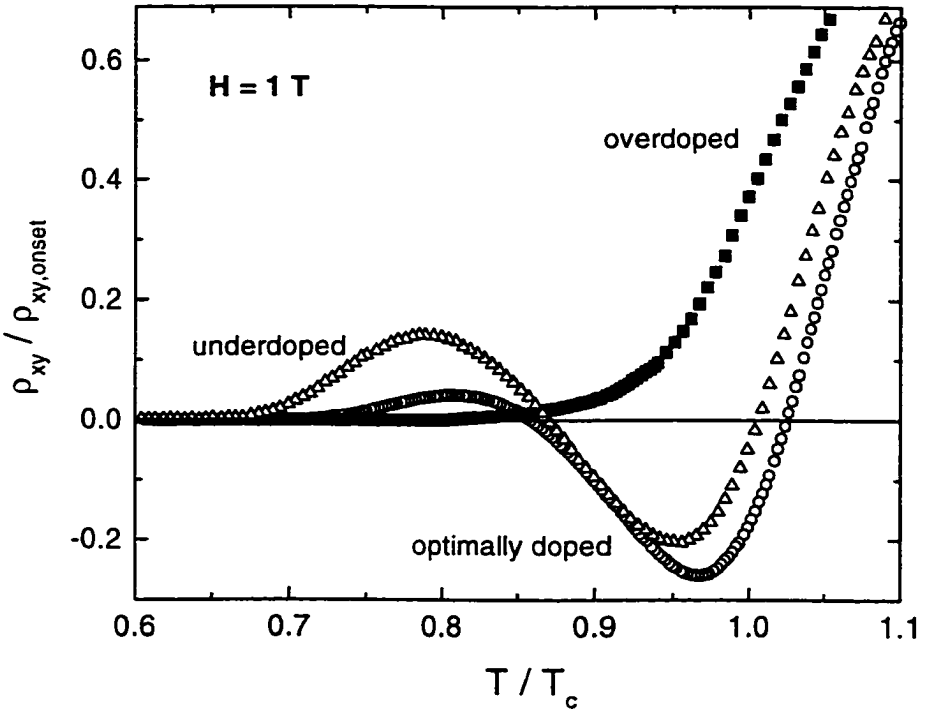

Fig. 3.3: The normalized ρ_{xy} vs. T/T_c for different oxygen levels at $H = 1$ T. Two sign reversals observed in the underdoped and optimally doped samples disappear in the overdoped sample.

presented in a function of the reduced temperature (T/T_c) rather than in a real temperature. Two sign reversals can be observed for both underdoped and optimally doped samples, but not for the overdoped sample. In other words, when the sample is overdoped, ρ_{xy} goes monotonically to zero with decreasing temperature without experiencing any sign change in the superconducting mixed state. This confirms experimentally, for the first time, that both two Hall sign reversals are determined by electronic band structure as suggested by the TDGL and microscopic theories. Moreover, since the underdoped and overdoped samples used for this experiment have T_cs very close to T_c^{opt} (T_c/T_c^{opt} is 0.99 for underdoped and 0.85 for overdoped), this experiment clearly shows that the Hall sign anomaly can be switched "on" or "off", depending on whether $n_h < n_h^{opt}$ or $n_h > n_h^{opt}$. This differs from the results in cation doping experiments where this boundary was shifted to the heavily doped region at $T_c/T_c^{opt} \sim 0.7$. As we argued earlier, this shift may be caused by the excess change in the electronic band structure in the cation doping case.

It should be pointed out that the occurrence of the Hall sign anomaly in the underdoped region disagrees with the prediction of the TDGL and microscopic theories, which would be otherwise successful in the interpretation of this experiment. This discrepancy between experiment and theory has also been recognized by Nagaoka *et al.* [61] and they attributed it to the failure of the simple *s*-wave weak coupling theory and suggested to consider the contribution of the vortex core in *d*-wave superconductors. However, it has been demonstrated [66] that from moderately clean systems to dirty systems, which most of the existing HTS systems are regarded as, the mechanism of vortex motion in a d-wave system remains qualitatively the same as that in an *s*-wave system. A simple d-wave consideration is thus not adequate to explain this discrepancy. It has been realized that the consideration of *s*-wave or *d*-wave causes a significant difference in the Hall effect in the superclean limit ($l/\xi >> \mu/\Delta$), but so far only "60 K" YBCO has been reported as a superclean *d*-wave superconductor [67] at $T \sim 0$ K and high applied magnetic field.

Based on cation and anion doping experiments for the systems with one sign reversal, it has been argued that the Hall sign is simply electron-like in the underdoped region and hole-like in the overdoped region [61]. Our experiment indicates that the electronic band structure in the superconducting state might be complicated. Since the Hall sign changes twice, it is electron-like at relatively high temperature (near T_c) and hole-like at lower temperature. As we argued earlier, two or more sign reversals may be a generic characteristic of HTSs. The Hall sign, therefore, may be either hole-like or electron-like in the underdoped region instead of being simply electron-like, suggesting a very complicated temperature/field dependence of the Fermi surface structure.

3.4 H-dependence of σ_{xy}

Examination of the field dependence of the σ_{xy} reveals further discrepancy between theory and experiment. According to the TDGL theory and the microscopic theory, $\sigma_{xy}(H)$ may be decomposed into three terms [21,22,68]; $\sigma_{xy}(H) = C_1/H + C_2 + C_3H$. The $1/H$ term from σ_{xy}^f dominates at low fields, while the H term from σ_{xy}^n dominates in high fields. The field-independent term is negligible for less anisotropic systems [12,69], but supersedes the third term for highly anisotropic systems [70]. The field dependence of σ_{xy} for different doping levels is plotted in Fig. 3.4 and the dashed line depicts the theoretical fitting. At relatively high fields, the data can be fitted well by the theory. In the low-field limit, however, there exists a threshold $H_k(T)$ below which the data deviate systematically from the fitting. The deviation of the data from the theory at $H < H_k$ may be caused by the effect of strong pinning since pinning is not considered in the theory.

The inconsistency of the TDGL and microscopic theories with experiment indicates that either significant modification for the current theory or development of

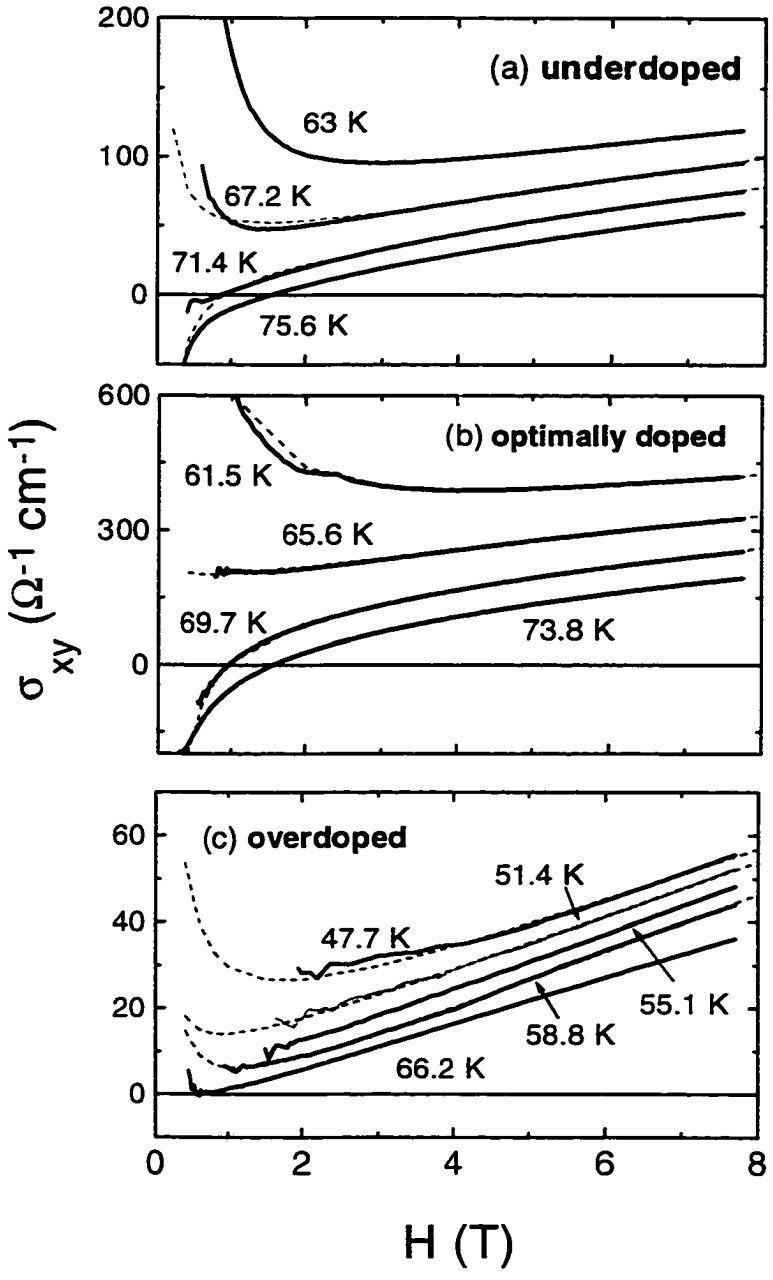

Fig. 3.4: The field dependence of σ_{xy} for different doping levels: (a) underdoped, (b) optimally doped and (c) overdoped samples. The dashed lines are the fits of the theory.

new theory is necessary to understand the Hall effect in the mixed state of HTSs. This experiment hence sets forth several criteria for the theory. First, the Hall sign anomaly is an intrinsic property of HTSs and is determined by electronic band structure. Second, the sign reversals occur only in the underdoped side and should be switched "off" when the system enters the overdoped region. Third, there is more than one sign reversal originating from the same mechanism. Fourth, the Hall sign may be either hole-like or electron-like in the superconducting state when the sample is underdoped.

Chapter 4

Effect of Pinning on Hall Sign Reversals

In the previous chapter, it is found that the two sign reversals observed in Tl-2201 films have the same mechanism and determined by electronic band structure. Since the observed number of the sign reversal in ρ_{xy} differs from system to system, for example, one sign reversal in strong pinning system such as YBCO and two sign reversals in moderate to weak pinning systems such as Bi-, Tl-, and Hg-based HTS cuprates, an immediate question is then what determines the appearance of the second sign reversal in ρ_{xy}.

Based on a phenomenological model, Vinokur *et al.* (VGFB) [19] proposed a general expression for ρ_{xy} in HTSs:

$$\rho_{xy} = \rho_{xx}^{2} f \tag{4.1}$$

where f is a function of T and ρ_{xy} changes sign when f changes sign. Even though the explicit form of f is unknown, f is predicted to be independent of pinning. In the vicinity of the resistive onset where pinning is effective, ρ_{xx} dominates the T-dependence of ρ_{xy} since f has a much weaker T-dependence in this region. Consequently, the features of f could be suppressed near the resistive onset. Considering that the resistive onset increases with pinning whereas f is pinning independent, it is thus suspected that the invisible second Hall sign reversal in a strong pinning system, such as YBCO, is due to a higher resistive onset in the system

[19].

Experimental investigations followed immediately by either increasing pinning in weak-pinning HTSs to suppress the second sign reversal [10,11,12,26], or by removing pinning in strong-pinning HTSs to uncover the second sign reversal [25,26]. The results, however, were inconsistent each other and thus inconclusive to confirm this model. In addition, these results cannot be used to exclude the existence of the second sign reversal since it is not clear where the transition from "pinned" to "unpinned" vortex phases occurs in the *H-T-J* phase diagram and whether the second sign reversal remains in the "pinned" region.

In chapter 3, it is observed that the theoretical fitting of σ_{xy} of Tl-2201 does not work below the threshold field $H_k(T)$, indicating that pinning is very effective in this region. Motivated by this result, we systematically studied the effect of pinning on the Hall sign reversals. In this chapter, the results of Hall measurement on Hg-1212 films while magnetic flux pinning is modified by addition of columnar defects are presented.

4.1 Experimental details

High-quality epitaxial *c*-axis oriented Hg-1212 films were prepared on (100) $SrTiO_3$ substrates by *rf* magnetron sputtering technique. The Hg-1212 films were fabricated by conventional thermal-reaction process with fast temperature ramping annealing (FTRA) as described in chapter 2 [49,54]. Three Hg-1212 films made from the same batch were used in this experiment. These films have T_c in the range of 123-124 *K*, with 2-3 *K* transition width in zero magnetic field and the zero-field critical current density at 77 *K* above $2x10^6$ A/cm^2. The films of about 800 *nm* thickness have atypical dimension of 6 x 4 mm^2. Five electrical contacts were made on each sample by sputtering about 100 *nm* thick *Ag* through a mask. The samples were then annealed at 350 °C for 20 minutes in flowing O_2 to insure low contact resistance. ρ_{xx} and ρ_{xy}

were measured simultaneously by a two-channel nanovoltmeter (HP34420A) in an 8 T superconducting magnet system using the standard five-probe *dc* method. The magnetic field was applied parallel to the *c*-axis of the Hg-1212 films.

Typical current density used for these measurements was ~ 250 A/cm^2. Before irradiation, one film was studied thoroughly for comparison with films irradiated by 5 *GeV* Xe-ion beam at the National Superconducting Cyclotron Laboratory at Michigan State University. The *Xe* beam was directed along the normal of the films which were kept at room temperature. No beam heating was expected. According to previous studies, linear tracks of amorphous and insulating material (columnar defects) were generated, which then act as the magnetic flux pinning centers. These columnar defects have diameter of ~ 6 - 10 *nm* and are parallel to the *c*-axis of the film. The irradiation doses were 0.5 x 10^{11}, 1.0 x 10^{11} and 1.5 x 10^{11} ions/cm^2. The numbers of defects thus generated are equivalent to the matching fields of B_ϕ = 1 T, 2 T and 3 T, respectively, assuming one flux quantum per columnar defect. No degradation of the sample was observed after the irradiation.

4.2 *H*-dependence of tan θ_H

Two Hall sign reversals can be observed in tan θ_H as shown in Fig. 4.1 on the pristine Hg-1212 films. The arrow $T_k(H)$ on each curve, shown as the solid circles in the inset of Fig. 4.1, divides the vortex-liquid phase into two regions where tan θ_H shows different behaviors. Above the arrow, tan θ_H is linearly proportional to H and below the arrow tan θ_H shows very complicated field dependence. The linear H-dependence of the Hall angle is a typical normal-state behavior. This suggests that pinning is negligible above $T_k(H)$.

Neglecting the effect of pinning, Dorsey [21] and Kopnin, Ivlev, and Kalasky (KIK) [22] calculated tan θ_H by means of the TDGL theory [71,72]. They found that tan θ_H can be decomposed into two terms:

$$\tan\theta_H(T, H) = \tan\theta_n(T, H) + \tan\theta_M(T) \qquad (4.2)$$

where $\tan\theta_n(T, H)$ is field-dependent and originates from the contribution of vortex normal cores and $\tan\theta_M(T)$ is the field-independent Magnus term. Since $\tan\theta_M(T) = 0$ in the normal state, $\tan\theta_n(T, H)$ can be obtained from the normal-state Hall effect measurement on Hg-1212, which suggests $\tan\theta_n(T, H) \sim AH/T^2$ [73]. In our experiment, $A = 39.5$ for the Hg-1212 thin film. Since the $\tan\theta_n(T, H)$ is positive for HTSs, the Hall sign reversal is due to $\tan\theta_M(T)$. In Fig. 4.2, $\tan\theta_M = \tan\theta_H - \tan\theta_n$ is plotted as function of T at different applied fields using the data in Fig. 4.1. Above T_c, $\tan\theta_M$ is zero as expected from the theory. Below T_c, $\tan\theta_M$ is negative at higher T's and swings to positive at $T \leq 108$K, corresponding to the two sign changes observed in $\tan\theta_H$. Above T_k, all $\tan\theta_M$ curves measured at different fields coincide, consistent with the KIK model [Eq. (4.2)]. Even though an explicit form for $\tan\theta_M$

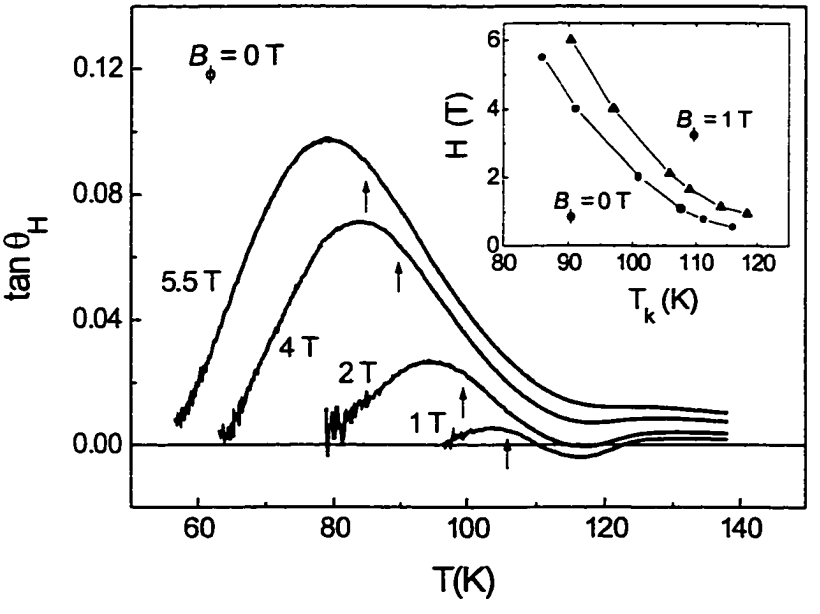

Fig. 4.1 Tan θ_H vs. T plots for Hg-1212 films at different magnetic fields. The inset shows H_k - T curves at $B_\phi = 0$ and 1 T, respectively.

(T) is yet available, this result confirms that the two Hall sign reversals have the same mechanism as observed in the anion doping study on Tl-2201 films [74]. Moreover, the result on Tl-2201 films also indicates, as predicted by the KIK model, that the Hall sign reversals are directly associated with the change of electronic band structure near the Fermi surface [22] and thus are an generic property of HTSs. More than two sign reversals, therefore, could be expected if band structure is modified by ion doping. Actually the third sign reversal has been observed in Zn-doped (0.4% and 0.6%) Bi-2212 films [75]. However, it is not clear yet whether this third sign reversal is caused by modified band structure or the formation of impurity phases due to doping. Further investigation is necessary to probe the details.

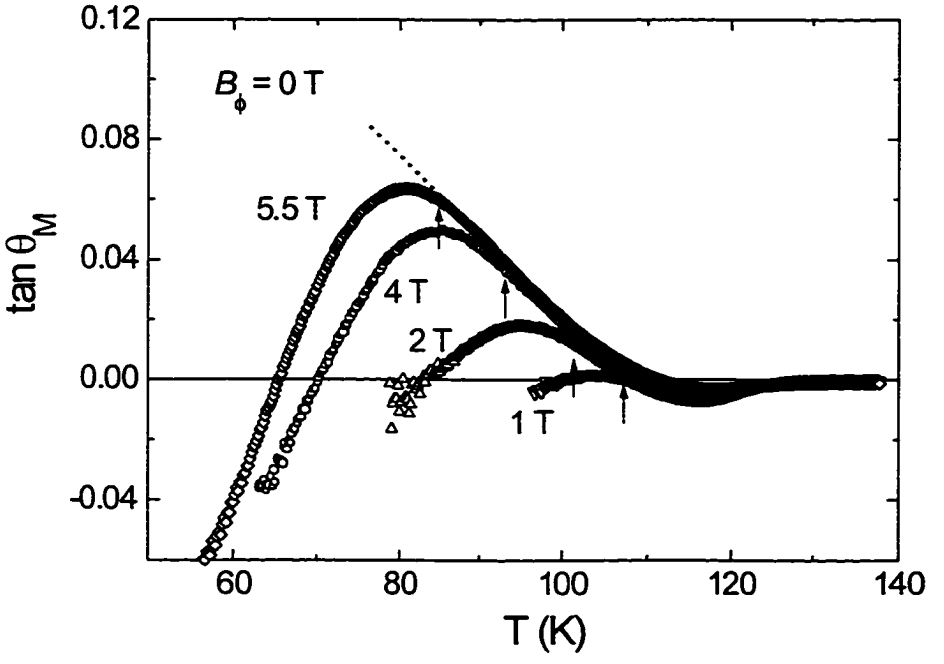

Fig. 4.2: Tan θ_M vs. T curves for a Hg-1212 film at different applied fields. The dashed line represents the field-independent part in tan θ_M.

Above T_k, tan θ_H has a linear H-dependence through the normal-core term tan θ_n. Near T_k (which is marked by the arrows in Fig. 4.2) the tan $\theta_M - T$ curve starts to deviate from the main trend indicating a nonlinear H-dependence of tan θ_H below $H - T_k$ where pinning sets in. It should be mentioned that fitting of experimental data with the KIK model was only attempted previously on YBCO films [25]. Tan θ_M (T) in YBCO was shown to be field independent near T_c, which agrees with our experiment. A complicate field dependence was observed in tan θ_M (T) at slightly lower temperatures in YBCO, which was not fully understood due to the lack of knowledge on flux motion.

4.3 Pinning dependence of Hall sign reversals

After the columnar defects are added to the sample, pinning is enhanced. Consequently, the $H - T_k$ curve is shifted to higher T and H (see the solid triangles in the inset of Fig. 4.1). If the second Hall sign reversal is not very far from T_k and if the applied field H is less than or comparable to the matching field B_ϕ, this shift could be so dramatic that the second sign reversal falls into the pinning effective region. Such an example can be found in Fig. 4.1 for tan θ_H - T at H = 1 T. The second Hall sign reversal occurs at $T \sim$ 110 K which is only 2-3 K above the T_k. After irradiation of B_ϕ = 1 T, the T_k was moved to ~ 117K as shown in Fig. 4.3. Even though the second sign change is still visible, the tan θ_H - T curve becomes fussy below T_k. Upon further increase of the pinning, for example at B_ϕ = 3 T, the second Hall sign reversal disappears (Fig. 4.4). In other words, sign reversals existing in the GL region could be diminished by pinning as predicted earlier by VGFB model [19]. On the other hand, the first Hall sign reversal and the ρ_{xy} - T curve above T_k are nearly unaffected by the pinning increase as shown in Fig. 4.4. This contradicts with the earlier results on Tl-2223 films [10] where both sign reversals disappeared when the pinning was increased. Our result, however, agrees well with others on YBCO and Tl-2212

[25,26]. Since the first sign reversal occurs near T_c where pinning is not important, other effects, such as degradation of weak links between superconducting grains during the ion beam irradiation, need to be considered. Furthermore, it is not difficult to see from Fig. 4.4 that the ρ_{xy} - T curve for Hg-1212 film with B_ϕ = 3 T looks the same as that for YBCO. One may argue that the second sign reversal is invisible in YBCO because of the strong intrinsic pinning in YBCO. Recently the second sign reversal is observed in YBCO films by suppressing pinning using high current densities of the order of 10^6 A/cm^2 [76]. This confirms our arguments that two (or more) Hall sign reversals are generic to most HTSs and the appearance of the sign reversals may be affected by pinning. On the other hand, the result of Ref. [76]

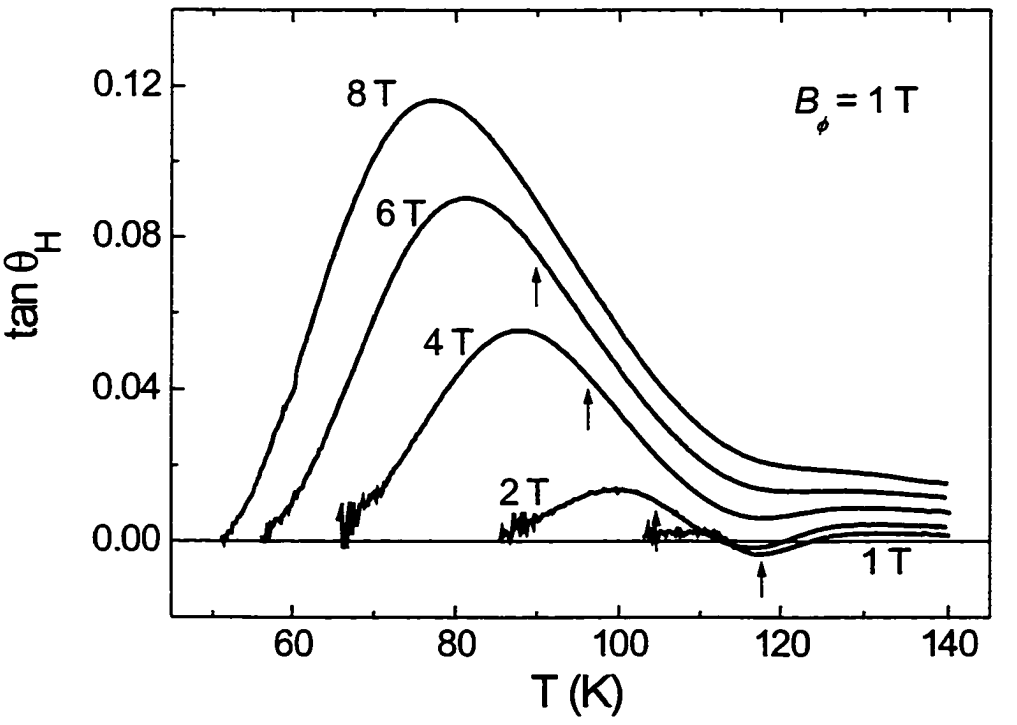

Fig. 4.3: Tan θ_H as function of T for Hg-1212 films after irradiated by 5 *GeV* Xe ions for B_ϕ = 1 T dose.

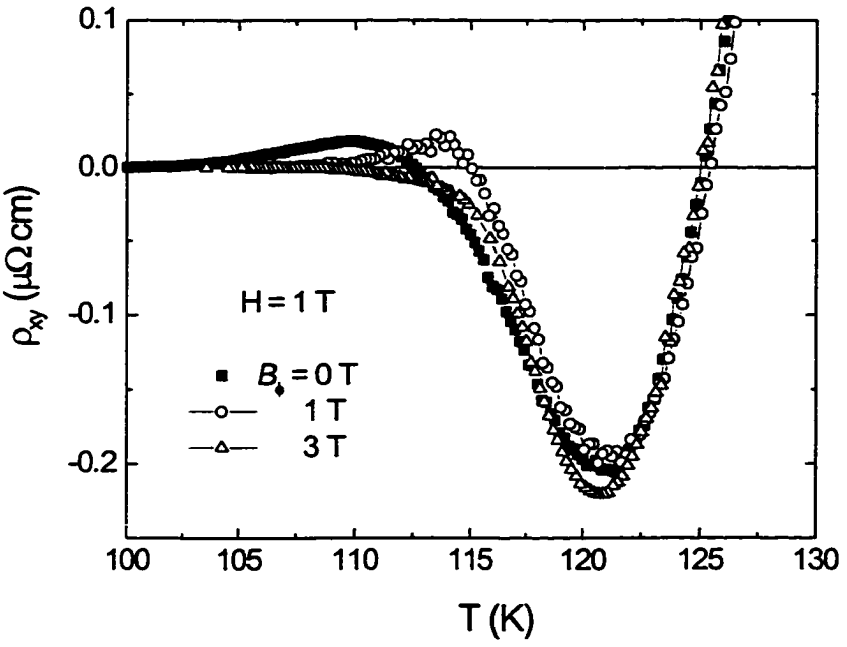

Fig. 4.4: ρ_{xy} as function of T for Hg-1212 films at different columnar defect concentrations of $B_\phi = 0$, 1 T and 3 T, respectively. The applied field is 1 T.

suggested that the Hall sign reversals might occur in the vortex-solid state, contrary to the current theories, which predict the Hall sign reversals occur only in the vortex-liquid region. From the studies on the Hall sign of Tl-2201 films [74], we have also found several discrepancies from the theories. Therefore, further investigations both in theory and experiment are necessary to clarify the existence of the Hall sign reversals in the vortex-solid state.

Chapter 5

Vortex-Liquid Phase Diagram

In chapter 3 and 4, it is observed that both in Tl-2201 and Hg-1212 systems, $\tan\theta_H$ and σ_{xy} fit well with the TDGL model only above the $H_k - T$ curve and deviate from the theoretical fitting below the $H_k - T$ curve. Since the effect of pinning is not considered in the TDGL model, this result suggests that in the vortex-liquid phase, there exists the region in which pinning is very significant. A thorough study of the vortex-liquid phase is thus necessary to understand the puzzling mixed-state Hall effect. In this chapter, we present a systematic study of the vortex-liquid phase diagram of HTS thin films.

5.1 Inter-vortex correlation in dirty superconductor

The observation of vortex lattice melting in "clean" or "pinning-free" high-T_c superconductors (HTSs) has stimulated an extensive investigation of the vortex phase diagram [77]. The key signature of the phase transition (melting) from vortex lattice to vortex liquid is a sharp drop in resistivity and magnetization combined with a hysteretic trace, suggesting a first-order phase transition across the melting line [78-84]. Theoretical support for the existence of such a first-order melting transition has been found in numerical simulations, showing a clear hysteretic behavior and finite

latent heat as the temperature is varied across the melting line [85].

The vortex phase diagram becomes much more complicated in superconductors with disorders, due to the existence of the magnetic flux pinning. On the vortex solid side, pinning randomizes the distribution of vortices, resulting in a vortex-glass phase in which the long-range order of the vortices is destroyed [86]. Since different types of disorder may affect the vortex system in a different way, it is not surprising to see different vortex-glass phases showing fine differences in their physical properties. For example, for a HTS with *correlated* disorders in the forms of twin boundaries, grain boundaries or columnar defects, Nelson and Vinokur [87] predict a new solid phase, "Bose-glass", at low temperatures with localized vortex lines and an infinite tilt modulus. Experimental support for the existence of this new phase has been reported by several groups on heavy-ion irradiated YBCO single crystals [88,89].

The vortex glass melts into a vortex liquid via a dramatically different route from that for a vortex-lattice. The nature of this transition is not yet fully understood. First of all, the signature of the first-order phase transition disappears. A high-order phase transition is hence suggested by a smooth transition in resistivity and magnetization [90], reported both on twinned [79] and electron irradiated untwinned YBCO crystals [81,82]. It is well known that vortices in the "clean" superconductor become completely uncorrelated upon melting as confirmed in strictly Ohmic *I-V* characteristics in the vortex liquid [79,91,92]. In the presence of pinning, however, this process may be different. For example, in twinned YBCO crystals and films, non-Ohmic behavior in longitudinal resistivity (ρ_{xx}), Hall resistivity (ρ_{xy}) and *I-V* characteristic have been reported by several groups [9,18,93,94]. This non-linear *I-V* characteristics in vortex liquid phase was attributed, in the vortex-glass (VG) model [86], to the coexistence of correlated and uncorrelated single vortices above the vortex glass-liquid transition (H_g-T). It is argued that when the applied current density (J) is below J_{th}, only single vortices could be driven to move, resulting in an Ohmic response. When $J \geq J_{th}$, the response becomes non-Ohmic due to the dissipation of

correlated vortices. Since this inter-vortex correlation is induced by pinning, a crossover from correlated to uncorrelated vortex-liquid phase is expected at higher field and temperature, at which pinning becomes ineffective. Questions are then raised as to where the crossover is, how it correlates with pinning, and to what extent the dissipation mechanisms differ in the two vortex-liquid states. The answers to such questions are of primary importance to the understanding of vortex dynamics in practical superconductors with strong pinning.

5.2 Experimental details

Measurement of ρ_{xx} and ρ_{xy} in a sweeping magnetic field is an effective way to probe the transition between a correlated and an uncorrelated vortex-liquid. In the correlated liquid, locally ordered vortex bundles may exist around the pinning site. The inter-vortex distance (a_0) in the bundles decreases monotonically as the applied field increases. On the transition line, the a_0 becomes comparable with the thermally induced vortex lateral displacement, resulting in complete destruction of the vortex ordering. In this chapter, I present experimental results of ρ_{xx} and ρ_{xy} measurements with sweeping magnetic fields. Several systems were chosen ranging from weak pinning (Tl-2212 film), moderate pinning (Hg-1212 films) and strong pinning (Hg-1212 films with columnar defects). This experiment allows a direct investigation on (1) the crossover from correlated to uncorrelated vortex-liquid state; (2) the correlation of such a crossover with pinning; and (3) dissipation mechanisms in both correlated and uncorrelated vortex liquids.

High-quality *c*-oriented $HgBa_2CaCu_2O_{6+\delta}$ (Hg-1212) and $Tl_2Ba_2CaCu_2O_{8-\delta}$ (Tl-2212) thin films were used for this experiment. The Hg-1212 films were fabricated by the recently developed cation-exchange method as described in chapter 2 [95]. The detailed fabrication process of Tl-2212 films has been described

elsewhere [47]. The films with 0.24-0.28 μm thickness were patterned using standard photolithography techniques to form 20-50 μm wide bridges. ρ_{xx} was measured using a standard four-probe configuration with a current of 1 μA, which gives a current density of about 8 and 25 A/cm^2 for Hg-1212 and Tl-2212 films, respectively. Magnetic field was applied along the c-axis of the samples in a 5.5 T SQUID magnetometer. The Hall measurement was performed only on Hg-1212 films. ρ_{xx} and ρ_{xy} were measured simultaneously by a two-channel nano-voltmeter (HP34420A) using a standard five-probe dc method. Typical current densities used for the Hall measurements were ~ 250 A/cm^2. Irradiation was conducted at the National Superconducting Cyclotron Laboratory at Michigan State University. Before the irradiation, one sample was studied thoroughly for comparison with films irradiated by 5 GeV Xe ions. The Xe-ion beam was directed along the c-axis so that the defects are parallel to the applied field. The irradiation dose was 5 x 10^{10} ions/cm^2 which are equivalent to the matching field of B_ϕ = 1 T, the field at which the density of vortices and defects are equal.

5.3 Scaling law of ρ_{xx}

Fig. 5.1 shows the field dependence of ρ_{xx} of Hg-1212 thin films at several temperatures below T_c. Since activated behavior is expected, ρ_{xx} is fitted by $\rho_{xx} \sim \exp(-U_e/T)$ with U_e representing activation energy. For most HTSs, $U_e(T, H) \sim U_0(1-T/T_c)^m H^{-a}$ is reported [5,7,30-33] with m ranging from 1.0 to 1.5 and a from 0.5 to 1.0 for YBCO [7,30,31] and Bi/Tl-compound [5,32,33], respectively. For Hg-1212 films, $m \cong 1.0$ and $a \cong 0.5$ were found in the field range of 0.05 T – 5 T. The scaling law of U_e is discussed in detail in chapter 6. By plotting log ρ_{xx} as a function of $1/\sqrt{H}$, the U_0 (which is proportional to the height of the activation energy barrier) can be

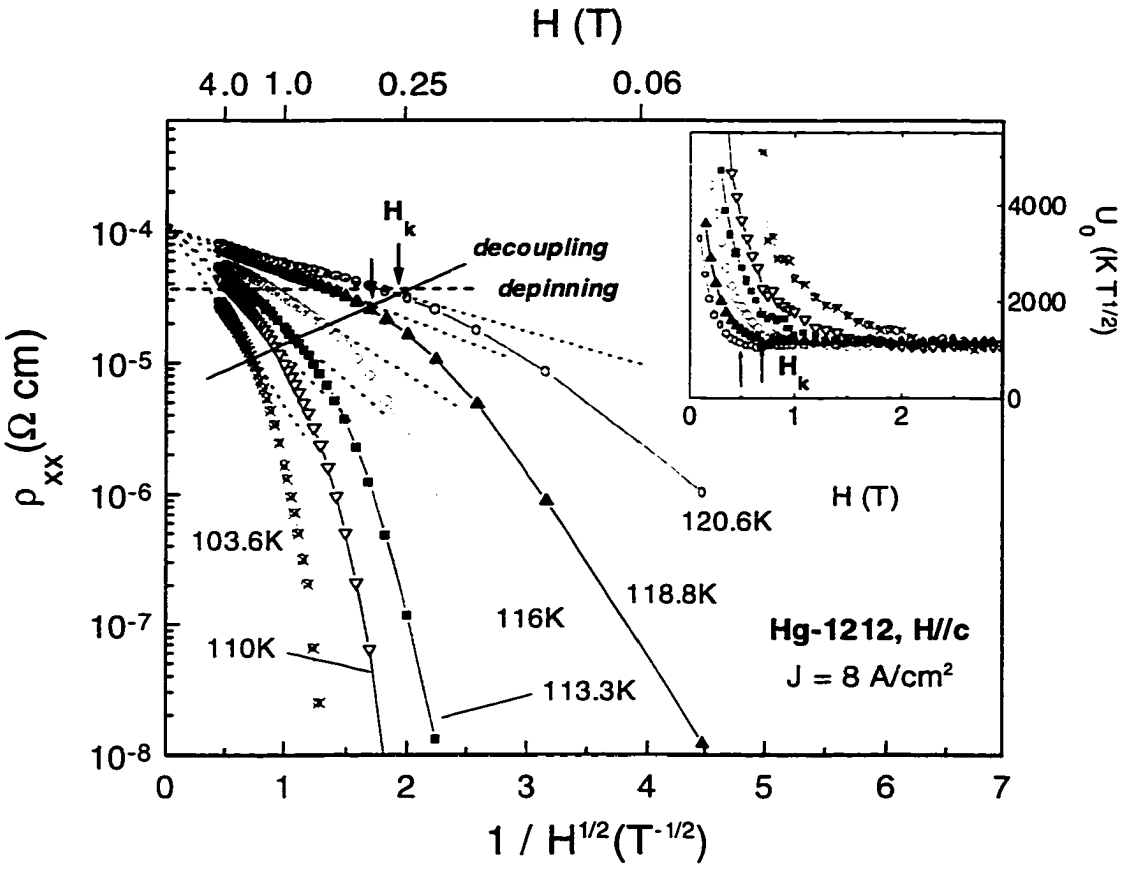

Fig. 5.1: log ρ_{xx} as a function of $1/\sqrt{H}$ for Hg-1212 films at different temperatures. The dotted lines are the fits of data at a high field region. The dashed line depicts the depinning line and the solid line is the H_k -T curve (decoupling line). Inset: U_0 vs. H plot at the same temperatures in the main panel.

obtained from the slope of the curve for each temperature. In Fig. 5.1, it is clearly shown that each curve consists of two parts separated by a kink (defined as H_k). U_0 shows dramatically different behaviors above and below the H_k as detailed in the inset of Fig. 5.1. At $H > H_k$, U_0 is independent of field while for $H < H_k$, U_0 increases rapidly with decreasing field by nearly an order of magnitude, indicating differing dissipation mechanisms in these two regions. Similar results were observed on twinned YBCO crystals [7], where H_k was identified as a crossover field from activated motion ($H < H_k$) to diffusive motion ($H \geq H_k$).

In a weakly pinned vortex liquid, a constant U_0 is expected in the thermally assisted flux flow (TAFF) region [40]. This seems to be supported by early experiments on HTSs [5,32,33], where a constant U_0 was extracted from the ρ_{xx} vs. T measurements at *constant* fields. On the melting line, U_0 (as well as U_e) increases abruptly to infinite when the vortex liquid freezes into the vortex solid, where vortices become strongly correlated. The gradual increase of U_0 with decreasing field as in the case of Hg-1212 films suggests that vortices may remain correlated within a finite band $H^* < H < H_k$, defining the onset field of ρ_{xx} as H^* [96]. Consequently, local ordering of the vortices may exist near the pinning centers and the distribution of vortices is highly non-uniform inside this band.

In the region $H^* < H < H_k$, ρ_{xx} shows a strong current dependence as shown in Fig. 5.2. At $H \geq H_k$, all log ρ_{xx} curves at different currents coincide nicely, indicating Ohmic behavior in this region. In contrast, non-Ohmic behavior, typically found in the vortex-glass phase, is observed in $H^* < H < H_k$. Consequently, calculated U_e (J) rapidly approaches infinity with decreasing current, similar to the characteristic of the vortex-glass phase. The I-V measurements conducted on Hg-1212 (inset of Fig. 5.2) also verify a non-Ohmic behavior in $H^* < H < H_k$.

The crossover from a correlated to an uncorrelated vortex liquid is also reflected in the behavior of the Hall angle [$\theta_H \equiv \tan^{-1}(\rho_{xy}/\rho_{xx})$] across the H_k-T curve. According to the time-dependent Ginzburg-Landau (TDGL) theory [21,22],

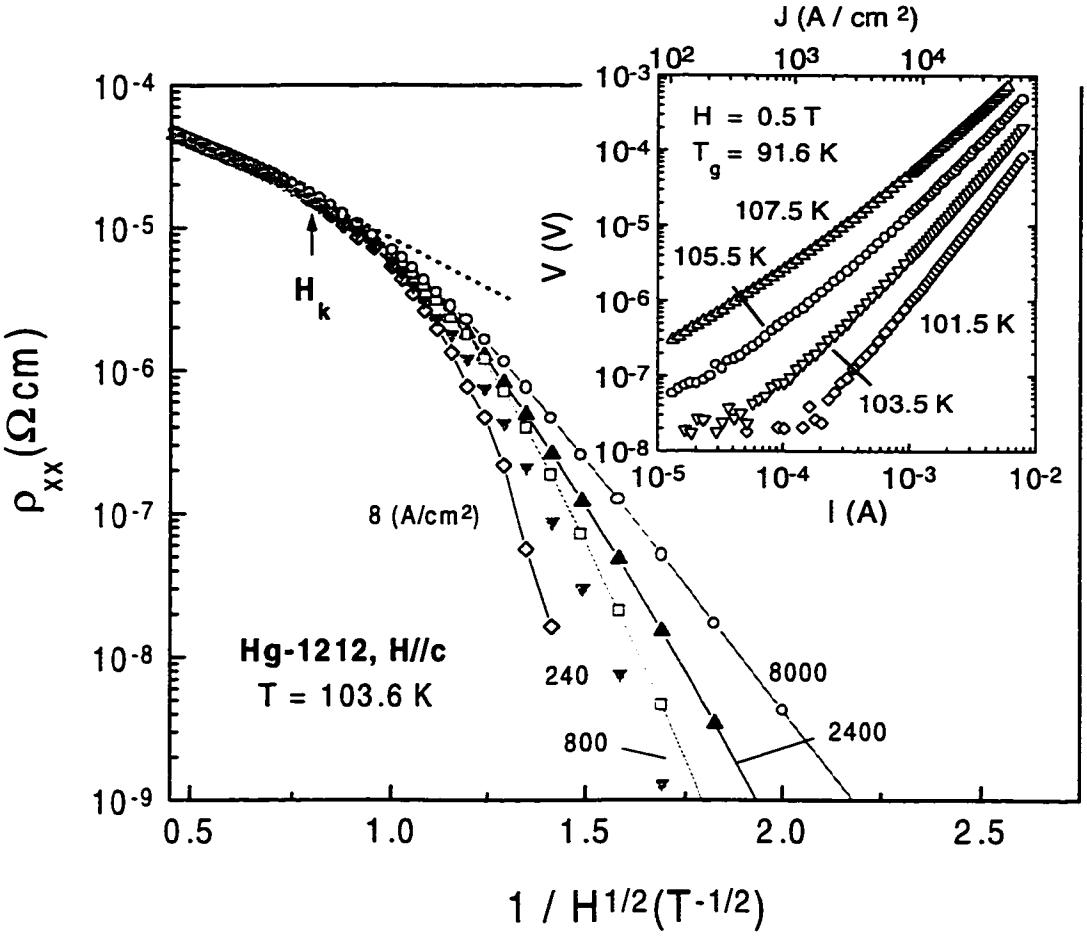

Fig. 5.2: log ρ_{xx} vs. $1/\sqrt{H}$ plots of Hg-1212 at several current densities. Ohmic behavior above H_k and non-Ohmic behavior below H_k are clearly shown. Inset: Four I -V curves for the temperature near 103.6 K at $H = 0.5$ T.

the mixed-state Hall angle contains two contributions: a normal-core term (tan θ_n), which is linearly proportional to the field, and a Magnus term (tan θ_M), which is predicted to be field-independent in a free-flow vortex liquid. In Fig. 5.3, tan θ_M is plotted as a function of temperature for several different applied fields. Here tan θ_n = $39.5H/T^2$ was derived from the normal-state Hall effect measurement [73]. Above the H_k -T, tan θ_M is independent of the field while below the H_k -T, it shows a complicated field- dependence. In other words, above the H_k -T line, pinning is ineffective so vortices are in free-flow vortex liquid while below H_k -T, pinning is effective and affects the vortex motion, which leads to deviation of tan θ_M from the theoretical prediction. This argument is supported by the fact that on the H_k -T line U_e is comparable with T. This implies that above the H_k -T line vortices are depinned so that the vortex motion is diffusive. Generally, such a depinning line (H_d -T), which separates the activated (TAFF) and diffusive (or free flux flow) regions,

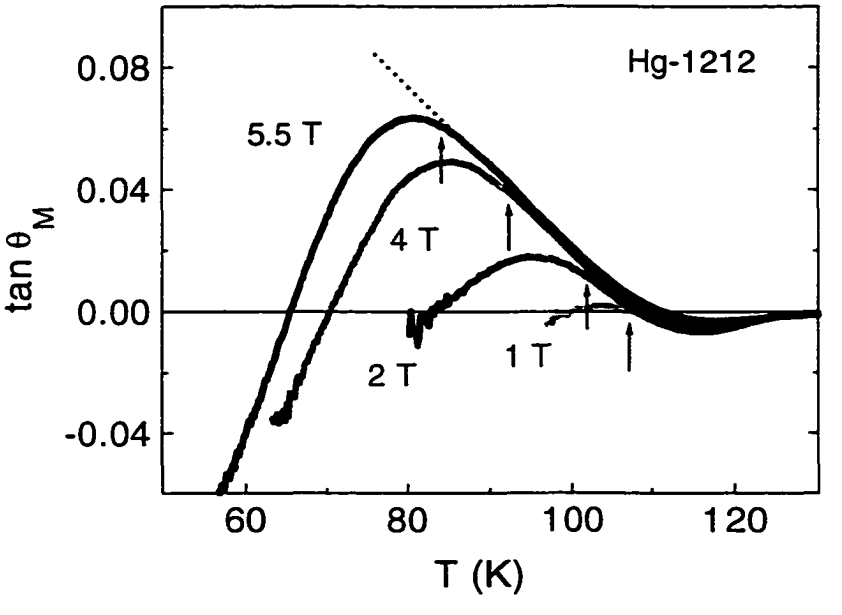

Fig. 5.3: Tan θ_M as a function of temperature for several applied fields. The dashed line represents the field-independent part of tan θ_M.

may be defined as $U_e = T$ [97]. It is clearly shown in Fig. 5.1 that this depinning line (dashed line) is very close to the H_k-T line (solid line). This seems to suggest that H_k-T is also the vortex depinning line for Hg-1212, which is, however, difficult to understand since vortex decoupling and vortex depinning are two different concepts.

5.4 Pinning dependence of vortex-liquid phase

In order to resolve this issue, the same measurements were repeated on a weak

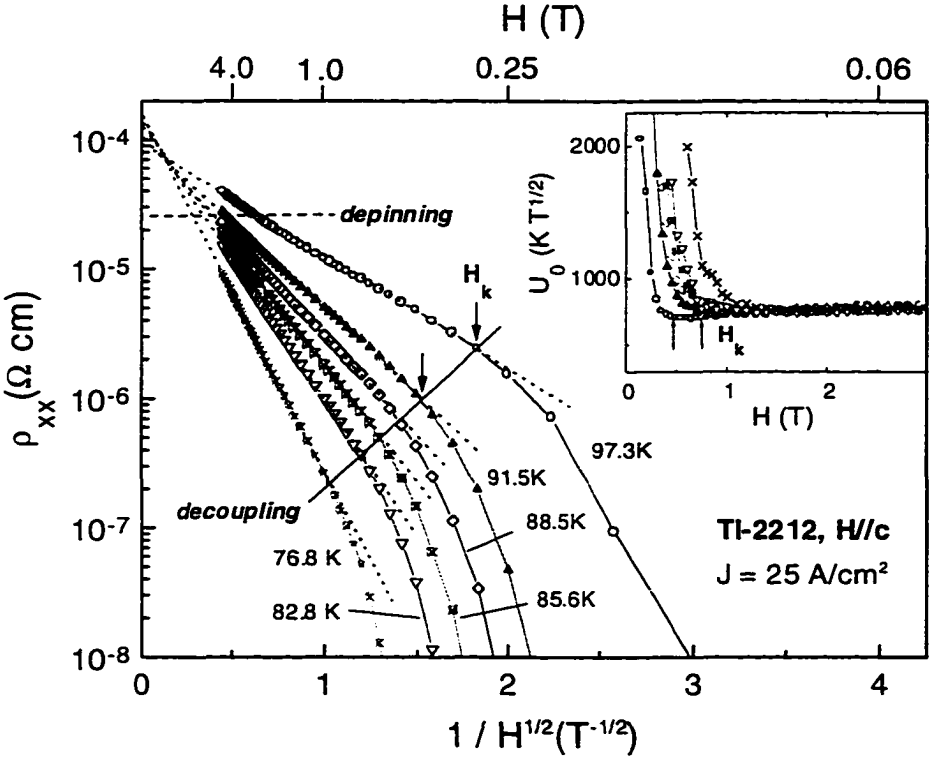

Fig. 5.4: log ρ_{xx} vs. $1/\sqrt{H}$ for Tl-2212 films. The dashed line and the solid line indicate the depinning line and the H_k-T curve (decoupling line), respectively. Inset: U_0 vs. H plot for Tl-2212 film at the same temperatures in the main panel.

pinning system, Tl-2212 thin films, and the results are shown in Fig. 5.4. The temperature range examined for Tl-2212 is 0.73 T_c - 0.92 T_c (T_c = 106 K), which is comparable to the range of 0.84 T_c - 0.98 T_c for Hg-1212 (T_c = 123 K). General trends in Tl-2212 such as two regions distinguished by the H_k with a gentle slope (above H_k) and a steep slope (below H_k) are the same as on Hg-1212. There exist, however, several differences between the two systems. Below H_k, U_0 for Tl-2212 increases more rapidly than for Hg-1212 as the field decreases, consequently yielding a narrower region for $H^* < H < H_k$. In the case of Tl-2212, this much lower H_k -T (solid line) is well separated from the depinning line (dashed line) defined from U_c = T as shown in Fig. 5.4. This indicates that the vortex liquid experiences decoupling at the H_k -T but remains pinned until the depinning line is reached. The region enclosed by the H_k -T curve (lower boundary) and the H_d -T curve (upper boundary) should thus be regarded as the TAFF of single vortices, which was confirmed by the Ohmic behavior observed for ρ_{xx} above H_k.

5.5 Glassy liquid and regular liquid

Fig. 5.5 depicts the magnetic phase diagrams of both the Hg-1212 and the Tl-2212 (inset) systems. The upper critical field H_{c2} (T) and the vortex solid-liquid transition line (H_g -T), extracted from I-V measurements [98], serve as the upper and lower boundaries of the vortex liquid phase, respectively. The resistive onset (H^*-T), also regarded as the vortex solid-liquid transition line [82,96], is shown obviously higher than the H_g -T line for both Hg-1212 and Tl-2212 films. A possible explanation would be the different criteria adopted in the two methods, which leaves the definition of the region between the H_g -T and H^* -T controversial. Nevertheless, the region above H^* -T can be regarded unambiguously as the vortex liquid phase.

This experiment therefore reveals several new features of the vortex liquid. (1)

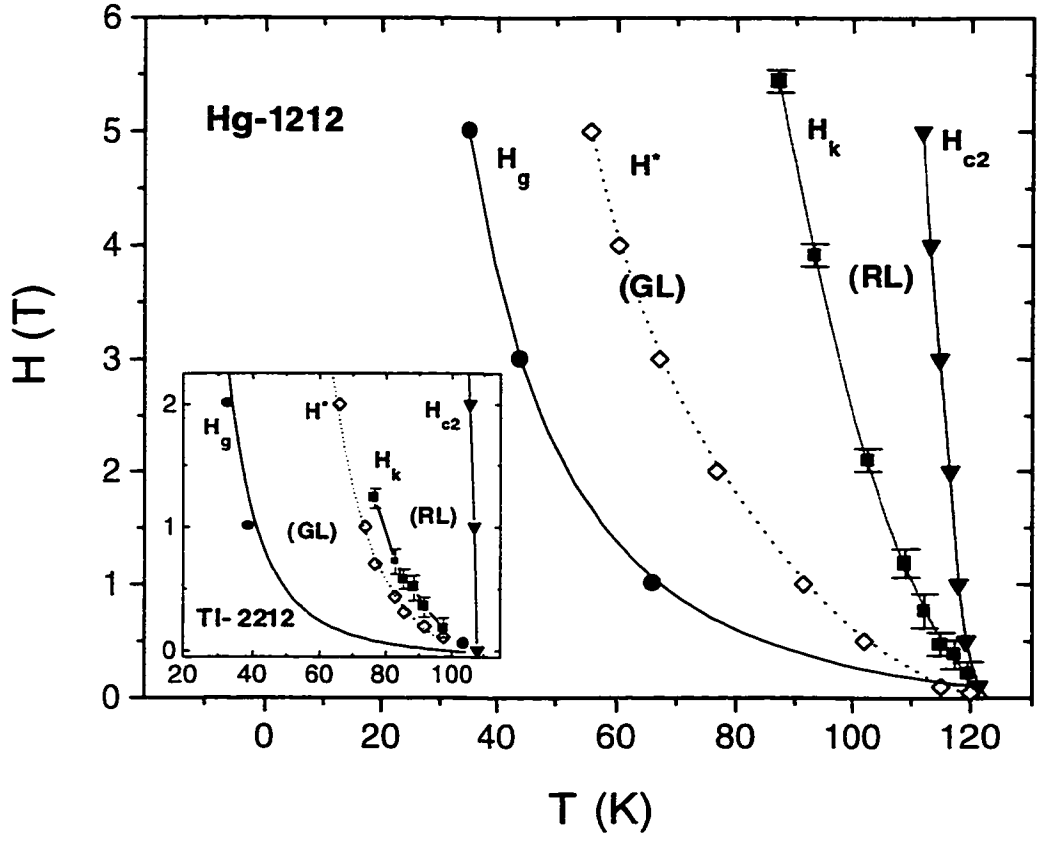

Fig. 5.5: Phase diagram for Hg-1212 thin films. The H_{c2} is from the mid-transition of ρ_{xx}-T and the H_k are identified from the kinks in the ρ_{xx}-H. The resistivity onset H^* is from Albert *et al.* [76] and the melting field H_g is extracted from I-V characteristics [79]. The solid and dotted lines are guides for eye. Inset: Phase diagram for Tl-2212 films. The H_k-T curve is much closer to the H^*-T than Hg-1212.

It is clearly shown in Fig. 5.5 that the H_k-T curve divides the vortex liquid into two states, the liquid of single vortices ($H \geq H_k$) and the liquid of correlated vortices ($H^* < H < H_k$). For convenience, we call the former "regular" liquid (RL) and the latter "glassy" liquid (GL) due to its resemblance to the vortex-glass phase. Both ρ_{xx} and tan θ_H are found to change their behaviors dramatically across the H_k-T; (2) The H_k-T curve strongly depends on the pinning. At moderate to strong pinning, there exists a wide GL region. The vortex glass melts into a liquid but remains correlated, most probably locally around the pinning centers due to non-uniformity of vortices. This GL region can be further increased with increasing pinning as shown in our recent experiment in Hg-1212 films irradiated with 5 *GeV* Xe-ions [99]. On the other hand, the GL region reduces with decreasing pinning (see the inset of Fig. 5.5) and becomes too narrow to be observed at low pinning limit. This consists of the Ohmic ρ_{xx} observed in HTS single crystals immediately above the H^*-T [79,81]; (3) Both GL and RL state could be pinned but the activation energy for the GL is nearly an order of magnitude higher than that for RL. This difference may be attributed to a large coherent "volume" for the vortex bundles in the GL region and this "volume" will be significantly reduced to that for single vortices in the RL region; and (4) Vortex depinning may occur either directly from correlated vortices in the strong pinning system including YBCO, Hg-1212 and Hg-1212 with columnar defects, or after the correlated vortices decouple into single vortices in the weak pinning system such as Tl-2212. In the former case, the high decoupling line merges approximately with the depinning line and in the latter case, the two lines are well separated so that single vortices are pinned in the region $H_k \leq H \leq H_d$. Above the H_d-T, vortex motion is diffusive and pinning becomes inefficient.

Chapter 6

Scaling Laws of ρ_{xx} and ρ_{xy}

6.1 T- and H-dependence of ρ_{xx}

At finite temperatures, thermally activated flux motion produces dissipation as follows:

$$\rho_{xx} = \rho_0 \exp(-U_e / kT) \tag{6.1}$$

where ρ_0 is the preexponential factor and k is the Boltzman constant. U_e is the effective activation energy which generally depends on the temperature and magnetic field such that

$$U_e(T, H) = U_0 \beta(T) g(H) \tag{6.2}$$

where U_0 is the unperturbed activation energy and the functions β and g incorporate the temperature and magnetic field.

For most HTSs, $\beta(T)$ and $g(H)$ are observed to have forms $\beta(T) \sim (1 - T/T_c)^m$ and $g(H) \sim H^{-a}$. From the measurement of ρ_{xx} with sweeping magnetic field as shown in Fig. 5.1 and 5.3, for Hg-1212 films, $U_e(H) \sim 1/\sqrt{H}$ is obtained both in the GL and RL for the magnetic field range of 0.05 T – 8 T. This $1/\sqrt{H}$ field dependence is the reported scaling for Bi/Tl –2212. The slope of the each curve gives directly the quantity $U_e\sqrt{H} / kT$ at a given temperature.

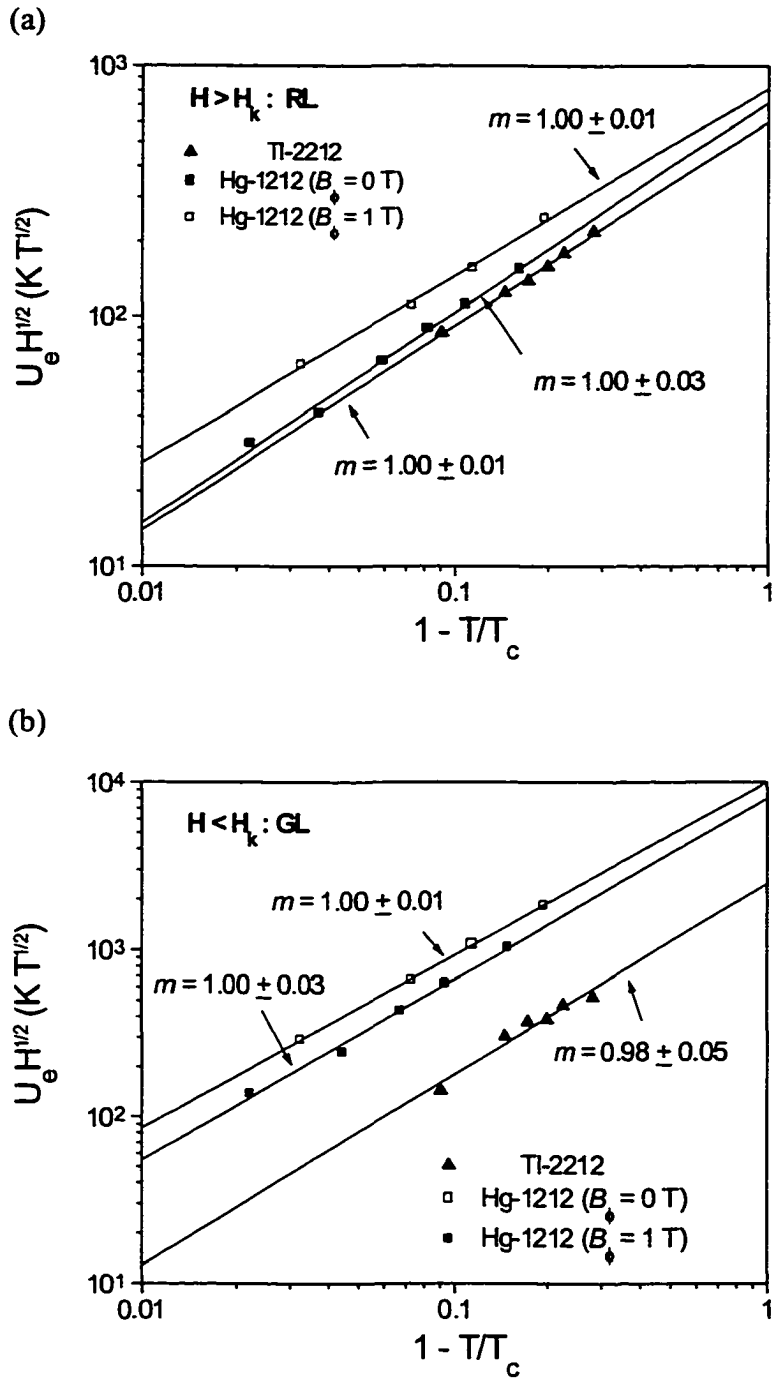

Fig. 6.1: Power law dependence of U_e plotted as a product $U_e\sqrt{H}$ (a) in the RL region; and (b) in the GL region.

The temperature dependence of U_e can be extracted from the slope of ρ_{xx} vs. $1/\sqrt{H}$ curves. Assuming a general power law for the temperature dependence of $U_e(T) \sim (1 - T/T_c)^m$, the product $U_e\sqrt{H}$ vs. $(1 - T/T_c)$ is plotted for both liquid phases, the GL and the RL, in Fig. 6.1. Also shown are the temperature scaling of weak pinning system, Tl-2212, and strong pinning system, Hg-1212 with columnar defects. As discussed in chapter 5, U_e's in the GL are about an order of magnitude higher than those in the RL for all three systems. As pinning increases, U_e increases in both regions, and the Hg-1212 with columnar defects has the highest U_e due to the strongest pinning. A linear regression of these data gives the exponent for the temperature scaling. Interestingly, m's for all three systems obtained in both phases are very close to 1.0 within error range, though their U_e values are very different. Therefore $U_e(T, H)$ of Hg-1212 without and with columnar defects can be described by the scaling law of $U_e(T, H) \sim (1 - T/T_c) / \sqrt{H}$.

This temperature and field scaling law of U_e consists with the model proposed by Vinokur *et al.* [40]. According to this model, the vortex-liquid phase can be separated into the flux flow and the thermally activated flux flow (TAFF). U_e in TAFF regime is associated with the plastic motion of the vortices. It should be noted, however, that in this model, the vortex-liquid phase is defined as an Ohmic regime while the GL is found to be non-Ohmic.

6.2 *T*- and *H*-dependence of tan θ_H

In chapter 4, *T*- and *H*-dependence of the tangent of the Hall angle (tan θ_H) is described. Based on the TDGL theory [21,22] neglecting the effect of pinning, tan θ_H can be decomposed into two terms:

$$\tan\theta_H(T, H) = \tan\theta_n(T, H) + \tan\theta_M(T) \qquad (6.5)$$

where tan θ_n (T, H) is field-dependent and originates from the contribution of vortex normal cores, and tan θ_M (T) is the field-independent Magnus term. Tan θ_n (T, H) is obtained from the normal-state Hall effect measurement on Hg-1212, which suggests tan θ_n (T, H) ~ AH / T^2 [73]. In our experiment, the coefficient A = 39.5 is obtained for the Hg-1212 thin film. As shown in Fig. 4.2 and discussed, T-dependence of the Magnus term (tan θ_M) at different applied fields shows clearly different behaviors in the two liquid states. In the RL region, all the tan θ_M curves that are measured at different fields come to coincide, indicating that tan θ_H has a linear H-dependence through the normal-core term tan θ_n, which is consistent with the KIK model [see Eq. (4.2)]. Near T_k (which is marked by the arrows in Fig. 4.2) the tan θ_M - T curve starts to deviate from the main trend showing a nonlinear H-dependence of tan θ_H in the GL region where pinning sets in. Therefore, the TDGL model does not fit with our data in the GL region since the effect of pinning is not considered. It should be mentioned that fitting of experimental data with the KIK model was only attempted previously on YBCO films [25]. Tan θ_M (T) in YBCO was shown to be field independent near T_c, while a complicate field dependence was observed in tan θ_M (T) at slightly lower temperatures, which agrees with our experimental results.

6.3 H-dependence of σ_{xy}

According to the TDGL [21] and microscopic theory [68], σ_{xy} can be decomposed into three terms:

$$\sigma_{xy} = C_1 / H + C_2 + C_3 H \tag{6.6}$$

The $1/H$ term comes from σ_{xy}^f and dominates at low fields, while the H term is from σ_{xy}^n, which dominates in high field. The second term is negligible for less anisotropic system such as YBCO [69] but supersedes the third term for highly anisotropic

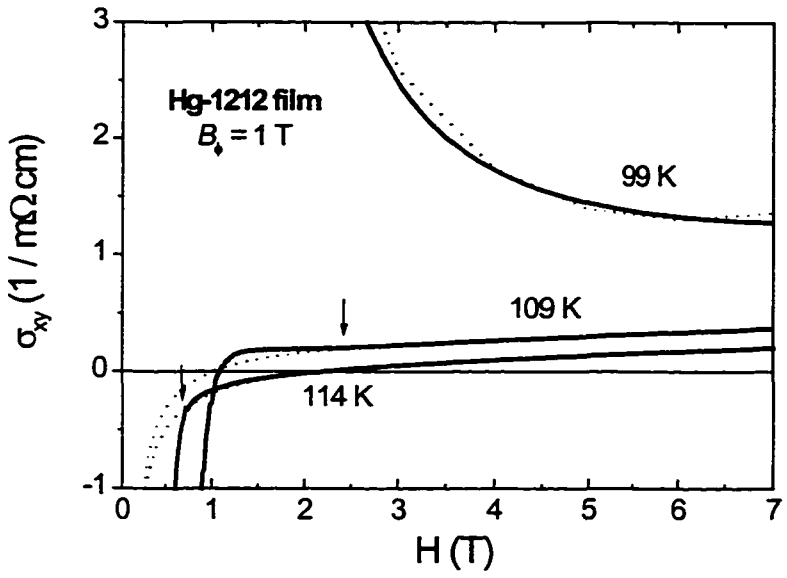

Fig. 6.2: Field dependence of σ_{xy} of Hg-1212 films (B_ϕ = 1 T) at several temperatures. The arrows indicate deviations from the theoretical fitting.

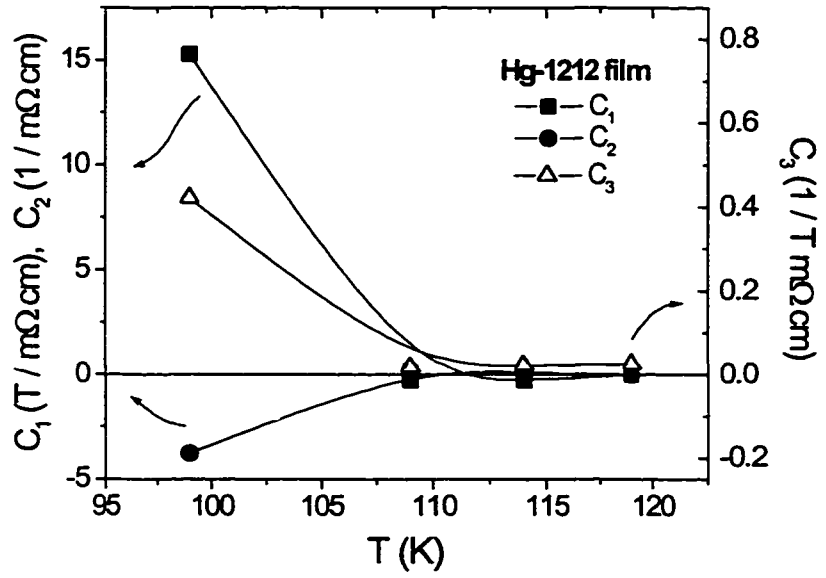

Fig. 6.3: Temperature dependence of coefficients C_1, C_2 and C_3 of Hg-1212 films

systems such as Tl-2212 [70]. The coefficient C_1, C_2 and C_3 are independent of fields, but are expected to depend on temperature. In Fig. 6.2, the field dependence of σ_{xy} is plotted at several temperatures below T_c. Dashed lines depict the theoretical fitting using the relation (6.6). At relatively high fields, there exists a threshold H_k (T) (marked by arrows) below which the data deviate systematically from the fitting. The deviation of σ_{xy} from the theoretical model in the low field region has also been reported for other HTSs including YBCO [69], LSCO [24] and Tl-2212 [70]. This deviation can be explained by the existence of the GL region. Since Eq. (6.6) is based on the assumption of unpinned vortex liquid, this relation should be applied only at $H > H_k$ (T) for Hg-1212 system in which depinning and decoupling occurs nearly simultaneously.

Temperature dependence of the coefficients C_1, C_2 and C_3 is plotted in Fig. 6.3. Upon cooling from T_c, C_1 and C_2 become negative at certain temperature range, while C_3 monotonically increasing with decreasing temperature. According to Eq. (6.6), the sign of σ_{xy} is determined by the competition between these three terms.

Chapter 7

Behavior of σ_{xy} in GL and RL

From the study of the vortex-liquid phase diagram described in chapter 5, it has been found that vortices are correlated in the glassy-liquid (GL) phase near the onset of resistivity and behave very differently from the regular-liquid (RL) phase due to the inter-vortex correlation. Based on this observation, we investigate behaviors of σ_{xy} in these two regions. Two systems are examined: (1) Hg-1212 in which vortex depinning occurs directly from correlated vortices, so vortices can move freely after they are uncorrelated at $H_k(T)$; (2) Tl-2212 in which the depinning and decoupling lines are well separated, so that single vortices are pinned in the region $H_k < H < H_d$. In this chapter we report a systematic study of σ_{xy} on the Hg-1212 and Tl-2212 films before and after columnar defects are added. The irradiation doses were the matching field of B_ϕ = 1 T and 1.2 T for Hg-1212 and Tl-2212, respectively.

7.1 Pinning dependence of GL and RL

In Fig. 7.1 in the following, the field dependence of ρ_{xx} before (B_ϕ = 0 T) and after irradiation (B_ϕ = 1 T) is shown at the same reduced temperatures below T_c. As shown in Fig. 7.1, the same $1/\sqrt{H}$ dependence of ρ_{xx} is observed for both B_ϕ = 0 and 1

T in the field range of 0.05 T – 8 T. Enhanced pinning by irradiation does not change the general trend of curves such as the distinction of two regions (the GL and the RL) by the H_k –T, but it modifies the detailed features of the curves. The $H_k - T$ (dashed arrow) is shifted toward higher fields and temperatures (solid arrow) after irradiation, resulting in a wider GL region. Since the $H_k - T$ curve represents disappearance of the inter-vortex correlation of vortices in the vortex-liquid phase, it is not surprising to see the correlation caused by stronger pinning sustains at higher fields and temperatures. Above the $H_k - T$ the slope of curves before and after irradiation, which represents an activation energy U_e, is nearly the same, confirming that pinning is no longer effective in this region since vortices are decoupled and depinned as well.

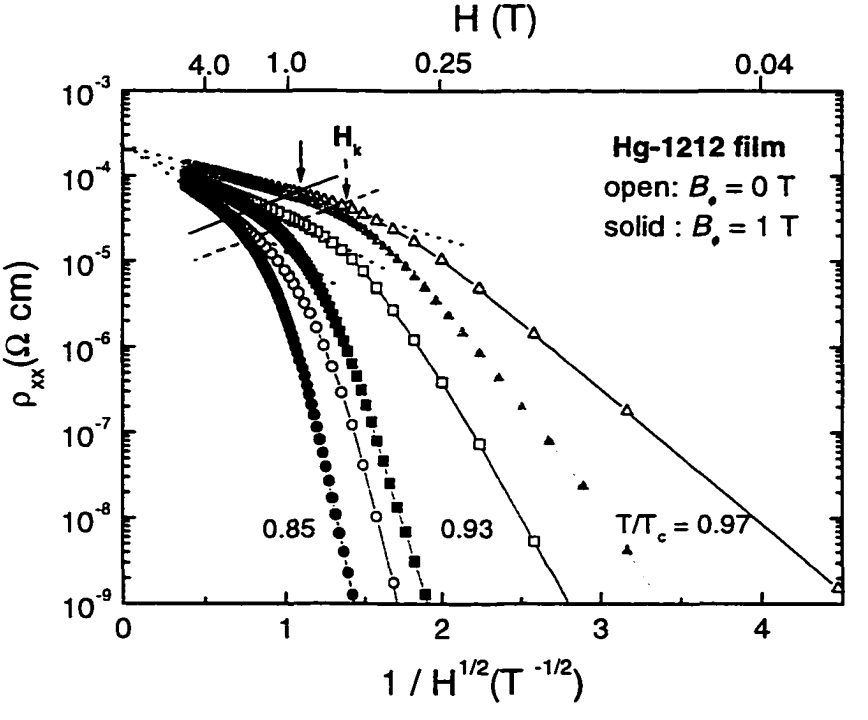

Fig. 7.1: Log ρ_{xx} as a function of $1/\sqrt{H}$ for Hg-1212 thin films before and after irradiation. After irradiation, the boundary field H_k (dashed arrow) between the RL and the GL is shifted to a higher field (solid arrow).

In contrary, the slope of the curves below the $H_k - T$ curve significantly steepens with columnar defects, confirming a dominant effect of pinning in the GL region.

7.2 σ_{xy} of Hg-1212 films in GL and RL

Fig. 7.2 (a) depicts the detailed phase diagram of the vortex-liquid phase of Hg-1212 film including the decoupling lines (H_k -T), at which the inter-vortex correlation disappears, before and after irradiation. Also shown are the H_{c2} from the mid-transition of ρ_{xx} -T curves, the H^* indicating the onset of resistivity [96] and the depinning line (H_d -T) defined by the criteria of $U_e \equiv T$ [97]. Notice that the H_k -T is shifted to higher H and T after pinning is enhanced by irradiation, resulting in nearly mergence into the H_d -T.

σ_{xy} is found to behave very differently in the two vortex-liquid regions. In Fig. 7.2 (b), $\sigma_{xy} = \rho_{xy}/\rho_{xx}^2$ is plotted for several applied fields before and after irradiation. In order to take into account the T_c difference of 0.8 K, the figure is presented in a reduced temperature T/T_c. It can be clearly seen that σ_{xy} before and after irradiation coincides above arrows and starts to diverse below arrows. In order to define a deviation of σ_{xy} consistently for all applied fields and also for the other system, a criterion of ~ 1 % deviation is used. If we apply the temperatures of arrows for different applied fields to the phase diagram in Fig. 7.2 (a), they stay on the H_k -T curve for the irradiated sample. This result shows that σ_{xy} is independent of pinning in the RL region, while it is strongly dependent on pinning in the GL region. However, it is not clear yet whether this pinning dependence of σ_{xy} in the GL region is caused either by pinning or by an inter-vortex correlation, since for Hg-1212 decoupling and depinning occur nearly simultaneously.

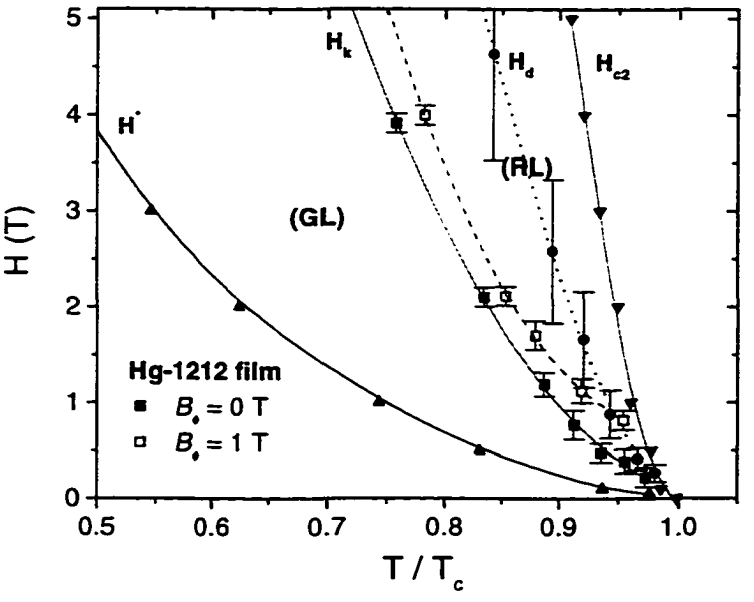

Fig. 7.2 (a): Phase diagram of the vortex-liquid phase for Hg-1212 films. The H_k -T is extracted from the ρ_{xx} -H curves before and after irradiation, and the H_d -T is determined by the criteria of $U_c = T$.

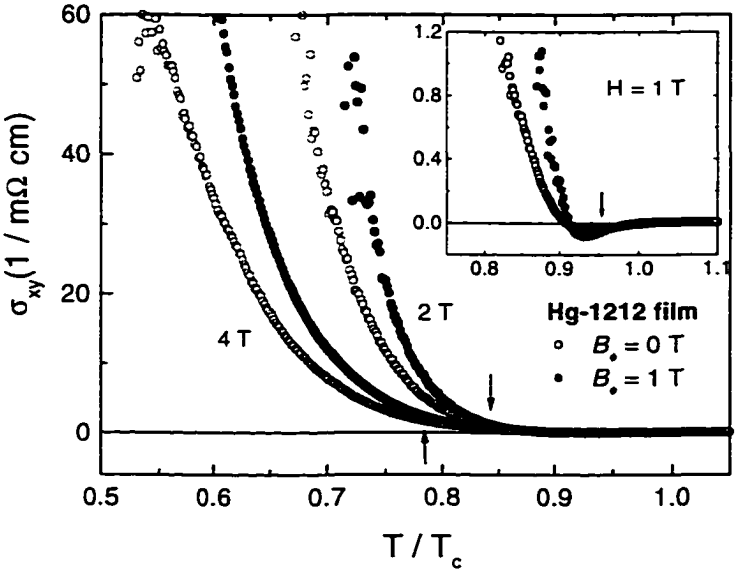

Fig. 7.2 (b): σ_{xy} *vs.* T plot before and after irradiation at H = 1 (inset), 2 and 4 T. σ_{xy} starts to deviate at the arrows, which stay nearly at the decoupling line for the irradiated sample in Fig. 7.2(a).

7.3 σ_{xy} of Tl-2212 films in GL and RL

In order to make sure if pinning dependence of σ_{xy} in the GL is caused either by the inter-vortex correlation or by pinning, we repeat the same measurement in Tl-2212 films, in which the decoupling and the depinning lines are well separated as shown in Fig. 7.3 (a). In Fig. 7.3 (b), σ_{xy} is plotted for H = 1 T and 2 T before and after irradiation. Similar to the result of the Hg-1212 films, σ_{xy} coincides above the arrow and diverses below the arrow. These arrows that are determined based on the same criterion as in Hg-1212 (marked by *) stay a little higher than the H_k -T in Fig. 7.3 (a). If we assume a shift of the H_k -T after the heavy ion irradiation as in the Hg-1212, the deviation of σ_{xy} starts approximately at the H_k -T of the irradiated sample. This result clearly indicates that the pinning dependence of σ_{xy} is induced by the inter-vortex correlation, not by pinning itself. If pinning causes the deviation of σ_{xy} before and after irradiation, this deviation must start from the depinning line H_d –T, which is far above the H_k –T.

Our results suggest the following physical picture: In the presence of pinning, vortices remain correlated in the GL region, so that the effect of pinning is reflected in ρ_{xx} and ρ_{xy} in a complicated way that can not be canceled out in σ_{xy}. Since the pinning dependence of σ_{xy} is caused by the inter-vortex correlation, this explains why the VGFB model in which the pinning effect is considered can not be applied to a low T and H regime for the YBCO and Hg-1212 systems [8,9,12]. In this model, the non-linear interaction term is considered to be averaged out over disorder and vortex positions. This simple average may not work at a region below the H_k –T, where the distribution of vortices near the pinning center is highly non-uniform due to the local ordering of vortices.

Depending on pinning, there exist two possibilities for uncorrelated single vortices in the RL region. For the moderate to strong pinning systems such as the YBCO and Hg-1212 films, decoupling and depinning occur nearly simultasneously.

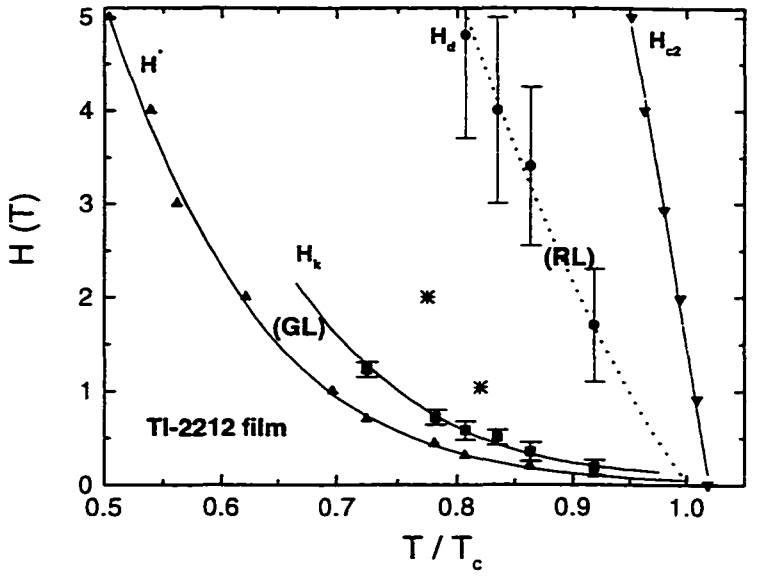

Fig. 7.3 (a): Phase diagram of the vortex-liquid phase for Tl-2212 films. Compared to that for Hg-1212 films, the H_k-T and H_d-T are well separated.

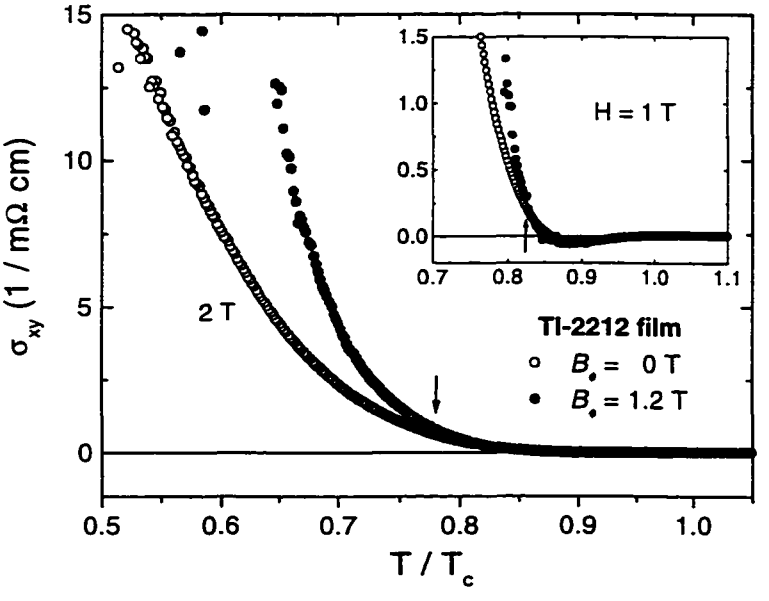

Fig. 7.3 (b): The same σ_{xy} *vs.* T plot before and after irradiation at H = 1 T and 2 T (inset). The deviation of σ_{xy} locates little above the H_k-T in the phase diagram.

Thus vortex motion is not affected by pinning after vortices are uncorrelated. Consequently, σ_{xy} is pinning independent. In contrary, for the weak pinning system such as the Tl-2212 films the H_k -T and the H_d -T lines are well separated, so vortices are uncorrelated, but still remain pinned at the region enclosed by the H_k -T (lower boundary) and the H_d -T (upper boundary) lines. Although pinning affects ρ_{xx} and ρ_{xy} respectively at this region, these effects are canceled out when σ_{xy} is calculated. This analysis can explain the pinning independent σ_{xy} in Tl-2212 films that was reported by Samoilov *et al.* [26]. In Ref. [26] σ_{xy} is not extended to a very low T regime to be able to reach the GL phase, so σ_{xy} before and after irradiation is compared only in the RL phase. Since vortices are completely uncorrelated in this region, the VGFB model should be valid.

The pinning-dependent σ_{xy} at low T and H regime appears to agree with the WDT model qualitatively. The question of how the backflow current inside normal core relates with the inter-vortex correlation, however, needs further investigation. In addition, a smaller β than 1.5 ($\beta \cong 1$) has been observed recently on Hg-1212 films at very low field [101], which can not be explained by this model.

Chapter 8

Concluding Remarks

In this dissertation, we presented the study on the mixed-state Hall effect of high-T_c superconductors (HTSs). In order to understand the mechanisms of the puzzling phenomena in the mixed-state Hall effect of HTSs, the Hall sign anomaly and scaling behavior, Hall measurements are conducted in several HTSs with various pinning from weak to strong, or with various oxygen content from underdoped to overdoped.

The mechanism of the sign reversal of the Hall resistivity is investigated from the study of the Hall effect in Tl-2201 films when the electronic band structure is varied through the underdoped, optimally doped, and overdoped region. Two sign reversals observed both in the underdoped and optimally doped samples disappear simultaneously when the sample is overdoped. These results confirm that the Hall sign reversal is an intrinsic property of HTSs and both Hall sign reversals are determined by electronic band structure.

Although pinning is not found to be the mechanism behind sign reversals, pinning can modify the detail of the Hall sign reversal. By enhancing pinning of Hg-1212 films by irradiation to trap the second sign reversal into the pinning effective region, the second sign reversal can be suppressed completely. Therefore, it is concluded that two (or more) sign reversals represent a generic behavior of HTSs.

From a systematic study of the vortex phase diagram, several new features of

the vortex liquid are discovered. In the presence of pinning, vortex liquid is composed of two states, a glassy liquid (GL) and a regular liquid (RL). In the GL state, vortices remain correlated as manifested in non-Ohmic resistivity whereas in the RL state, resistivity becomes Ohmic as vortices become uncorrelated. Generally the boundary (H_k -T) between the GL and the RL is lower than the depinning line (H_d –T). As pinning increases the H_k -T may approach the H_d -T, thus vortices are decoupled and depinned simultaneously for a strong pinning system. For the weak pinning system, on the other hand, the $H_k - T$ and the $H_d - T$ are well separated so that single vortices remain pinned in the region $H_k \leq H \leq H_d$.

The presence of the GL is reflected in the scaling laws of ρ_{xx} and ρ_{xy}. The scaling law of U_e for Hg-1212 system is obtained as $U_e(T, H) \sim U_0 (1 - T/T_c) / \sqrt{H}$ both in the GL and the RL despite different U_e values in the two regions. The magnetic field dependence of tan θ_H is found to be linear in the RL and non-linear in the GL. The temperature and field dependence of tan θ_H and σ_{xy} fits well with the TDGL theory only in the RL region while they do not fit in the GL region because the effect of pinning is not considered in this model.

σ_{xy} is found to behave very differently in the GL and the RL. In the GL σ_{xy} is observed dependent on pinning due to the inter-vortex correlation whereas in the RL σ_{xy} is independent of pinning because the pinning effect is scaled out.

These observations shed many insights onto the understanding of the Hall sign reversals and the scaling behavior. However, several problems still remain unsolved in the mixed-state Hall effect of HTSs. For example, the mechanism of how electronic band structure determines the Hall sign is not clear yet. In addition, an application of the TDGL model to the Hall angle of Tl-2201 (or Tl-2212) films reveals an interesting fine feature, which is different from that of the strong pinning systems such as YBCO or Hg-1212 films. These problems are left for future research.

Chapter 9

Future Experiment Proposal

Based on our observations shown in the previous chapters, we propose the Hall effect measurements of Tl-2201 thin films (1) with various oxygen contents and (2) with various irradiation doses. By measuring ρ_{xx} and ρ_{xy} of Tl-2201 films, we will carefully investigate the dependence of the Hall resistivity or the Hall angle on (1) charge carrier density, and (2) pinning strength.

9.1 Hall effect on Tl-2201 films with various oxygen contents

In chapter 3, we have investigated the intimate relation between the Hall sign reversals and electronic band structure on Tl-2201 films with oxygen contents varying from slightly underdoped to overdoped. However, it is not clear yet how the electronic band structure controls the mixed-state Hall sign. The systematic study on the relation between the Hall sign anomalies and charge carrier density is thus necessary to understand the mechanism of the Hall sign reversals in HTSs.

Tl-2201 thin films are an ideal system for such a study since their electronic band structures can be perturbed by anion doping instead of cation doping, which may produce an unnecessary effect on the Fermi surface. Through collaboration with

the State University of New York (SUNY) at Buffalo, we will extend the Hall effect measurements on Tl-2201 films in order to cover a wide range on oxygen contents from underdoping to overdoping with fine intervals. From this experiment, we will investigate (1) the dependence of both of the two sign reversals on charge carrier density; (2) at which doping level, both of the two Hall sign reversals disappear; and (3) the dependence of the Hall resistivity on charge carrier density in the overdoped region.

9.2 Hall effect on Tl-2201 films with columnar defects

The relation (4.2) has been reported to have a good agreement with tan θ_H of YBCO crystals (strong pinning system) [25] and Hg-1212 thin films with columnar

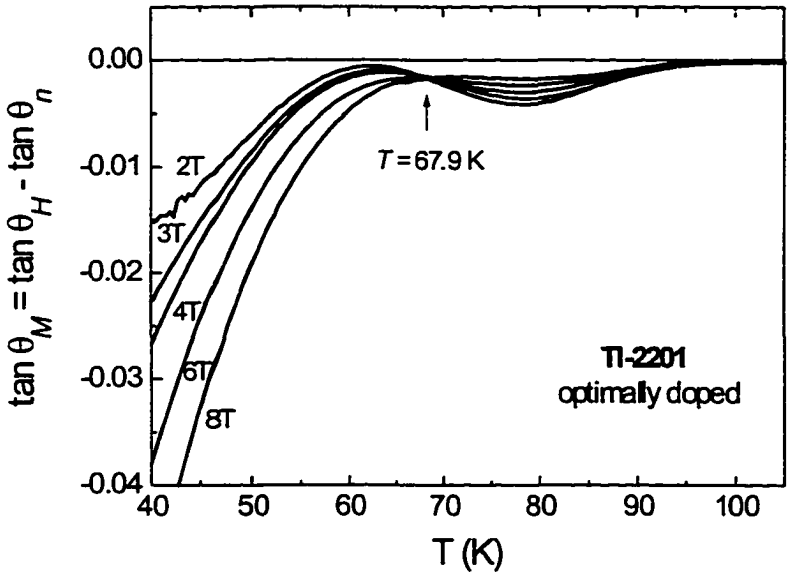

Fig. 9.1: Tan θ_M vs. T curves for a Tl-2201 film at different applied field ($H \geq 2$ T). The crossover at $T = 67.9$ K can be clearly seen.

defects (moderate pinning system) [102]. The application of the same analysis to Tl-2201 (weak pinning system), however, shows very different and interesting fine structures at high field region as shown in Fig. 9.1. This fine structure, which has also been observed in the Tl-2212 system, is not expected from any existing theories.

As we observed in chapter 5, the vortex state in the vortex-liquid phase of Tl-2212 is different from that of YBCO and Hg-1212. The vortex liquid experiences decoupling at the $H_k - T$ line, but remains pinned until the depinning line ($H_d - T$) is reached. Therefore, there exists a wide region for the TAFF of single vortices enclosed by the $H_k - T$ (lower boundary) and the $H_d - T$ (upper boundary), while in YBCO and Hg-1212, decoupling and depinning occurs nearly similtaneously. The fine structures of the Hall angle may associate with the decoupling of vortices. This argument is supported by the observation that tan θ_M vs. T plot for Tl-2201 at a low field region (Fig. 9.2) is very similar to that of Hg-1212 at a high field region (see

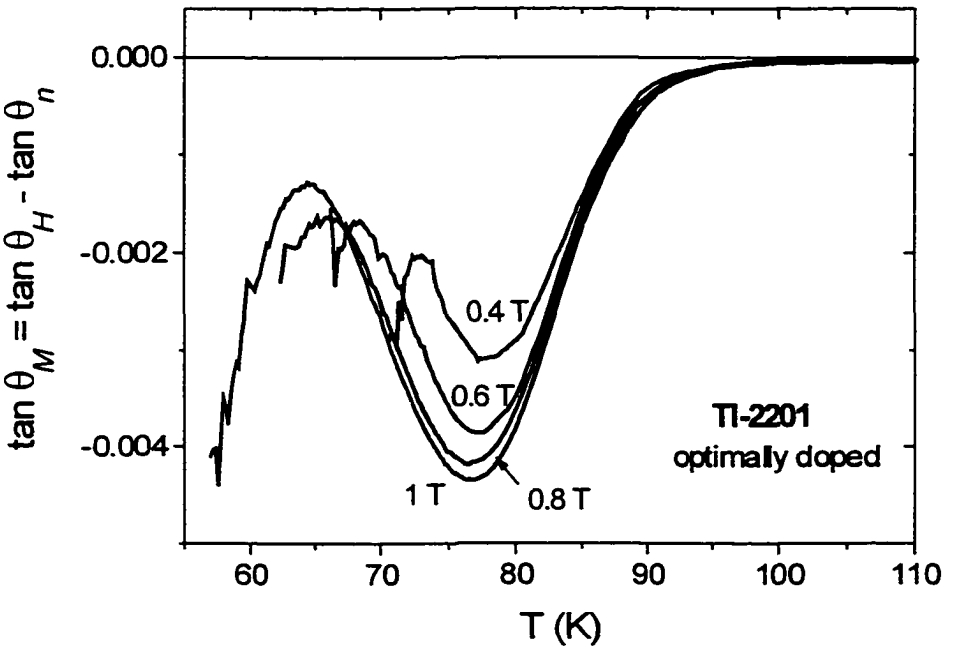

Fig. 9.2: Tan θ_M as a function of T for a Tl-2201 film at different applied fields ($H \leq 1$ T). At a low field region, tan θ_M behaves differently from that at high field region

Since the pinning of Hg-1212 is stronger than that of Tl-2201 (or Tl-2212) due to smaller anisotropy, the same fine structure is expected to occur at a higher field region ($H > 8$ T) for Hg-1212. Therefore, the Tl-2201 system provides a relatively wide field region for the study of detailed fine structures in the Hall angle. A careful analysis of the Hall angle of Tl-2201 with different pinning, which can be modified by using ion beam irradiation, will be conducted in high (1 – 8 T), moderate (0.1 – 1 T) and low (0.01 – 0.1 T) field regions, using a lock-in amplifier to improve the resolution of the measurement. It has been found that the decoupling line shifts to higher temperatures and fields as pinning enhances by heavy ion beam irradiation [100]. In collaboration with the SUNY at Buffalo and Sandia laboratory, we will prepare a set of Tl-2201 samples with different irradiation doses. Measurement of the Hall angle on Tl-2212 films as a function of irradiation dose will thus provide a quantitative understanding of the mechanism of these fine structures.

Bibliography

[1] J. Bardeen and M.J. Stephen, *Phys. Rev.* **140**, A1197 (1965).

[2] P. Noizieres and W.F. Vinen, *Philos. Mag.* **14**, 667 (1966).

[3] M. Galffy and E. Zirngiebl, *Solid State Commun.* **68**, 929 (1988).

[4] Y. Iye, S. Nakamura and T. Tamegai, *Physica C* **159**, 616 (1989).

[5] K.C. Woo, K.E. Gray, R.T. Kampwirth, and J.H. Kang, *Physica C* **162-164**, 1011 (1989).

[6] S.J. Hagen, C.J. Lobb, R.L. Greene, and M. Eddy, *Phys. Rev. B* **43**, 6246 (1991).

[7] T.R. Chien, T.W. Jing, N.P. Ong, and Z.Z. Wang, *Phys. Rev. Lett.* **66**, 3075 (1991).

[8] J. P. Rice, N. Rigakis, D.M. Ginsberg, and J.M. Mochel, *Phys. Rev. B* **46**, 11050 (1992).

[9] J. Luo, T.P. Orlnado, J.M. Graybeal, X.D. Wu, and R. Muenchausen, *Phys. Rev. Lett.* **68**, 690 (1992).

[10] R.C. Budhani, S.H. Liou and Z.X. Cai, *Phys. Rev. Lett.* **71**, 621 (1993).

[11] A. V. Samoilov, *Phys. Rev. Lett.* **71**, 617 (1993).

[12] W.N. Kang, D.H. Kim, S.Y. Shim, J.H. Park, T.S. Hahn, S.S. Choi, W.C. Lee, J. D. Hettinger, K.E. Gray, and B. Glagola, *Phys. Rev. Lett.* **76**, 2993 (1996).

[13] W.N. Kang, S.H. Yun, J.Z. Wu, and D.H. Kim, *Phys. Rev. B* **55**, 621 (1997).

[14] K. Noto, S. Shinzawa and Y. Muto, *Solid State Comm.*, **18**, 1081 (1976).

[15] J.M. Graybeal, J. Luo and W.R. White, *Phys. Rev. B* **49**, 12923 (1994).

[16] T.W. Clinton, A.W. Smith, Qi Li, J.L. Peng, R.L. Greene, C.J. Lobb, M. Eddy, and C.C. Tsuei, *Phys. Rev. B* **52**, R7046 (1995).

[17] A.T. Dorsey and M.P.A. Fisher, *Phys. Rev. Lett.* **68**, 694 (1992).

[18] P.J. M. Wöltgens, C. Deer, and H.W. de Wijn, *Phys. Rev. Lett.* **71**, 3858 (1993).

[19] V.M. Vinokur, V.B. Geshkenbein, M.V. Feigel'man, and G. Blatter, *Phys. Rev. Lett.* **71**, 1242 (1993).

[20] Z.D. Wang, J. Dong, and C.S. Ting, *Phys. Rev. Lett.* **72**, 3875 (1994).

[21] A. Dorsey, *Phys. Rev. B* **46**, 8376 (1992).

[22] N.B. Kopnin, B.I. Ivlev and A.V. Kalatsky, *J. Low Temp. Phys.* **90**, 1 (1993).

[23] Z.D. Wang and C.S. Ting, *Phys. Rev. B* **46**, 284 (1992); *Phys. Rev. Lett.* **67**, 3618 (1991).

[24] Y. Matsuda, T. Nagaoka, G. Suzui, K. Umagai, M. Suzuki, M. Machida, M. Sera, M. Hiroi, and N. Kobayashi, *Phys. Rev. B* **52**, R15749 (1995).

[25] M.N. Kunchur, D.K. Christen, and C.E. Klabunde, *Phys. Rev. Lett.* **72**, 2259 (1994).

[26] V. Samoilov, A. Legris, F. Rullier-Albenque, P. Lejay, S. Bouffard, Z.G. Ivanov, L.-G. Johansson, *Phys. Rev. Lett.* **74**, 2351 (1995).

[27] L.M. Wang, H.C. Yang, and H.E. Horng, *Phys. Rev. Lett.* **78**, 527 (1997)

[28] A.W. Smith, T.W. Clinton, Wu Liu, C.C. Tsuei, A. Pique, Qi Li, and C.J. Lobb, *Phys. Rev. B* **56**, R2944 (1997)

[29] D.H. Kim, J.H. Park, Y.H. Kim, J.M. Lee, T.S. Hahn, J.D. Hettinger, and K.E. Gray, preprint

[30] E. Zeldov, N.M. Amer, G. Koren, A. Gupta, R.J. Gambino, and M.W. McElfresh, *Phys. Rev. Lett.* **62**, 3093 (1989); *Appl. Phys. Lett.* **56**, 680 (1990).

[31] S. Zhu, D.K. Christen, C.E. Klabunde, J.R. Thompson, E.C. Jones, R. Feenstra, D.H. Lowndes, and D.P. Norton, *Phys. Rev. B* **46**, 5576 (1992).

[32] J.T. Kucera, T.P. Orlando, G. Virshup, and J.N. Eckstein, *Phys. Rev. B* **46**, 11004 (1992).

[33] M. Nikolo, W. Kiehl, H.M. Duan, and A.M. Hermann, *Phys. Rev. B* **45**, 5641 (1992).

[34] D.R. Harshman, L.F. Schneemeyer, J.V. Waszczak, G. Aeppli, R.J. Cava, B. Batlogg, L.W. Rupp, E.J. Ansaldo, R.F. Kiefl, G.M. Luke, T.M. Riseman, and P.L1. Williams, *Phys. Rev. B* **39**, 851 (1989).

[35] D.E. Farrell, S. Bonham, J. Foster, Y.C. Chang, P.Z. Jiang, K.G. Vandervoort, D.J. Lam, and V.G. Kogan, *Phys. Rev. Lett.* **63**, 782 (1989).

[36] D.E. Farrell, R.G. Beck, M.F. Booth, C.J. Allen, E.D. Bukowski, and D.M. Ginsberg, *Phys. Rev. B* **42**, 6758 (1990).

[37] Y. Yeshurun and A.P. Malozmoff, *Phys. Rev. Lett.* **60**, 2202 (1988).

[38] M. Tinkham, *Phys. Rev. Lett.* **61**, 1658 (1988).

[39] V. Geshkenbein, M. Feigel'man, A. Larkin, and V. Vinokur, *Physica C*, **162-164**, 239 (1989).

[40] V.M. Vinokur, M.V. Feigel'man, V.B. Geshkenbein, and A.I. Larkin, *Phys. Rev. Lett.* **65**, 259 (1990).

[41] O. Brunner, L. Antognazza, J.-M. Triscone, L. Miéville, and Ø. Fisher, *Phys. Rev. Lett.* **67**, 1354 (1991).

[42] J.J. Sun, L.Z. Zheng, B.R. Zhao, B.Xu, J.W. Li, B. Yin, F. Wu, S.L. Jia, L. Li, and Z.X. Zhao, *Physica C* **270**, 343 (1996)

[43] N.P. Ong, *Phys. Rev.* **43**, 193 (1991).

[44] C.P. Poole, Jr., H.A. Farach, and R.J. Creswick, *Superconductivity* (Academic press, 1995) Chap.14, p 470-471

[45] S.N. Putilin, E.V. Antipov, O. Chmaissem, and M. Marezio, *Nature* **362**, 226 (1993).

[46] Schiling, M. Cantoni, J.D. Guo, and H.R. Ott, *Nature* **363**, 56 (1993).

[47] S.L. Yan, L. Fang, Q.X. Song, J. Yan, Y.P. Zhu, J.H. Chen, and S.B. Zhang, *Appl. Phys. Lett.* **63**, 1845 (1993).

[48] Z.F. Ren, J.H. Wang, and D.J. Miller, *Appl. Phys. Lett.* **69**, 1798 (1996).

[49] J.Z. Wu, S.L. Yan, and Y.Y. Xie, submitted to *Science*.

[50] S.H. Yun and J.Z. Wu, *Appl. Phys. Lett.* **68**, 862 (1996).

[51] S.H. Yun, J.Z. Wu, S.C. Tidrow, and D.W. Eckart, *Appl. Phys. Lett.* **68**, 2565 (1996).

[52] F. Foong, B. Bedard, Q.L. Xu, and S.H. Liou, *Appl. Phys. Lett.* **68**, 1153 (1996).

[53] C.C. Tsuei, A. Gupta, G. Trafas, and D. Mitzi, *Science* **263**, 1259 (1994).

[54] J.Z. Wu, S.H. Yun, A. Gapud, B.W. Kang, W.N. Kang, S.C. Tidrow, T.P. Monahan, X.T. cui, and W.K. Chu, *Physica C* **277**, 219 (1997).

[55] M.P. Siegal, E.L. Venturini, and T. L. Aselage, *J. Mat. Res.* **12**, 2825 (1997).

[56] L. Krusin-Elbaum, C.C. Tsuei, and A. Gupta, *Nature* 373, 679 (1995).

[57] H. Fukuyama, H. Ebisawa, and T.Tsuzuki, *Prog. Theor. Phys.* **46**, 1028 (1971).

[58] A.G. Arnov, S. Hikami, and A.I. Larkin, *Phys. Rev. B* **51**, 3880 (1995).

[59] A. Ino, T. Mizokawa, and A. Fujimori, *Phys. Rev. Lett.* **79**, 2101 (1997).

[60] R.P. Vasquez, Z.F. Ren, and J.H. Wang, *Phys. Rev. B* **54**, 6115 (1996).

[61] T. Nagaoka, Y. Matsuda, H. Obara, A. Sawa, T. Terashima, I. Chong, M. Takano and, M. Suzuki, *Phys. Rev. Lett.* **80**, 3594 (1998).

[62] Y. Shimakawa, Y. Kubo, T. Manako and H. Igarashi, *Phys. Rev. B* **40**, 11400 (1989).

[63] Z.F. Ren, J.H. Wang, and D.J. Miller, *Appl. Phys. Lett.* **71**, 1706 (1997)

[64] Y. Kubo, Y. Shimaawa, T. Manao, and H. Igarashi, Phys. Rev. B **43**, 7875 (1991).

[65] C.A. Wang, Z.F.Ren, J.H. Wang, D.K. Petrov, M.J. Naugton, W.Y. Yu, and A. Petrou, *Physica C* **262**, 98-102 (1996).

[66] N.B. Kopnin, *Physica B* **210**, 267 (1995).

[67] J. M. Harris, Y.F. Yan, O.K.C. Tsui, Y. Matsuda, and N.P. Ong, *Phys. Rev. Lett.* **73**, 1711 (1994).

[68] N.B. Kopnin and A.V. Lopatin, *Phys. Rev. B* **51**, 15291 (1995).

[69] D.M. Ginzberg and J.T. Manson, *Phys. Rev. B* **51**, 515 (1995).

[70] A.V. Samoilov, Z.G. Ivanov, and L.-G. Johansson, *Phys. Rev. B* **49**, 36 (1994).

[71] A. Schmid, *Phys. Kondon. Mater.* **5**, 302 (1966).

[72] M. Cyrot, *Rep. Prog. Phys.* **36**, 103 (1973).

[73] J.M. Harris, H. Wu, N.P. Ong, R.L. Meng, and C.W. Chu, *Phys. Rev. B* **50**, 3246 (1994).

[74] B.W. Kang, J.Z. Wu, W.N. Kang, Q.Y. Chen, W.K. Chu, Z.F.Ren and W.H. Wang, "Effect of anion doping on the Hall sign anomaly in the mixed state of Tl-2201 thin films", *Philos. Mag. Lett.* (in press).

[75] C. Li-Xin, N. Amatatsu, H. Ikeda, and R. Yoshizaki, *Adv. in Sup., Proc. of 9th International Symposium on Superconductivity (ISS 96)*, vol. **1**, p. 97-100

[76] K. Nakao, K. Hayashi, T. Utagawa, Y. Enomoto, and N. Koshizuka, *Phys. Rev.*

B **57**, 8662 (1998).

[77] G.W. Crabtree and D. R. Nelson, *Physics Today* **50**, 38 (1997).

[78] H. Safar, P.L.Gammel, D.A. Huse, D.J. Bishop, W.C. Lee, J. Giapintzakis, and D.M. Ginzberg, *Phys. Rev. Lett.* **69**, 824 (1992); *Phys. Rev. Lett.* **70**, 3800 (1993).

[79] W.K. Kwok, J. Fendrich, S. Fleshler, U. Welp, J. Downey, and G.W. Crabtree, *Phys. Rev. Lett.* **69**, 3370 (1992); *Phys. Rev. Lett.* **72**, 1088 (1994).

[80] M. Charalambous, J. Chaussy, P.Lejay, and V. Vinokur, *Phys. Rev. Lett.* **71**, 436 (1993).

[81] J.A. Fendrich, W.K. Kwok, J. Giapinzakis, C.J. van der Beek, V.M. Vinokur, S. Fleshler, U. Welp, H.K. Viswanathan, and G.W. Crabtree, *Phys. Rev. Lett.* **74**, 1210 (1995).

[82] D. López, E.F. Prghi, G. Nieva, F. de la Cruz, *Phys. Rev. Lett.* **76**, 4034 (1996); *Phys. Rev. B* **53**, R8895 (1996).

[83] U. Welp, J.A. Fendrich, W.K. Kwok, G.W. Crabtree, and B.W. Veal, *Phys. Rev. Lett.* **76**, 4809 (1996).

[84] E. Zeldov, D. Majer, M. Konczykowski, V.B. Geshkenbein, V.M. Vinokur, and H. Shtrikman, *Nature* **375**, 373 (1995).

[85] R. E. Hetzel, A Sudbo and D.A. Huse, *Phys. Rev. Lett.* **69**, 518 (1992).

[86] D.S. Fisher, M.P.A. Fisher and D.A. Huse, *Phys. Rev. B* **43**, 130 (1991).

[87] D.R. Nelson and V.M. Vinokur, *Phys. Rev. B* **48**, 13060 (1993).

[88] L. Krusin-Albaum, L. Civale, G. Blatter, A.D. Marwick, F. Holtzberg, and C. Feild, *Phys. Rev. Lett.* **72**, 1914 (1994).

[89] A.V. Samoilov, M.V. Feigel'man, M. Konczykowski, and F. Holtzberg, *Phys. Rev. Lett.* **76**, 2798 (1996).

[90] G. Blatter, M.V. Feigel'man, V.B. Geshkenbein, A.I. Larkin, and V.M. Vinokur, *Rev. Mod. Phys.* **56**, 1125 (1994).

[91] T.K. Worthington, F.H. Holtzberg, and C.A. Field, *Cryogenics* **30**, 417 (1990).

[92] T.T.M. Palstra, B. Batlogg, R.B. van Dover, L.F. Schneemeyer, and J.V. Wasczak, *Appl. Phys. Lett.* **54**, 763 (1989).

[93] R.H. Koch, V. Foglietti, W.J. Gallagher, G. Koren, A. Gupta, and M.P.A. Fisher, *Phys. Rev. Lett.* **63**, 1511 (1989).

[94] P.L. Gammel, L.F. Schneemeyer and D.J. Bishop, *Phys. Rev. Lett.* **66**, 953 (1991).

[95] S.L. Yan, Y.Y. Xie, J.Z. Wu, T. Aytug, A.A. Gapud, B.W. Kang, L. Fang, M. He, S.C. Tidrow, K.W. Kirchner, J.R. Liu, and W.K. Chu, submitted to *Appl. Phys. Lett.*

[96] A.A. Gapud, J.Z. Wu, B.W. Kang, S.L. Yan, Y.Y. Xie, M.P. Siegal, *Phys. Rev. B* (in press).

[97] T.T.M. Palstra, B. Batlogg, L.F. Schneemeyer, and J.V. Waszczak, Phys. Rev. B **43**, 3756 (1991).

[98] A.A.Gapud *et al.*, unpublished.

[99] B.W. Kang, J.Z. Wu, W.N. Kang, A.A. Gapud, D.K. Christen, R. Kerchner, preprint

[100] B.W. Kang, J.Z. Wu, A.A. Gapud, W.N. Kang, D.K. Christen and H.R. Kerchner, submitted to *Phys. Rev. Lett.*

[101] W.N. Kang, B.W. Kang, Q.Y. Chen, J.Z. Wu, S.H. Yun, A.A. Gapud, J.Z. Qu, W.K. Chu, D.K. Christen and C.W. Chu, submitted to *Phys. Rev. B*

[102] J.Z. Wu, B.W. Kang, W.N. Kang, S.H. Yun, A.A. Gapud, D.K. Christen and H.R. Kerchner, Q.Y. Chen, and W.K. Chu, submitted to *Phys. Rev. B*

Publications

Flux Dynamics

1. **B.W. Kang,** J.Z. Wu, A.A. Gapud, W.N. Kang, D.K. Christen and R. Kerchner, *"Glassy vortex-liquid phase in high-T_C superconductors"*, submitted to Phys. Rev. Lett. Sept. 1998

2. J.Z. Wu, **B.W. Kang**, W.N. Kang, S.H. Yun, A.A. Gapud, D.K. Christen, R. Kerchner, Q.Y. Chen, and W.K. Chu, *"Sign reversals in the mixed-state Hall effect of high-T_C superconductors"*, submitted to Phys. Rev. B, Sept. 1998.

3. W.N. Kang, **B.W. Kang**, Q.Y. Chen, J.Z. Wu, S.H. Yun, A.A. Gapud, J.Z. Qu, W.K. Chu, D.K. Christen, R. Kerchner, and C.W. Chu, *"Scaling of the Hall resistivity in epitaxial $HgBa_2CaCu_2O_{6+\delta}$ thin films with columnar defects"*, submitted to Phys. Rev. B, April 1998.

4. **B.W. Kang,** J.Z. Wu, W.N. Kang, Q.Y. Chen, W.K. Chu, and Z.F. Ren, *"Effect of anion doping on Hall sign anomaly of Tl-2201 films"*, to appear in Philos. Mag. Lett.

5. A.A. Gapud, J.Z. Wu, **B.W. Kang**, S.L. Yan and Y.Y. Xie, *"Nature of giant T_C shift in '1212' superconductors due to Hg/Tl exchange"*, to appear in Phys. Rev. B.

6. **B.W. Kang**, J.Z. Wu, W.N. Kang, Q.Y. Chen, W.K. Chu, D.K. Christen, H.R. Kerchner and A. Gapud, *"Mixed-state Hall effect in $HgBa_2CaCu_2O_{6+\delta}$ thin films with columnar defects"*, J. of Supercond. **11**, 163 (1998).

7. A.A. Gapud, J.Z. Wu, S.L. Yan, Y.Y. Xie, **B.W. Kang**, Z.F. Ren, S.H. Yun, M.P. Siegal, D.K. Christen, J.R. Thompson and H.R. Kerchner, *"Magnetic flux pinning in Hg-based HTS thin films"*, Proceeding of 8th US-Japan workshop on high-T_c superconductivity (1998).

8. **B.W. Kang**, W.N. Kang, S.H. Yun and J.Z. Wu, *"Scaling behavior of activation energy of $HgBa_2CaCu_2O_{6+\delta}$ thin films"*, Phys. Rev. B **56**, 7862 (1997)

9. A.A. Gapud, J.R. Liu, J.Z. Wu, W.N. Kang, **B.W. Kang**, S.H. Yun and W.K. Chu, *"Effects of 1-Mev proton irradiation in Hg-based cuprate thin film"*, Phys. Rev. B **56**, 862 (1997).

Material Process

1. S.L. Yan, Y.Y. Xie, J.Z. Wu, T. Aytug, A.A. Gapud, **B.W. Kang**, L. Fang, M. He, S.C. Tidrow, K.W. Kirchner, J.R. Liu, and W.K. Chu, *"High critical current density in epitaxial $HgBa2CaCu_2O_x$ thin films"*, submitted to Appl. Phys. Lett., Sept. 1998.

2. L. Fang, S.L. Yan, T. Aytug, A.A. Gapud, **B.W. Kang**, Y.Y. Xie, and J.Z. Wu, *"Growth of superconducting Hg-1212 very thin films"*, submitted to IEEE transactions on Applied Superconductivity (1998)

3. T. Aytug, **B.W. Kang**, S.L. Yan, Y.Y. Xie, and J.Z.Wu, *"Stability of Hg-based high-T_C superconducting thin films"*, Physica C **307**, 117 (1998).

4. T. Aytug, A.A. Gapud, S.H. Yoo, **B.W. Kang** and J.Z. Wu, "*Effect of sodium doping on oxygen distribution of Hg-1223 superconductors*", to appear in Physica C.

5. A.A. Gapud, T. Aytug, S.H. Yoo, Y.Y. Xie, **B.W. Kang**, S.D. Gapud, J.Z. Wu, S.W. Wu, W.Y. Liang, X.T. Cui, J.R. Liu, and W.K. Chu, "*Lithium-doping-assisted growth of $HgBa_2CaCu_3O_{8+\delta}$ superconducting phase in bulks and thin films*", to appear in Physica C.

6. **B.W. Kang**, A.A. Gapud, X. Fei, T. Aytug and J.Z. Wu, "*Minimization of detrimental effect of air in $HgBa_2CaCu_2O_{6+\delta}$ thin film processing*", Appl. Phys. Lett. **72**, 1766 (1998).

7. J.Z. Wu, S.H. Yoo, T. Aytug, A. Gapud, **B.W. Kang**, S. Wu, and W. Zhou, "*Superconductivity in lithium- and sodium-doped mercury based cuprates*", J. of Supercond. **11**, 169 (1998)

8. J.Z. Wu, S.H. Yun, A. Gapud, **B.W. Kang**, W.N. Kang, S.C. Tidrow, T.P. Monahan, X.T. Cui and W.K. Chu, "*Epitaxial growth of $HgBa_2CaCu_2O_{6+\delta}$ thin films on $SrTiO_3$ substrates*", Physica C **277**, 219-224 (1997)

9. J.Z. Wu, S.H. Yun, A.Gapud, **B.W. Kang**, W.N. Kang, S.C. Tidrow, D. Eckart, X.T. Cui and W.K. Chu, "*Fast temperature ramping Hg-vapor annealing process for fabrication of Hg-based superconducting thin films*", IEEE transactions on Applied Superconductivity **7**, 1907 (1997)

10. S.H. Yun, J.Z. Wu, **B.W. Kang**, A.N. Ray, A. Gapud, Y.Yang, R. Farr, G.F. Sun, S.H. Yoo, Y. Xin and W.S. He, "*Fabrication of c-oriented $HgBa_2Ca_2Cu_3O_{8+\delta}$ superconducting thin films*", Appl. Phys. Lett. **67**, 2866 (1996)

IMAGE EVALUATION
TEST TARGET (QA-3)

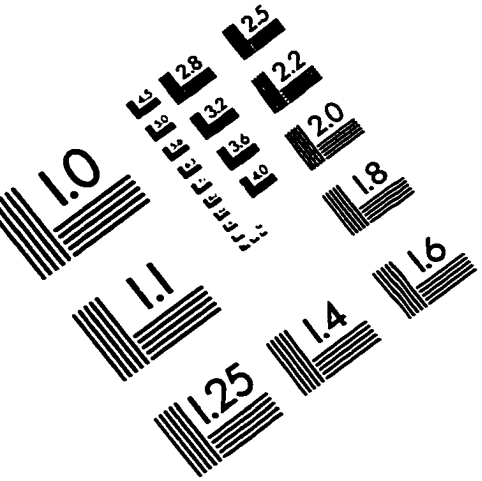

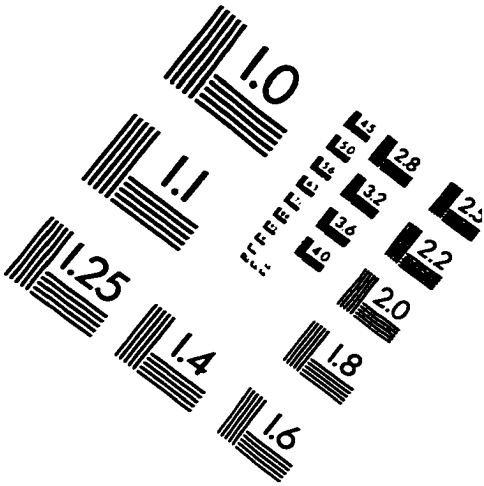

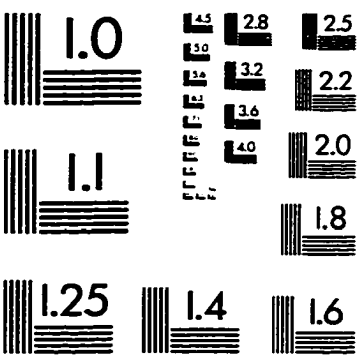

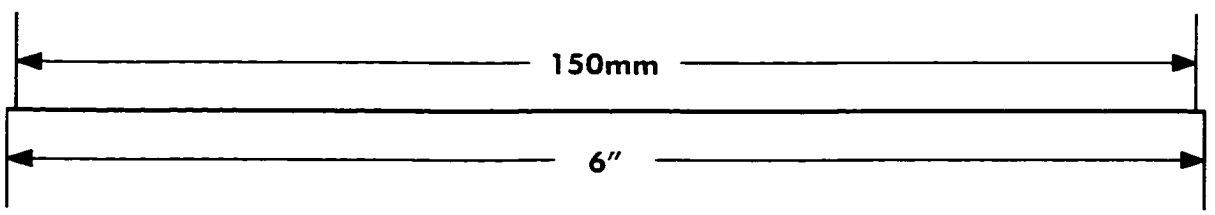

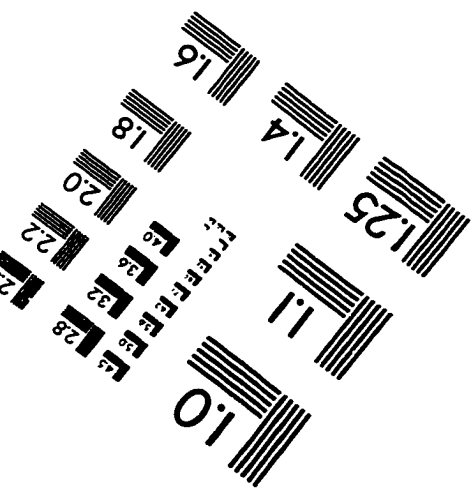

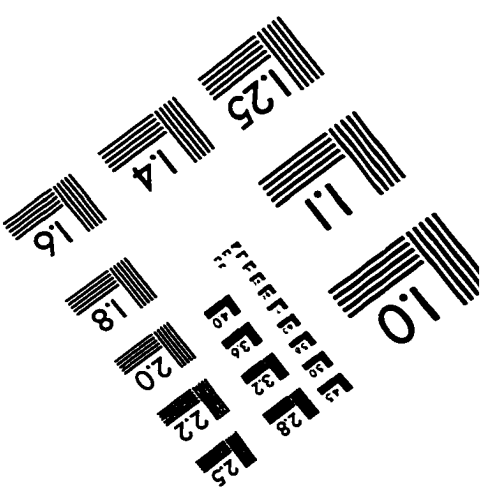

APPLIED IMAGE, Inc
1653 East Main Street
Rochester, NY 14609 USA
Phone: 716/482-0300
Fax: 716/288-5989